

Cite this: *Mater. Adv.*, 2025,  
6, 909

# Translational paradigm of MXene nanocomposites: biophysical advancements to modern applications

Sriparna De,<sup>a</sup> Shaikh Sheeran Naser,<sup>b</sup> Aditya Nandi,<sup>b</sup> Arpita Adhikari,<sup>d</sup> Arbind Prasad,<sup>e</sup> Kunal Sarkar,<sup>f</sup> Adrija Sinha,<sup>b</sup> Sushil Kumar Verma,<sup>i</sup> Ateet Dutt,<sup>b,c</sup> Dipankar Chattopadhyay,<sup>b,d</sup> Nagendra Kumar Kaushik,<sup>b,g</sup> Aishee Ghosh<sup>\*b,h</sup> and Suresh K. Verma<sup>b</sup>

The expanding potential of 2D MXenes opens up promising avenues for flexible biomedical applications. MXenes, a new family of two-dimensional materials with exceptional mechanical, electrical, and chemical properties, have garnered attention for their potential to revolutionize healthcare. These properties enable MXenes to interface seamlessly with biological systems, offering innovative diagnostics, therapeutics, and regenerative medicine solutions. In the biomedical domain, MXenes have shown promise in antibacterial applications, drug delivery, biosensing, photothermal therapy, and tissue engineering, and their biocompatibility and ease of functionalization enhance their utility in real-world healthcare settings. Their large surface areas make them ideal for drug delivery systems, enabling precise encapsulation and release of therapeutic molecules. High electrical conductivity of MXenes has opened new possibilities for neuroprosthetics and brain-machine interfaces, potentially restoring lost functions. Their excellent mechanical properties, biocompatibility, and corrosion resistance make MXenes promising for durable orthodontic devices. Furthermore, their surface-modification capabilities allow for innovative biosensing and diagnostic platforms for sensitive disease detection. MXenes are compatible with imaging techniques, making them suitable contrast agents that can enhance the resolution of medical imaging. MXenes also hold potential in wearable health monitoring devices, advanced bioelectronics, and smart implants, bridging the gap between laboratory research and clinical deployment. However, there are certain challenges regarding their biocompatibility, long-term effects, and large-scale production, which need further research to ensure their safe integration into biomedical applications. This review presents the advancements in the biophysical fabrication of 2D MXenes and their antimicrobial properties and biocompatibility, along with their applications in diagnostics, imaging, biosensing, and therapeutics.

Received 4th September 2024,  
Accepted 14th December 2024

DOI: 10.1039/d4ma00894d

[rsc.li/materials-advances](https://rsc.li/materials-advances)

<sup>a</sup> Department of Allied Health Sciences, Brainware University, 398, Ramkrishnapur Road, Kolkata-700125, India

<sup>b</sup> School of Biotechnology, KIIT Deemed to be University, Bhubaneswar, 751024, Odisha, India. E-mail: sureshverma22@gmail.com

<sup>c</sup> Instituto de Investigaciones en Materiales, UNAM, CDMX, 04510, Mexico

<sup>d</sup> Department of Polymer Science & Technology, University of Calcutta, Acharya Prafulla Chandra Road, Rajabazar, Kolkata-700009, India

<sup>e</sup> Katihar Engineering College (Dept. of Science, Technology & Tech. Ed, Govt. of Bihar), Katihar, India

<sup>f</sup> Department of Zoology, University of Calcutta, 35, Ballygunge Circular Road, Kolkata, West Bengal, 700019, India

<sup>g</sup> Plasma Bioscience Research Center, Department of Electrical and Biological Physics, Kwangwoon University, 01897 Seoul, South Korea.

E-mail: kaushik.nagendra@kw.ac.kr

<sup>h</sup> Department of Physics and Astronomy, Uppsala University, Box 516, Uppsala, SE-751 20, Sweden. E-mail: aishee.ghosh@physics.uu.se

<sup>i</sup> Department of Chemical Engineering, CoE-Suspol, Indian Institute of Technology Guwahati, Guwahati 781039, India

## 1. Introduction

Nanomaterials in biomedical research are increasingly getting integrated into clinical prospects, launching a new era of cutting-edge biomedical applications. With their distinctive characteristics at the nanoscale level, nanomaterials present a wide range of possibilities for transforming several facets of healthcare. Nanomaterials can be tailored to encapsulate therapeutic molecules and selectively release them at particular sites, reducing side effects and improving treatment effectiveness.<sup>1</sup> Their adaptability extends to tissue engineering, where scaffolds made of nanomaterials can imitate the natural extracellular matrix to aid in tissue regeneration. The use of precise diagnostics and therapies catered to specific patient profiles, through the use of nanomaterials, has the potential to



architect customized medicine. In biomedicine as well as nanobiotechnology, numerous unique nanoscience-based techniques have been developed, allowing theragnostic modalities like synergistic therapy and multimodal imaging, which are promising alternatives in treating a variety of ailments. Materials having layered 2D structures have received a lot of attention since graphene was discovered in 2004 as a result of their proven biochemical and physical characteristics that set them apart from their bulk counterparts.<sup>1</sup> Utilising novel 2D-based systems with fascinating features for versatile technical applications is the major objective.<sup>2</sup> The topic emerged again with attention of scientific communities on graphene, the first 2D layered structure, and further led to a huge success in terms of applicability. Since then, dichalcogenides, phosphorenes, hexagonal boron nitride, *etc.* have been explored as 2D materials and extensively researched for various potential applications.<sup>3,4</sup> A broad family of transition metal nitrides and/or carbides known as the MXenes was recently developed by the Gogotsi research team at Drexel University.<sup>5</sup> To synthesize MXenes from 'MAX' phases, layers of 'A' element are particularly etched. The transition metal-based nitrides and carbides that make up the MAX phases are connected by the 'A' element to form strong bonding (ionic, metallic, and covalent) with the 2D layers.<sup>6</sup> A typical MXene 2D flake has the general characteristic formula of  $M_n+1X_nT_x$ , which denotes the presence of carbon or

nitrogen intermingled with surface functions such as F, Cl, O, and OH, Sc, Ti, V, Cr, Mn, Fe, Y, Zr, Nb, Mo, Hf, Ta, and W.

A number of top-down synthesis methods including electrochemical etching,<sup>7,8</sup> thermally driven electrochemical,<sup>9</sup> hydrothermal techniques in the presence of NaOH<sup>10</sup> and KOH solutions,<sup>11</sup> Lewis acid molten salt replacement reaction,<sup>12</sup> and salt-templated approaches<sup>13</sup> were adopted. Amongst them recently fluorine-free synthesis methods are attracting considerable attention for their safe and promising gateway to chemical synthesis of MXenes (Fig. 1).

MXene nanosheets possess high specific surface areas making them suitable carriers of drugs or proteins with lots of anchoring sites and reservoirs. MXenes have intriguing physicochemical characteristics, such as photothermal conversion, X-ray attenuation, electron switching ability, and localized surface plasmon resonance, as well as biological behaviours, such as enzyme-assisted biodegradation, cellular endocytosis, distinctive biodistribution, and metabolism pathway, because of their ultrathin layered structure with almost single-atomic thickness.<sup>14</sup> Owing to its 2D planar arrangement, hydrophilic nature, infinite and open possibilities towards functionalization and chemical substitution, substantial absorption characteristics in the near-infrared region, and excellent attributes, MXenes are considered one of the most favourable materials for use in biomedical uses. Despite diligent research on MXene,

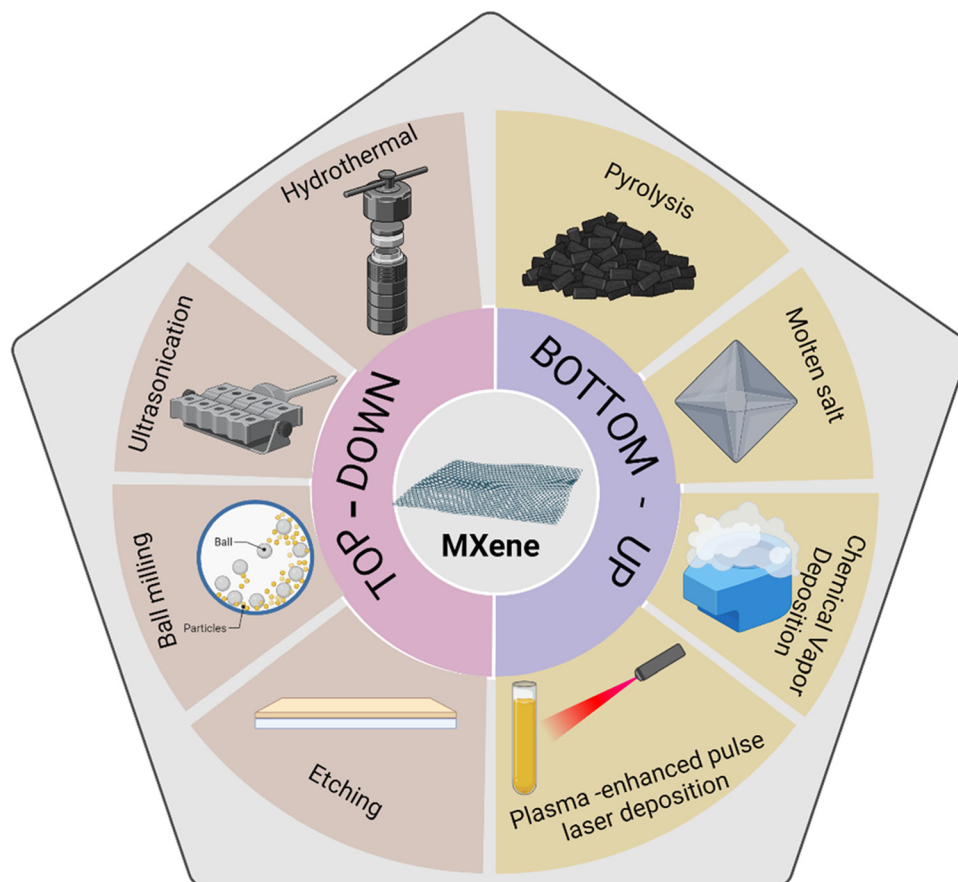


Fig. 1 Schematic of surface functionalization techniques for MXenes.



the remarkable features of these materials are still insufficient to meet all the pre-requisites of several biomedical applications. The upgrade of the functional characteristics and performance through surface coupling with different materials and polymers added new horizon for nanomedicine application.<sup>14</sup>

MXenes and their composites, which are ideal biomaterials for biomedical applications, can be engineered to exhibit various chemical, physical, and mechanical properties,<sup>15</sup> but they must also be physiologically compatible with dependable mechanical strength, sustainability, and the capacity to resist biological refutation. Despite their limited exploration, a number of MXenes and their composites have demonstrated that they are biocompatible and nontoxic to living things,<sup>16</sup> and MXenes such as niobium carbide have demonstrated that they are biodegradable in mice,<sup>17</sup> making them promising for *in vivo* applications and offering tremendous potential for revolutionary uses. To ensure MXenes' safe integration into clinical practice, it is crucial to conduct extensive studies into their long-term biocompatibility, possible immunological reactions, and biodegradability as their potential for use in medicine is investigated.

The development of skin-like electronic devices for human-machine interaction has drawn widespread attention owing to its characteristic features, such as stretchability, self-healing, transparency, biocompatibility, and wearability. This review paper emphasizes the latest developments in MXenes, a promising material that shows potential for creating soft, skin-like electrodes that are malleable. A lot of work has been done on creating skin-like electrodes for various applications including signal monitoring, electrocardiograms (ECGs), biomedical applications, energy storage devices, transistors, pressure sensors, energy harvesters, and soft, malleable electrodes that resemble skin, which have replaced rigid electrodes in recent years. These electrodes maintain their electrical conductivity even under the most severe mechanical damage and deformations. A "hospital-on-a-chip" system-integrated MXene nanosheet-based multifunctional microneedle electrodes have been recognized for their versatility for biosensing applications. Through micro-needling technique, dozens of tiny needles were utilized for fabricating effective transdermal patch for drug delivery and biosensing applications through penetrating the dermal layer within the human body. Miniaturized MXene nanosheet-based microneedles can also sense the movement-specific variation of human eye and musculoskeletal contraction.

Wearable microfluidic biosensors provide new avenues to strengthen healthcare and life productivity. These gadgets make it possible for body-worn sensors to wirelessly send critical data, transforming healthcare technology by enabling prognosis and diagnosis using bodily fluids or physiological signals. However, the inability to recover data from the human body and the requirement for flexible, lightweight, and water-resistant sensors make the implementation of these technologies problematic. Wearable microfluidic biosensor technologies have been developed to address these issues. MoS<sub>2</sub>

transistors have been used as the key sensing material in wearable smart contact lenses because of their multilayer dangling bond-free surface, high surface area, superior biocompatibility, charge transfer capabilities, and adjustable bandgap.<sup>18</sup> These lenses offer a high current on/off ratio, a quick reaction time, and great sensitivity and responsiveness for picture recognition.

Exfoliated MXenes (Ti<sub>3</sub>C<sub>2</sub>T<sub>x</sub>) with PB composites showed superior electrochemical performance over graphene/PB and CNT/PB composites against H<sub>2</sub>O<sub>2</sub> detection in Lei *et al.*'s introduction of MXene-based microfluidic wearable electrochemical biosensors for sweat detection. Custom sensors made to track other analytes can be used to replace the sensor device's interchangeable component.<sup>19</sup> A novel wearable impedimetric immunosensor for the non-invasive measurement of cortisol in human sweat was described by Noh *et al.* Although microfluidic technologies have made it possible to employ microchip-based platforms in biology and life science, they frequently improve upon or offer equivalent options to current macroscale experiments.<sup>20</sup> Further research and vigorous characterization are urged to tune the applicability of microfluidic wearable biosensors in various area.<sup>21</sup> In this review, we systematically summarize the significant biomedical prospects of MXenes and functional MXenes, and their composites in the field of drug administration, cancer therapeutics, wound healing, smart sensing, and tissue engineering field. MXenes offer an exciting new direction for biomedical research, with their unique features primed to transform medical monitoring, treatments, and diagnostic methods. Despite these amazing developments, strategic concerns provide insights into potential toxicity, long-term consequences and scalable production techniques to ensure the safe and successful transfer of nanomaterials from the laboratory to the clinical settings.

## 2. Synthesis of MXenes and their derivatives

MXenes, a family of two-dimensional materials, are synthesized primarily through two approaches: top-down and bottom-up methods (Fig. 1).<sup>22</sup> The top-down method involves selectively etching the A-layer from MAX phases (ternary carbides or nitrides) using chemical treatments, such as hydrofluoric acid or fluoride-containing solutions, followed by exfoliation to produce nanosheets. This technique is widely adopted due to its efficiency and scalability. The bottom-up approach, though less common, relies on chemical vapor deposition or molecular assembly for precise control over the material structure. Surface modifications of MXenes and their derivatives achieved through functionalization with polymers or biomolecules enhance their stability, biocompatibility, and suitability for diverse applications.<sup>23</sup> Currently, the top-down synthesis from the MAX phase is the most widely used method.

MXenes are typically synthesised by a top-down etching technique using stacked ternary MAX phases as precursors. The MAX phase is a catch-all phrase for many types of

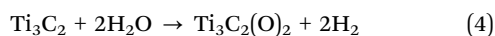
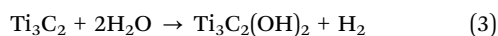
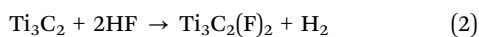
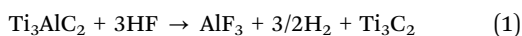


metal-based carbides and nitrides, having the chemical formula  $M_{n+1}AX_n$ .<sup>24</sup> It is a three-dimensional crystal structure generated by subsequent chemical bonding and stacking of two-dimensional layers. Herein, the “M” signifies transition metals, “A” is associated with 13 and 14 group elements, “X” belongs to C and N, and  $n$  ranges from 1 to 4. The distorted octahedron of [XM6] forms lateral edge-sharing configuration. Metal bonds connect the “A” and “M” atoms in the “A” layers, which are positioned on either side of “M–X” layer. The 2D layer of materials generated by omitting the “A” layers from the MXenes have alternate ordered structure of “M” ( $n + 1$  layer) and “X” ( $n$  layer) with F, OH, O, or Cl (denoted as  $T_x$ ) used as surface termination.<sup>25</sup>

The method of synthesizing MXenes involves wet chemical etch processing of the MAX phase with hydrofluoric acid (HF) or a HF derivative as the etchant or *in situ* production of HF, such as eliminating the specific chemical element from the layered structure of MAX phase ( $M_{n+1}AX_n$ ) or removal of Al element layer from  $Ti_3AlC_2$ .<sup>26</sup>

## 2.1 Etching strategies of MXenes

**2.1.1 HF etching method.** The first documented etchant for obtaining MXenes from their respective MAX phase as precursors was HF acid. The etching mechanism is shown in Fig. 2. Except for the Al layer, the stoichiometric compound  $Ti_3C_2T_x$  was similar to the comparable  $Ti_3AlC_2$  MAX phase.<sup>27</sup> Furthermore, MXenes with lots of surface terminations such as  $-F$ ,  $-OH$ , and  $-O$  were synthesized *via* this aqueous etching procedure. The following chemical treatment might be applied to the etching process:



The HF concentration, etching temperature, and time all affect product quality during etching. As  $Ti_3C_2T_x$  was removed during etching, the HF etchant strength affects surface termination species. Easy-to-use and low-temperature chemical reactions make HF etching appropriate for etching Al from the MAX phase and a portion of non-MAX phase. However, HF etchant is poisonous, corrosive, hazardous during reaction, and environmentally harmful.

**2.1.2 *In situ* HF-forming etching methods.** To reduce corrosion from the HF-based etchant, another etching method that involves *in situ* HF treatment is examined. In *in situ* HF-producing systems, due to their great reactivity, the F ion can mix with the Al element of MAX precursors to form fluoride,  $H_2$ , and MXenes. *In situ* HF-based methods are easier to operate, require less energy, and decrease chemical risk during etching than standard HF treatment since direct HF usage is limited. Ghidui *et al.* initially etched  $Ti_3AlC_2$  at 40 °C using HCl/LiF in 2014.<sup>32</sup> This developed high-plasticity  $Ti_3C_2T_x$  clay that can be

roller-pressed into film. Multi-layered accordion-like MXenes are produced by HCl/LiF etching, like HF.

**2.1.3 Electrochemical etching methods.** MXenes are made by electrochemically etching the aluminium atomic layer at a specified voltage using the MAX phase as an electrode (Fig. 2). Electrochemically creating carbide-derived carbon (CDC) from the MAX phase may use NaCl, HF, or HCl.<sup>33</sup>

Standard electrochemical etching disrupts the M–A bond and removes the MAX phase A-layer with cyclic voltammograms between 0 and 2.5 V. As the voltage increases, more M-layer is destroyed, forming amorphous carbon compounds. Selectively removing A atoms requires adjusting the etching voltage window (etching potential) within the reaction potential range between A and M layers and precisely controlling the etching time. This allows precise MXene synthesis control.

The electrode is commonly obtained from the MAX phase; therefore, the etching process begins on its surface with the production of CDC layers that prevent further etching. Thus, controlling the applied voltage for etching the MAX phase is crucial. Sun *et al.* electrochemically etched the MAX phase at 0.6 V (against Ag/AgCl) using three electrodes.<sup>34</sup> Bulk  $Ti_2AlC$  was cut into tiny cubic blocks as working electrodes, while Ag/AgCl, HCl, and platinum were used as the reference, electrolytic system, and counter electrodes, respectively. Electrochemical etching transforms  $Ti_2AlC$  into  $Ti_2CT_x$  and CDC layers, with the CDC coatings on the  $Ti_2AlC$  surface restricting etching and creating an MXene-enabled materials. The MAX phase became CDC as electrochemical etching increased. The study also examined how electrochemical exposure, etching duration, and electrolyte concentration affected final products.

**2.1.4 Molten salt etching methods.** At low operating temperatures, the aqueous-based etchings are acceptable for most Al-enabled MAX compounds, yielding hydrophilic MXenes.<sup>13</sup> Urbankowski *et al.* etched  $Ti_4AlN_3$  with mixed molten salts of alkali fluorides at 550 °C for 1/2 h to get the nitride-based MXenes, *i.e.*,  $Ti_4N_3T_x$ , demonstrating the capabilities of molten salt towards the formation of MXenes with a high formation energy.<sup>35</sup> Excluding molten salt etching, it is strenuous to synthesize nitride MXenes. According to reports, HF-etched  $Mo_2C$  may be transformed into  $Mo_2N$  MXenes by heating at 600 °C in an  $NH_3$  environment.<sup>13</sup> The molten salt-based etching methodology is preferred for synthesizing MXenes that exhibit high formation energy, such as nitride-based MXenes.

**2.1.5 Alkali etching methods.** The alkali is also anticipated to allow for selective etching of the MAX phase. Because of the alkali's high binding capacity with Al, alkaline etchants may be useful in etching  $Ti_3AlC_2$  or other layered precursors. Xie *et al.* studied a two-step etching methodology that includes soaking  $Ti_3AlC_2$  in a 1 M NaOH solvent for 100 h and then in a 1 M  $H_2SO_4$  solution at 80 °C for 2 h, allowing the etching of MAX surface into  $Ti_3C_2T_x$ .<sup>36</sup> The alkali was utilised in this method to remove Al constituents from the MAX phase, whereas  $H_2SO_4$  drives the removal of Al from the surface. The approach allowed for efficient MAX phase etching using alkali as an etchant at low concentrations; however, only the superficial layer of the



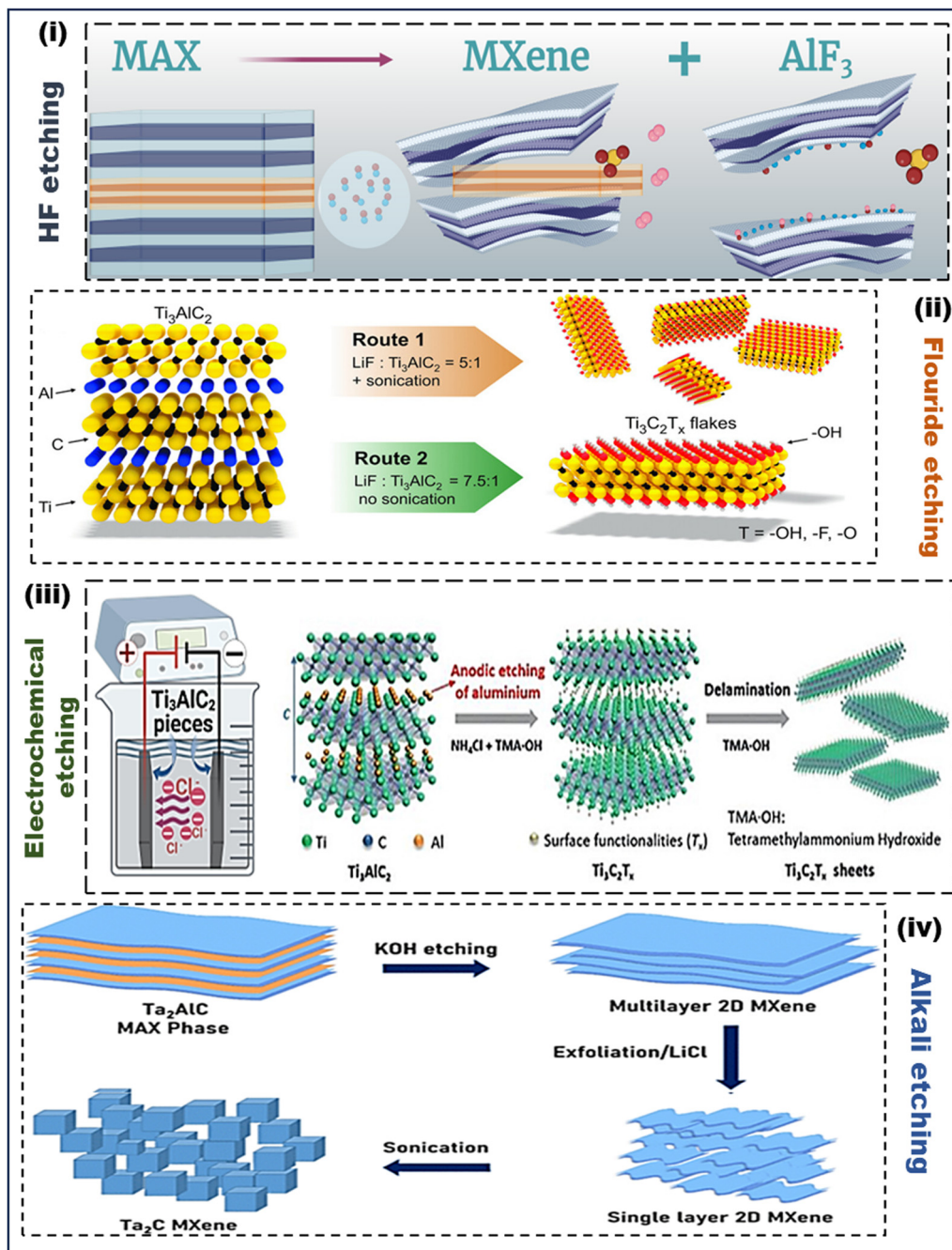


Fig. 2 Schematic of etching strategies for MXene production. (i) HF etching. Reproduced from ref. 28 with permission from Elsevier, copyright 2020, (ii) Fluoride etching. Reproduced from ref. 29 with permission from Wiley, copyright 2016. (iii) Electrochemical etching. Reproduced from ref. 30 with permission from Wiley, copyright 2018. (iv) Alkali etching. Reproduced from ref. 31 with permission from the Royal Society of Chemistry, copyright 2018.

MAX phase that could lead poor etching to yield MXenes. Furthermore, the resulting MXenes' separation from their precursor phase is quite challenging. Another impediment to alkali etching yields the formation of additional oxide/hydroxide layers, developed over the MAX phase. In one example, when 2 M KOH was used to etch  $\text{Ti}_3\text{SiC}_2$  at a temperature of 200 °C *via* a hydrothermal reaction, it results in a core-shell  $\text{MAX}@K_2\text{Ti}_8\text{O}_{17}$  composite,<sup>37</sup> whereas NaOH caused the development of a  $\text{Na}_2\text{Ti}_7\text{O}_{15}$  layer on the MAX phase, preventing the

process from yielding pure MXenes. The use of intense alkali for etching the MAX phase is effective, yielding extremely hydrophilic substances with F-free terminations. However, the risks of using concentrated alkali and high temperatures confine its use to the production of significant amounts of MXenes. Furthermore, the resulting chemical products are often multilayered MXenes with accordion-like shape, which induce further intercalation and delamination to form mono-layer MXene nanosheets.<sup>38</sup>



**2.1.6 Other etching methods.** Multiple synthesis routes are constantly being studied to find MXenes that are safe, efficient, and environmentally friendly. Recently, a number of new methods have been outlined. Halogen has also been described as a MAX etching etchant. Shi *et al.* used  $I_2$  to etch  $Ti_3AlC_2$  at  $100\text{ }^\circ\text{C}$  in anhydrous acetonitrile ( $CH_3CN$ ), yielding accordion-like  $Ti_3C_2I_x$ .<sup>39</sup> After that, the resulting product was treated with HCl (1 M) to eliminate  $AlI_3$  produced during etching. It has also been proposed to employ electromagnetic waves and mechanical strength to etch the stacked ternary predecessors. Mei *et al.* etched  $Mo_2Ga_2C$  to generate  $Mo_2C$  in a phosphoric acid medium for 3–5 hours using an ultraviolet light (100 W).<sup>40</sup>

**2.1.7 Bottom-up synthesis.** Bottom-up synthesis, a less widely recognized protocol for MXene synthesis,<sup>28</sup> typically commences with minute organic or inorganic molecules/atoms. Following this, a crystal is formed, which can be utilized to create a 2D-ordered layer.<sup>23</sup> Among the methods employed for bottom-up synthesis, the chemical vapor deposition (CVD) technique is frequently used and is known for producing high-quality thin films on various substrates. Generally, CVD results in thin films of very low thickness, often organized into multilayered structures with at least six layers.<sup>41</sup> A study exploring the application of the chemical vapor deposition (CVD) approach for synthesizing molybdenum carbide ( $Mo_2C$ ) employed methane ( $CH_4$ ) and copper/molybdenum (Cu/Mo) foils at temperatures of  $1085\text{ }^\circ\text{C}$ .<sup>42</sup> This method yields high-quality, thin, and substantial nanosheets with minimal flaws. Beyond CVD, current literature details alternative MXene synthesis approaches,<sup>43</sup> including template techniques and plasma-enhanced pulsed laser deposition (PEPLD), with examples such as 2D nitrides ( $MoN$ ,  $V_2N$ , and  $W_2N$ ).<sup>44</sup> Bottom-up synthetic methods offer precise control over MXene's size distribution, shape, and surface termination.

**2.1.8 Mxene–polymer composites.** Polymers have established themselves as credible contenders among the 2D materials predating MXenes. Comprising long chains of carbon molecules assembled with other molecules, polymers can modify their chemical and mechanical properties. The inherent flexibility of polymers has sustained them as an ever-expanding subject of study.<sup>45</sup> Renowned for their low-cost and ease of production, polymer composites exhibit distinguished attributes such as abrasion resistance, corrosion resistance, fatigue resistance, impact resistance, great strength, fracture resistance, and significant stiffness. The synergistic collaboration between polymers and MXene yields exceptional electrical, mechanical, and thermal characteristics.<sup>46</sup> The formation of polymer/MXene nanocomposites employs various techniques, resulting in diverse interactions between the polymer and the MXene.<sup>47</sup> For instance, Jin *et al.* developed a nanocomposite of poly(vinyl alcohol)/ $Ti_3C_2T_x$  (PVA/MXene), illustrating a multi-layered casting procedure to create PVA/MXenes<sup>48</sup> (Fig. 3). The incessant MXene layer was generated using aqueous dispersion, and the polymer was casted at  $45\text{ }^\circ\text{C}$  to achieve a multilayered structure. In another study, Wu *et al.* reported a  $Ti_3C_2T_x$  MXene-based poly(dimethylsiloxane) (PDMS) nanocomposite. MXene was combined with sodium alginate (SA) to form MXene/SA.<sup>49</sup> Subsequently, PDMS-coated MXene/SA was

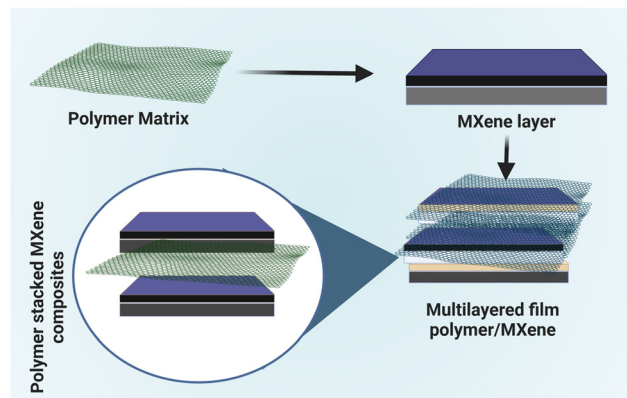


Fig. 3 General schematic of polymer/Mxene composite layered structure.

created through a freeze-drying procedure. This involved forming MXene/SA and coating the hybrid by dipping it in PDMS. The resulting polymer/MXene nanostructures exhibited remarkable thermal stability, thermal conductivity, electrical conductivity, and mechanical properties. Although polymer/MXene nanocomposites demonstrate exceptional physical properties, the combination of functional MXenes with polymers enhances these attributes, resulting in high-performance polymer/MXene-based nanocomposites. The selective, stimuli-responsive, contrast-enhancing, and sensitive nature of various polymer-functionalized MXene composites makes them suitable for biomedical applications such as photothermal therapy, drug delivery, diagnostic imaging, biosensing, bone regeneration, and antibacterial activity.

### 3. Translational applications of MXenes

MXenes, a versatile class of two-dimensional materials, have shown immense promise in biomedical applications due to their unique properties such as high electrical conductivity, biocompatibility, and tunable surface chemistry. They are utilized in multiple biomedical applications such as wound healing, antibacterial agents, and biosensing technologies for the accurate detection of biomarkers, significantly improving disease diagnostics (Table 1). In drug delivery, MXenes act as efficient carriers, allowing controlled and targeted release of therapeutic agents. Their photothermal and photodynamic properties make them effective in cancer treatment, enabling minimally invasive therapies. Furthermore, MXenes are used in tissue engineering as scaffolds to support cell growth and regeneration, while their flexibility makes them ideal for wearable health-monitoring devices.

#### 3.1. Employment of MXenes in wound healing applications

The skin is the body's principal barrier, preventing microbial, chemical, and radioactive damage. Medical professionals worry about delayed wound healing in skin injury. Hydrogels, gelatin sponges, films, and bandages are being tested for wound dressing to speed healing. These compounds are essential for





Table 1 Applications of MXenes in the biomedical sector

MXene-based NMs	Significant parameters	Application area	Characteristics features	Ref.
Poly-L-lysine/glucose oxidase/Ti <sub>3</sub> C <sub>2</sub> Prussian blue/Ti <sub>3</sub> C <sub>2</sub> MXene	4.0–20 μM 5 × 10 <sup>2</sup> –5 × 10 <sup>5</sup> particles μL <sup>-1</sup> 229 particles μL <sup>-1</sup> (LOD)	Biosensor Biosensor	NA Detection of exosomes secreted by various cancer cells with high specificity	50 51
MXene–MoS <sub>2</sub>	100 fm to 100 nm 26 fm	Biosensor	High selectivity, reproducibility, and stability	52
MXene N-Ti <sub>3</sub> C <sub>2</sub> quantum dot/Fe <sup>3+</sup>	0.5–100 μm 0.17 μm	Biosensor	Promising probe for detecting/showing cellular imaging of glutathione in MCF-7 cells.	53
MXene-derived quantum dot@Au	5 fm to 10 nm, 1.7 fm	Biosensor	MQD@Au NBs heterostructure in electrochemiluminescence sensing	54
MXene@Au NPs@ methylene blue	5 pg mL <sup>-1</sup> to 10 ng mL <sup>-1</sup>	Biosensor	Universal antifouling detection strategy by changing the recognition sequence of the peptides.	55
Ti <sub>3</sub> C <sub>2</sub> @ReS <sub>2</sub>	0.83 pg mL <sup>-1</sup> 0.1 fm to 1 nm 2.4 am	Biosensor	ReS <sub>2</sub> for photoelectrochemical bioanalysis and also a novel and efficient avenue by using Ti <sub>3</sub> C <sub>2</sub> -based semiconductors to boost the charge separation efficiency	56
Ti <sub>3</sub> C <sub>2</sub> /polyacrylamide		Drug delivery	97.5127.7 mg g <sup>-1</sup> drug-loading ability and percentage releases 62.1–81.4	57
Cellulose/DOX/Ti <sub>3</sub> C <sub>2</sub> MXene[10a]	235.2–313.6 ppm	Drug delivery	235.2–313.6 ppm – chemotherapeutic agent, synergistic chemotherapy and PTT with power density of 1.0 W cm <sup>2</sup>	58
Ti <sub>3</sub> C <sub>2</sub> T <sub>x</sub> MXene	Vacuum-assisted filtration	Potential antibacterial agent	Antibacterial activity to inhibit the growth of <i>E. coli</i> and <i>B. subtilis</i> by Ti <sub>3</sub> C <sub>2</sub> T <sub>x</sub> /polyvinylidene fluoride	5
Ti <sub>3</sub> C <sub>2</sub> T <sub>x</sub> /polyvinylidene fluoride	Vacuum-assisted filtration	Potential antibacterial agent	Inhibits the growth of <i>E. coli</i> and <i>B. subtilis</i>	59
Ultra-long hydroxyapatite nanowires/titanium carbide nanocomposite	Bone	Regenerative medicine.	Improved mechanical properties and hydrophilicity with enhanced cell adhesion, proliferation, and osteogenic differentiation	60
Muscle-inspired MXene/PVA hydrogel	Skin	Regenerative medicine.	Excellent mechanical properties (stressed up to 0.5 MPa and strained up to 800%) for local hyperthermia of infected sites under NIR laser.	61
Nb <sub>2</sub> C MXene titanium plate (Nb <sub>2</sub> C@TP)-based implant	Skin	Regenerative medicine.	The Nb <sub>2</sub> C@TP medical implant to promote angiogenesis and tissue remodeling.	62
Silica@Nb <sub>2</sub> C MXene-integrated 3D-printing bioactive glass scaffolds	Skin	Regenerative medicine.	Controllable NO release, highly efficient photothermal conversion, and stimulatory bone regeneration	63
MXene–amoxicillin–PVA nanofibrous membrane	Skin	Regenerative medicine.	Physical barrier to coload the amoxicillin, high antibacterial and accelerated wound healing capacity.	64

preventing microbial infections. Bioactive substances including antibiotics, nanoparticles, and growth factors improve their characteristics.

Traditional wound dressings focus on haemostasis and inflammation during skin repair. This is done by absorbing exudate, keeping the environment moist, and minimizing infection. Angiogenesis, tissue granulation, and ECM synthesis occur during the 2–10-day proliferation phase. This phase releases cytokines including FGF2/bFGF and VEGFA, speeding healing. Fibroblasts and myofibroblasts work together to form the ECM. The third phase of wound healing is remodelling, commencing about two to three weeks after the initial injury and lasting for a year or longer. During this stage, most macrophages and myofibroblasts undergo apoptosis, transforming the type III collagen framework into a type I collagen framework. Traditional dressings, such as gauze, play passive roles in the healing process, offering protection, hydration, exudate absorption, and damage prevention. External factors can impede wound closure, and a popular strategy involves enriching dressing materials with active ingredients that actively influence endogenous cells and factors while possessing natural antibacterial characteristics. By employing this approach, wound dressings can enhance their antibacterial and tissue-repair capabilities. Various bioactive substances have been incorporated into wound dressings to boost antibacterial capabilities and control the synthesis of endogenous growth factors.<sup>65</sup>

MXene has recently emerged as a notable active agent, distinguished by its unique physicochemical architecture. Li *et al.* pioneered the creation of anisotropic MXene@PVA hydrogels through a directional freezing-assisted salting-out technique.<sup>61</sup> These hydrogels exhibited finely tuned photothermal properties and demonstrated broad-spectrum antibacterial activity against both *E. coli* and *S. aureus*, with efficiency rates of 98.3% and 95.5%, respectively. The mechanical properties of the hydrogel were also finely tuned, offering substantial assistance with a stress of up to 0.5 MPa and a strain of up to 800% while fostering NIH-3T3 cell proliferation.

In a mouse wound model, the hydrogel showcased its efficacy in preventing wound infection and enhancing wound closure, achieving a remarkable rate of approximately 98%. Additionally, the simultaneous incorporation of MXene-based nanomaterials within chitin sponges (CH) accelerated hemophilicity and regulated blood vessel coagulation kinetics, making them effective for tissue engineering applications.<sup>66</sup>

Studies have demonstrated that the scaffold provides outstanding rheological properties, self-healing capabilities, electrical conductivity, and tissue adhesibility. Furthermore, the HPEM scaffold displays robust antibacterial activity against both Gram-positive and Gram-negative bacteria, including MRSA. Additionally, it can enhance cell proliferation and upregulate the production of genes related to muscle actin, COL III, and VEGF.<sup>67,68</sup>

The modulation of a photothermal agent leads to necrosis or apoptosis wherein near-infrared (NIR) laser-driven photothermal therapy (PTT) is applied locally to convert NIR radiation

into heat energy, thereby inducing cell death cascade. Researchers are increasingly finding that photothermal therapy can be utilized to improve skin wound healing in addition to the treatment of cancer. In order to create Ag/Ti<sub>3</sub>C<sub>2</sub>T<sub>x</sub> composites using MXene nanoparticles that have outstanding photothermal characteristics with Ag, Zhu *et al.* adopted the concept of photothermal therapy (PTT), wherein they have showed that the synergism between Ag and Ti<sub>3</sub>C<sub>2</sub>T<sub>x</sub> significantly induces photothermal sterilization when applied in combination.<sup>69</sup> Additionally, the cytotoxicity results demonstrated that Ag/Ti<sub>3</sub>C<sub>2</sub>T<sub>x</sub> had superior antibacterial effects. NIR instigates antibacterial potency to the implanted hydrogel, resulting in wound healing characteristics. In order to increase the ROS yields for antimicrobial applications, Li *et al.* built the Schottky junction of Bi<sub>2</sub>S<sub>3</sub>/Ti<sub>3</sub>C<sub>2</sub>T<sub>x</sub>.<sup>70</sup> They also designed various *in vitro* experimental set-ups wherein morphological staining pattern and immunohistochemistry (IHC) techniques were specifically tailored for scrutinizing the characteristic features in the cell cycle environment. The antibacterial properties of Bi<sub>2</sub>S<sub>3</sub>/Ti<sub>3</sub>C<sub>2</sub>T<sub>x-5</sub> on *Staphylococcus aureus* and *Escherichia coli* have been demonstrated using different methodologies. They have additionally directed emphasis to the synergistic benefits of combining reactive oxygen species (ROS) and photothermal therapy, which reveal more significant antibacterial characteristics in comparison to either ROS or photothermal therapy by themselves. In addition, it was discovered that the Bi<sub>2</sub>S<sub>3</sub>/Ti<sub>3</sub>C<sub>2</sub>T<sub>x</sub> Schottky knot enormously speed up the process of wound healing when it was illuminated by light with an 808 nm wavelength. Materials based on MXenes, such as MoS<sub>2</sub> and PLGA bioisomers, have properties that are analogous to those of glutathione, peroxidase, photothermal, and photodynamic energy. *In vivo* tests with a mouse wound model implied that this antibacterial platform showcased unprecedented potency and expedited the healing process for wounds. The employment of the photothermal agent in conjunction with other materials focuses on the prospect of MXenes as alternatives to antibiotics that have immense potential for the therapy of drug-resistant infections and wound care management.

### 3.2. Antibacterial potency and efficacy of MXene derivatives

Composites comprising MXenes have demonstrated great potential for invading microorganisms that are resistant to antibiotics. The underlying concept of the killing efficacy of pathogenic bacteria and their bactericidal mechanisms is still illusory. The sharp edges of MXene nanoflakes lead to the release of reactive oxygen species (ROS) and photothermal degradation of bacteria.<sup>71</sup> Studies reveal that MXenes adsorbed on bacterial membrane surfaces may instigate cell lysis through a cascade of topical phase transition followed by leakage of intracellular molecules at the phase boundary, resulting in cellular damage (Fig. 4). MXenes, specifically Ti<sub>3</sub>C<sub>2</sub>T<sub>x</sub>, possess a significant antibacterial potency through physical damage and direct mechanical destruction. Surprisingly, coatings made of hydrophilic MXenes (Ti<sub>3</sub>C<sub>2</sub>T<sub>x</sub>) articulated effective antibacterial properties against both *B. subtilis* and *E. coli*.<sup>5</sup>





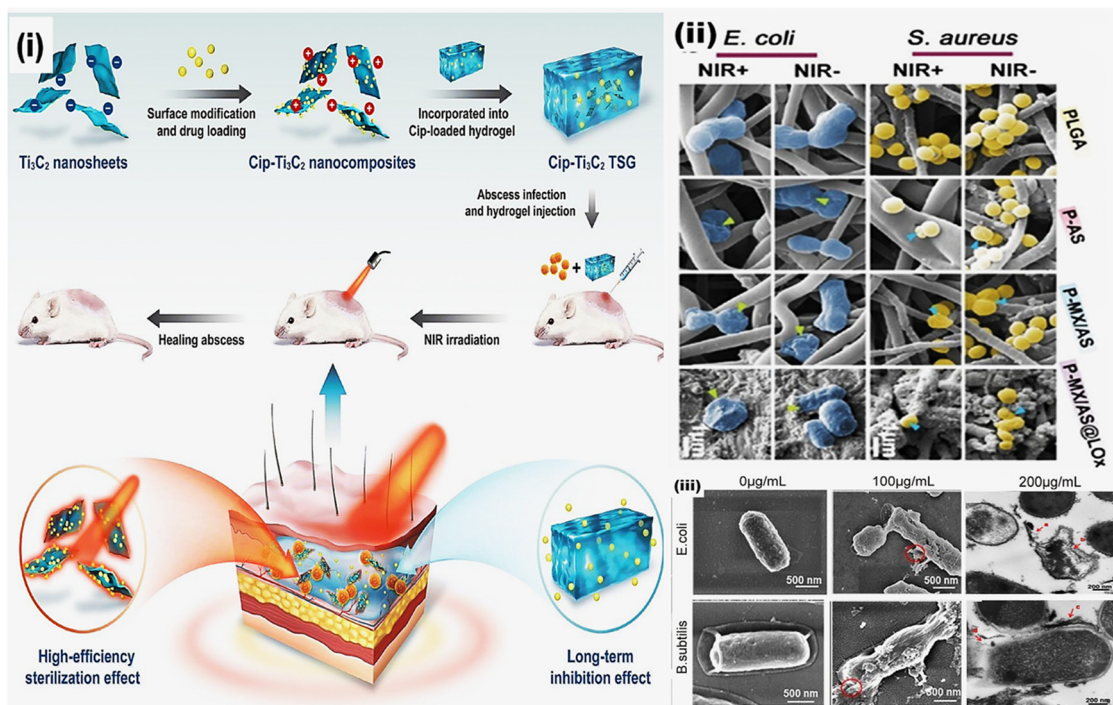


Fig. 4 (i) Schematic of the Cip-Ti<sub>3</sub>C<sub>2</sub> TSG simultaneously achieving high-efficiency sterilization and a long-term inhibition effect. Reproduced from ref. 72 with permission from Elsevier, copyright 2022. (ii) SEM morphologies of *S. aureus* and *E. coli* incubated with different samples consisting of electrospun poly(lactic-co-glycolic acid) (PLGA) scaffolds, Ag<sub>2</sub>S-loaded membranes (P-AS), MX/AS nano-HJ-incorporated electrospun membranes (P-MX/AS), and LO<sub>x</sub>-decorated P-MX/AS membranes (P-MX/AS@LO<sub>x</sub>) fibers. Reproduced from ref. 73 with permission from Wiley, copyright 2022. (iii) SEM images of *E. coli* and *B. subtilis* exposed to 100 μg mL<sup>-1</sup> Ti<sub>3</sub>C<sub>2</sub>T<sub>x</sub>. Reproduced from ref. 74 with permission from the American Chemical Society, copyright 2016.

According to Li *et al.*, MXene-hybridized silane films have antibacterial characteristics that cause physical harm and mechanical degradation directly (Fig. 5). Additionally, MXenes (Ti<sub>3</sub>C<sub>2</sub>T<sub>x</sub>) demonstrated concentration-dependent bactericidal activity, showcasing more significant antibacterial effects against pathogenic bacteria than graphene oxides.<sup>75</sup> At 200 mg mL<sup>-1</sup> of MXenes after 4 hours of exposure, it was possible to identify a loss of more than 98% of bacterial cell viability for both types of cells. It was feasible to detect a loss of more than 98% of bacterial cell viability for both types of cells at 200 mg mL<sup>-1</sup> of MXenes with exposure for 4 hours. These MXene-based structures rupture the architecture of bacterial cell membranes, thereby enabling the leakage of intracellular cytoplasmic content leading to cell damage.

Photothermal therapy (PTT) is a promising cancer treatment method. Nanomaterials convert light into heat energy to kill cancer cells. Research aims to develop photothermal agents that can self-modulate photothermal conversion efficiency and slow cancer cell growth. PTT may work non-invasively to fight infections. This tactical method for photo/thermal conversion on PTT agents generates hyperthermia, which inactivates proteins and regulates the cell cycle *via* DNA crosslinking, destroying bacterial cell membranes. This allows antibacterial agents to enter and destroy biofilms. Nanozyme technology may cure illnesses without medications. MXenes possess POD-like activities that have been widely used for antibacterial applications.<sup>76,77</sup>

Li *et al.* created Pt single-atom (Pt/Ti<sub>3</sub>C<sub>2</sub>)-based nanocomposites using Ti<sub>3</sub>C<sub>2</sub>-based materials. The one-atom Pt demonstrated strong POD-like activity to catalyze H<sub>2</sub>O<sub>2</sub> and produce hydroxyl radicals, which might eradicate biofilms and kill bacteria. In addition, Pt/Ti<sub>3</sub>C<sub>2</sub> showed extremely high photothermal conversion efficiency at low concentrations.<sup>78</sup> Atomic morphology and topologies control the antibacterial properties of MXenes. The antimicrobial potency of MXene derivatives such as Nb<sub>2</sub>CT<sub>x</sub> and Nb<sub>4</sub>C<sub>3</sub>T<sub>x</sub> was examined against resistant bacteria (*S. aureus* and *E. coli*), wherein sufficiently high growth inhibition was observed in both cultures.

However, in another study by Zhou *et al.*, Ti<sub>3</sub>C<sub>2</sub>T<sub>x</sub>-based composites showed methicillin-resistant *S. aureus*-infected wound healing applications. The composites made up of MXene/polydopamine interact with bacterial cell membranes and disrupt cell membranes, resulting in leakage of cytoplasmic content through vascular dilation, angiogenesis, and tissue granulation.<sup>79</sup> The use of MXene-based membranes as anti-biofouling membranes in wastewater treatment should be investigated further due to their outstanding significance against resistant microorganisms. Silver nanoparticle (Ag)-anchored MXene (Ti<sub>3</sub>C<sub>2</sub>T<sub>x</sub>) composites exhibit excellent antimicrobial potency towards *E. coli* and are utilized for water purification applications.<sup>80</sup> Simultaneously, the IC<sub>50</sub> values of 11.7 mg mL<sup>-1</sup> of MXene and a trace amount (0.04 mm) of gold nanoclusters manifested superb antimicrobial potency due to good synergism between the antimicrobial effect and the tuned



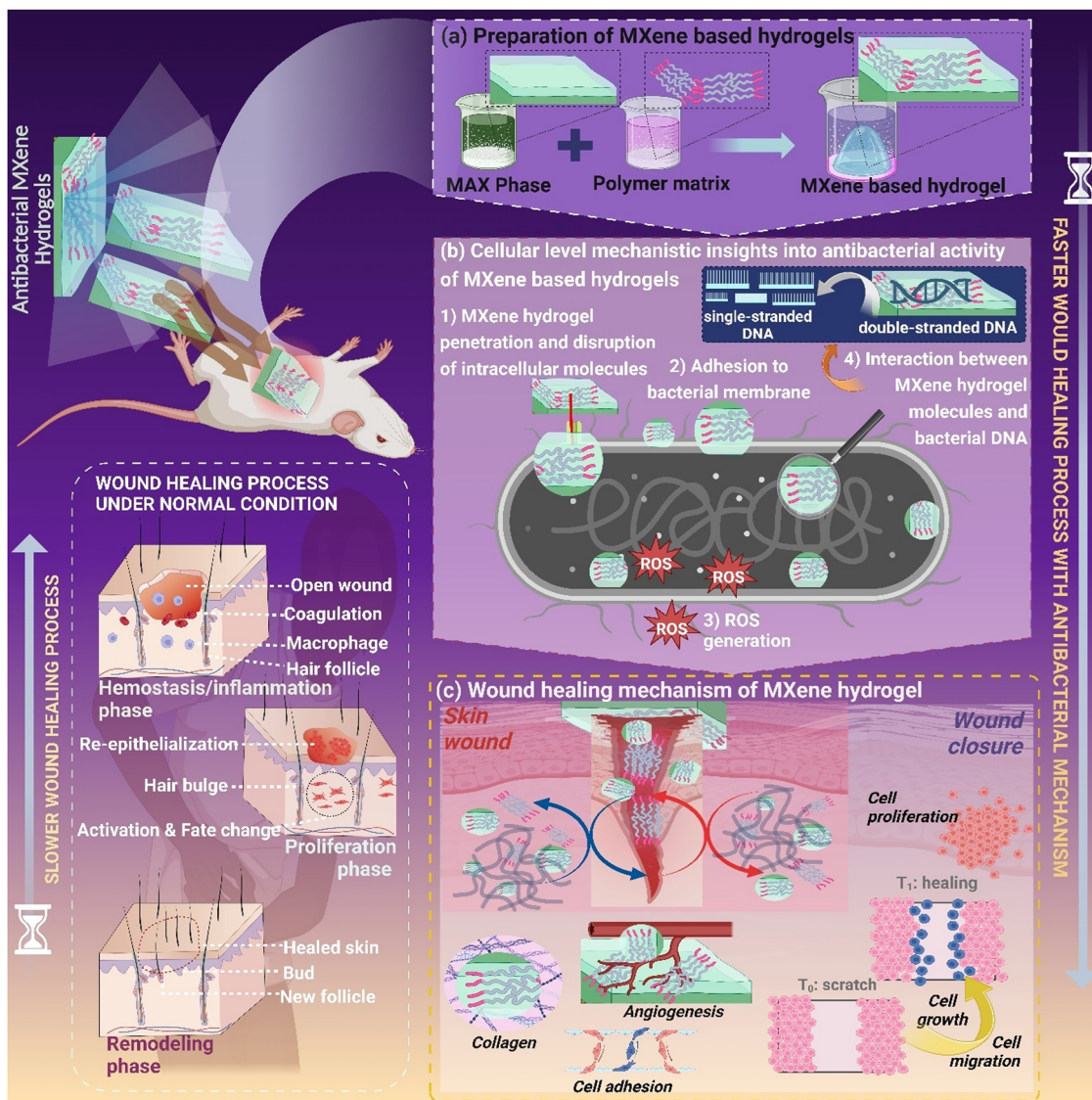


Fig. 5 Schematic of cellular level insights into MXene materials as potential antibacterial candidates for wound healing applications.

bactericide density for both Gram-positive and Gram-negative bacteria, which ultimately leads to the inhibition of biofilm formation.<sup>80</sup> In this case, antibiotic-resistant bacteria can be effectively combated with combinational therapy and multi-mechanism antimicrobial medicines that have synergistic effects.

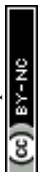
As the threat of antibiotic resistance continues to rise, the antimicrobial potential of MXenes stands as a beacon of hope in the fight against bacterial infections in the biomedical field. MXenes with their unique optical/thermal characteristics, high electrical conductivity, hydrophilicity, electro-mechanical properties and tuneable physicochemical properties can be thought of as appealing candidates for the designing of innovative micro- and nano-systems with significant bactericidal potency. Overall, the primary and potential mechanisms by which MXenes/derivatives deactivate or eradicate pathogenic bacteria are the rupture of cell membranes of bacteria *via* the sharp

edges of nanoflakes of MXenes, the inhibition of nutrient intake, the generation of reactive oxygen species (ROS), and photo-thermal-driven bacterial deactivation. Compiling toxicological, pharmacological/pharmacokinetics, and associated antibacterial mechanisms can aid in the development of avant-garde MXene-derived composites wherein they exhibit potential antibacterial properties in subsequent eras.

## 4. Insights into the biomedical application prospect of MXene-derived nanostructured materials

### 4.1 Drug delivery applications

MXene-based nanocomposites have emerged as a promising and innovative solution in the field of drug delivery, offering significant advancements in the way therapeutic agents are



administered and released within the human body. MXene-anchored nanostructured materials (NMs) have explored as drug carriers for targeted therapy because of their planar structures, abundant surface functional groups, and negatively charged surfaces. Their unique structural characteristics allow for efficient drug encapsulation and controlled release, addressing the critical challenges of conventional drug delivery systems. Functionalized  $\text{Ti}_3\text{C}_2$  nanosheets possess large surface areas for effective DOX drug loading efficacy, thus successfully inhibiting the tumor cell growth and proliferation in an acidic media.<sup>80,81</sup> A method of *in situ* growth was used to create sandwich-shaped  $\text{Ti}_3\text{C}_2@\text{Au}$  nanorods (GNRs)/polydopamine (PDA)/ $\text{Ti}_3\text{C}_2$  NCs, which demonstrated great drug loading efficiency and increased photothermal conversion competency. To further assess the drug-loading capacity and pH/NIR responsiveness of  $\text{Ti}_3\text{C}_2@\text{Au}$ , DOX was employed and the loading efficiency tuned to 95.88%. The drug loading efficacy is further influenced by electrostatic interactions between positively charged DOX and negatively charged NC molecules. A typical sandwich-like  $\text{Ti}_3\text{C}_2$  MXene-based nanoplateform  $\text{Ti}_3\text{C}_2@\text{GNRs}/\text{PDA}/\text{Ti}_3\text{C}_2$ , which improved photothermal effectivity, facile growth process, and pH/NIR sensitivity, was fabricated by Beibei *et al.*<sup>81</sup>

The hydroxyl functionalization of  $\text{Ti}_3\text{C}_2\text{T}_x$ , which was produced *via* tetra propylammonium hydroxide (TPAOH) intercalation, improved the photothermal sensitivity and ability energy harvesting from light in the NIR range. The outer layer of nanosheets was enriched with hyaluronic acid (HA), which improved the compatibility of the system by enabling precise targeting of cancer cells due to the overexpression of CD44 on their cell membranes.<sup>82</sup> A novel nano-drug-delivery system called  $\text{Ti}_3\text{C}_2\text{T}_x\text{-SP}$  also has an extraordinary drug-loading aptitude (up to  $\sim 212\%$ ), pH sensitivity, and NIR laser-engineered drug release. However, MXenes lack a constrained space for high drug loading, which could pose a problem for their use as drug delivery vehicles.

Hydrogels were conjugated with MXene-based NMs to effectively regulate the drug release efficacy. In this view, Yang *et al.* adopted a modified procedure for the fabrication of an MXene-based hydrogel structure that serves as a magnetic and photosensitive drug delivery vehicle as antidotal therapeutics for deep chronic wounds.<sup>83</sup> This system has a controllable drug delivery capacity, minimizes adverse drug reactions, mitigates bacterial infections, and promotes wound healing procedures. The practical application of the MXene-based hydrogel was tested on full-thickness cutaneous and subcutaneous wounds in rats. The hydrogel's drug delivery capacity is manageable, resulting in fewer detrimental drug side effects, reduced bacterial infections, and support for wound healing techniques. *In vivo* experiments were conducted on diabetic mice with open and epidermal skin lesions to assess the hydrogel technology. In the context of chronic wound healing, infection is a common hindrance. In the rat model, the MXene-based hydrogel system demonstrated a potential for accelerated wound closure without bacterial infection transmission.

Zhang *et al.* constructed a nanobiosensor employing  $\text{Ti}_3\text{C}_2$  MXenes to enhance the signals, acting as the transduction material and a nucleic acid probe. The specific region targeted was the 16s rDNA segment of *M. tuberculosis* H37Ra, used as a biomarker for identifying *M. tuberculosis*. Strong interactions between the phosphate groups of targeted assembly and Zr cross-linked  $\text{Ti}_3\text{C}_2$  MXenes led to a direct bond between the target segments and  $\text{Ti}_3\text{C}_2$  MXenes, and *M. tuberculosis* may be detected using this biosensor.<sup>84,85</sup>

*Mycobacterium tuberculosis*, the bacterium responsible for tuberculosis, is a highly dangerous pathogen. In their research, Zhang and their team developed a method to efficiently identify *M. tuberculosis* using  $\text{Ti}_3\text{C}_2$  MXenes, which amplified the signal for transduction.<sup>86</sup> They specifically focused on the 16s rDNA segment of *M. tuberculosis* H37Ra, a critical biomarker. Through strong interactions between phosphate groups in the target fragments and Zr-crosslinked  $\text{Ti}_3\text{C}_2$  MXenes, a direct connection was established (Table 2). This innovative biosensor enables the detection of *M. tuberculosis*.<sup>86</sup>

Both chemotherapy and photodynamic therapy (PDT), which are standard cancer treatment approaches, have the potential to affect healthy as well as cancerous cells. This problem can be substantially mitigated by developing responsive materials that can selectively target and sense tumor cells. In this context, Liu and colleagues engineered nanoplateforms using  $\text{Ti}_3\text{C}_2$  to combine chemotherapy, photothermal therapy (PTT) and photodynamic therapy (PDT). The resulting  $\text{Ti}_3\text{C}_2$ -based nanosheets exhibited impressive properties, including an extraordinary extinction coefficient of  $28.6 \text{ L g}^{-1} \text{ cm}^{-1}$ , an outstanding photothermal conversion efficiency of approximately 58%, and significant generation of singlet oxygen under exposure to an 808 nm laser.<sup>102,103</sup>

The recognition molecule Apt is very specific and has affinity. Mucin (MUC1) is a biomarker in MCF-7 tumor cells. Apt-M, MUC1 Apt, may target MCF-7 tumors.  $\text{Ti}_3\text{C}_2$  nanosheets, which exhibit reasonable photothermal efficiency, were prospective tumor nanoplateforms. The DOX/ $\text{Ti}_3\text{C}_2$ /Apt-M therapeutic nanoplateform released chemotherapeutic medicines in response to multimodal stimuli under acidic conditions and laser-induced local heating. DOX/ $\text{Ti}_3\text{C}_2$ /Apt-M + Laser MCF-7 xenograft mice showed a tumor surface temperature of  $58.3 \text{ }^\circ\text{C}$ , greater than other laser irradiation groups. DOX/ $\text{Ti}_3\text{C}_2$ /Apt-M nanoplateform rapidly accumulates in MCF-7 tumors with highly active spots for targeting and increased tumor suppression with combination therapy.<sup>104</sup>

## 4.2 Cancer therapeutics applications

The development of MXenes and various MXene-based composites with potential for diagnostic and therapeutic roles has been intensely investigated<sup>94,105,106</sup> (Table 2). However, little research has so far focused on the collective therapeutic and diagnostic usage of these functional materials<sup>107–109</sup> in comparison to other studied materials of 2D structure family, *e.g.* graphene and its derivatives. Specifically, for the *in situ* creation of superparamagnetic  $\text{Fe}_3\text{O}_4$  nanocrystals, MXenes with their distinctive topologies and surface chemistry were used in the



Table 2 Harnessing the biosafety of Mxene derivatives in Cancer therapeutics applications

Mxene derivatives	Significant strategy/approach	Applications/salient features	Ref.
Ti <sub>3</sub> C <sub>2</sub> /doxorubicin hydrochloride@Cellulose	Chemo photothermal therapy	Controlled and targeted drug delivery and significant instant destruction of tumor cells	58
Mo <sub>2</sub> C	Synergistic phototherapy of cancers using multi-modal imaging-guided strategy	Biocompatibility, minimal toxicity and hematotoxicity	87
Ti <sub>3</sub> C <sub>2</sub>	Cancer theranostics; photothermal elimination of cancerous cells and ablation of tumors; magnetic resonance imaging (MRI) of tumors	Significant T <sub>2</sub> relaxivity (~394.2 mM <sup>-1</sup> s <sup>-1</sup> ) with efficient contrast-enhanced MRI Excellent photothermal conversion efficiency (~48.6%) with high biocompatibility	88
Ti <sub>2</sub> C	Photothermal cancer therapy	NIR induced potential for cancer cell	89
Nb <sub>2</sub> C	Chemo/photothermal cancer therapy; diagnostic potential	Targeted chemotherapy with reduced toxicity Improved photothermal hyperthermia of cancer, low/noncytotoxicity (at 300 μg mL <sup>-1</sup> ) the photothermal conversion efficiency was ~28.6%	90
Nb <sub>2</sub> C	Chemo/photothermal cancer therapy; diagnostic potential	Enhanced photothermal hyperthermia, non-toxicity, tuned photothermal conversion efficiency	17
MnO <sub>x</sub> /Ti <sub>3</sub> C <sub>2</sub>	MR/PA guided photothermal cancer therapy, photoacoustic imaging	High biocompatibility, no toxicity, no remarkable histological abnormalities or lesions	91
MnO <sub>x</sub> /Ta <sub>4</sub> C <sub>3</sub>	MR/PA guided photothermal cancer therapy, photoacoustic imaging	High biocompatibility, no toxicity, no remarkable histological abnormalities or lesions	92
Mo <sub>2</sub> C	Photothermal cancer therapy	Photothermal ablation of tumors with high efficiency, rapid biodegradability	93
Ti <sub>3</sub> C <sub>2</sub> @Au	PA/CT guided photothermal cancer therapy	Enhanced stability, biocompatibility, low toxicity	94
V <sub>2</sub> C	MR/PA guided photothermal therapy	Good biocompatibility, low cytotoxicity, good efficiency for photothermal conversion	95
Ta <sub>4</sub> C <sub>3</sub>	Dual-mode photoacoustic/computed tomography (CT) imaging along with effective photothermal ablation of tumors ( <i>in vivo</i> )	Excellent photothermal conversion efficiency, Targeted photothermal ablation of tumors ( <i>in vitro</i> and <i>in vivo</i> )	96
Ti <sub>3</sub> C <sub>2</sub> -MXene-Au nanocomposites/gOX40	Photoacoustic (PA) and thermal dual-mode photothermal therapy (PTT) and enzyme dynamic therapy (EDT)	PTT/EDT/antitumor immune therapy, good biocompatibility and biosafety	97
Ti <sub>3</sub> C <sub>2</sub> T <sub>x</sub> -Pt-PEG/POD	Cell apoptosis and necrosis and NIR-II light irradiation with a low power density (0.75 W cm <sup>-2</sup> ).	Cell apoptosis and necrosis and NIR-II light irradiation with a low power density (0.75 W cm <sup>-2</sup> ).	98
Ti <sub>3</sub> C <sub>2</sub> T <sub>x</sub> MXene nanosheets coated with metal-polyphenol nanodots	Photothermal therapy (PTT)-induced inflammation and hyperthermia induced overexpression of heat shock proteins (HSPs), (-)-epigallocatechin gallate (EGCG) reduce the expression of HSPs act as an anti-inflammation	Satisfactory synergistic PTT/enzyme therapy, good photoacoustic imaging capability, hyperthermia-amplified nanozyme catalytic therapy	99
Polydopamine (PDA)/niobium carbide (Nb <sub>2</sub> C)	High specific surface area and a fascinating light-to-heat conversion rate, NIR-II photothermal therapy and immune therapy	Good photothermal conversion efficiency, <i>in vitro</i> and <i>in vivo</i> anti-cancer PTT effect and anti-inflammation capability	100
2D Ti <sub>3</sub> C <sub>2</sub> MXene/Cu <sub>2</sub> O nanosheet/multifunctional nanoplateform (3-BP@MCG NSs)	NIR-resolution photoacoustic imaging (PAI), near-infrared (NIR) region	Prevent tumor recurrence, potential RBC camouflaged nanoplateform for the combination of effective PTT and immune therapy	101
		Self-enhanced PTT/CDT synergistic therapy, highly efficient PAI-guided cooperation of hypoxia relief and <i>in situ</i> H <sub>2</sub> O <sub>2</sub> and NIR synergistic enhancement to improve therapeutic efficiency	



construction of superparamagnetic 2D MXene ( $\text{Ti}_3\text{C}_2$ )-based structures.<sup>109,110</sup> These biocompatible composites demonstrated excellent  $T_2$  relaxivity ( $394.2 \text{ mM}^{-1} \text{ s}^{-1}$ ) and effective contrast-enhanced MRI of tumors, opening up a new avenue for cancer theranostics.<sup>98</sup> Additionally, they established a high photothermal conversion efficiency of 48.6% for the *in vitro* and *in vivo* photothermal ablation of tumour tissues as well as the photothermal elimination of cancer cells. To enhance the durability of these biofriendly composites in biological conditions, soybean phospholipids were additionally modified.<sup>111</sup> These materials offer valuable tools for cancer theranostics, as they have applications in photothermal therapy (with an efficiency of approximately 32.5%) and excel in high-performance contrast-enhanced CT and  $T_2$ -weighted MRI for breast cancer diagnosis.

MXene-based architectures represent intriguing choices for cancer diagnosis and treatment, offering both biosafety and potential for clinical use. Their significant advantages include being hydrophilic and having low toxicity.<sup>112</sup> Furthermore, there is a need for more extensive exploration of these materials in the context of photoacoustic imaging and photothermal therapy, given their substantial efficiency in converting light into heat and their extensive and robust absorption of near-infrared (NIR) wavelengths.<sup>113,114</sup> Despite all these benefits, only a small portion of them have been explored for their potential medicinal applications, with the majority of research focusing on a small number of instances such as  $\text{Ti}_3\text{C}_2$ ,  $\text{Nb}_2\text{C}$ ,  $\text{Mo}_2\text{C}$ ,  $\text{V}_2\text{C}$ , and  $\text{Ta}_3\text{C}_4$ .<sup>108</sup> It is highly likely that innovative MXene-based configurations, when designed with diverse theranostic applications, excellent biocompatibility, and swift biodegradability, will see extensive adoption in the field of biomedicine and transition into clinical practice. Moreover, a novel approach to combat malignancies involves hyperthermia-mediated nanozyme catalytic therapy using MXene-anchored nanomaterials.<sup>115</sup>

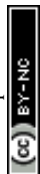
In this perspective, MXene 2D nanosheets can serve as platforms for anchoring valuable components such as nanodrugs and nanozymes. For instance, to create nanocomposites exhibiting peroxidase-like capabilities, synthetic platinum (Pt) nanozymes were attached to the surface of MXene ( $\text{Ti}_3\text{C}_2$ ) nanosheets. These composite materials could spontaneously catalyze hydrogen peroxide to generate hydroxyl radicals ( $\cdot\text{OH}$ ), which induced cellular apoptosis and necrosis. Furthermore, these composites exhibited favorable photothermal effects when exposed to low-power-density NIR-II light, opening up new avenues for synergistic photothermal/enzyme-based cancer treatment in combination with photoacoustic imaging for guiding therapeutic interventions.<sup>115</sup> Liu *et al.* introduced MXene ( $\text{Ti}_3\text{C}_2$ ) nanosheets (100 nm) for targeted treatment of tumors, employing a combination of photothermal, photodynamic, and chemotherapy. These nanomaterials demonstrated exceptional properties, including a high mass extinction coefficient of  $28.6 \text{ L g cm}^{-1}$  at a wavelength of 808 nm, a substantial photo-thermal conversion efficiency of  $\sim 58\%$ , and efficient production of singlet oxygen ( $^1\text{O}_2$ ) under 808 nm laser irradiation, all while maintaining good biocompatibility in both *in vitro* and *in vivo* settings.<sup>116</sup>

As theranostic agents,  $\text{Mo}_2\text{C}$  MXene nanospheres (50 nm) were created, and they harvested light across the whole NIR spectrum. Additionally, NIR radiation has the ability to simultaneously cause hyperthermia and the production of reactive oxygen species (ROS).<sup>87</sup> These extremely biocompatible nanospheres have the potential to be employed alongside photothermal and photodynamic cancer treatments for the eradication of cancer cells and the elimination of solid tumors, using the well-established liquefactive necrosis method. In a different investigation, Zhang and colleagues introduced a photo/sono-responsive theranostic nanoplatfrom designed for cancer treatment. This system combines photoacoustic and photothermal dual-mode imaging to guide NIR-II photothermal-enhanced sonodynamic therapy on MXene ( $\text{Ti}_3\text{C}_2$ ) surfaces. These nanocomposites exhibited enhanced tumor elimination in *in vivo* experiments, with no tumor reappearance and minimal systemic toxicity, accompanied by a significant localized hyperthermic effect.<sup>117</sup> Furthermore, MXene-based quantum dots showcase distinct optical properties, including light absorption, electrochemiluminescence, photoluminescence, optoelectronic catalysis, and optoelectronic functionality. Among these,  $\text{Ti}_2\text{N}$  quantum dots (5 nm) exhibited high photo-thermal conversion performance when exposed to laser irradiation in the NIR-I region at 808 nm (48.62%) and NIR-II region at 1064 nm (45.51%).<sup>118,119</sup> Recently by utilizing NIR-based photo/thermal therapy (PTT), small-size  $\text{Ti}_3\text{C}_2\text{T}_x$  MXene nanosheets were adopted for this study of cancer chemotherapeutics and anti-inflammation due to their high photothermal conversion efficiency in the area of NIR, high loading capacity, and noble free-radical scavenging aptitudes. Additionally, (–)-epigallocatechin gallate (EGCG) was added to the nanosheets to fabricate EGCG/Fe metal-polyphenol nanodots providing good tumor ablation capability with minimal inflammation.<sup>99</sup>

Despite having potential as biological fluorescent probes, red emissive gold nanoclusters anchored with 3D MXene materials showed efficient photothermal conversion (PTC) efficiency of  $\sim 43\%$  and a bright fluorescence, which enabled them to excite bio-imaging at a small concentration of  $12 \text{ g mL}^{-1}$ . The material also displayed outstanding applicability as a *in vitro* bioimaging and PTT agent. By examining apoptosis, ROS production and cell proliferation, *in vitro* examinations of the PTT-induced cell death pathways were carried out. Toxicity assessment, hematological investigation, and biochemical assay findings unveiled MXene gold nanoconjugates in various biomedical applications, with no adverse effects after intravenous or oral delivery.<sup>120</sup> Future approaches to cancer treatment should extend their exploration of MXenes beyond  $\text{Ti}_3\text{C}_2$ , taking into account the most suitable conditions and methods for functionalization. While MXenes have shown promise in photothermal cancer nanotherapy, enhancing cellular uptake necessitates surface modifications with ligands specific to cancer cells (Fig. 6 and 7). Additionally, it is worthwhile to investigate MXene-based architectures that exhibit biological responsiveness.

### 4.3 Biosensor and smart wearable monitoring device

Living organisms employ their biological sensors to detect specific substances with precision and sensitivity. Typically,



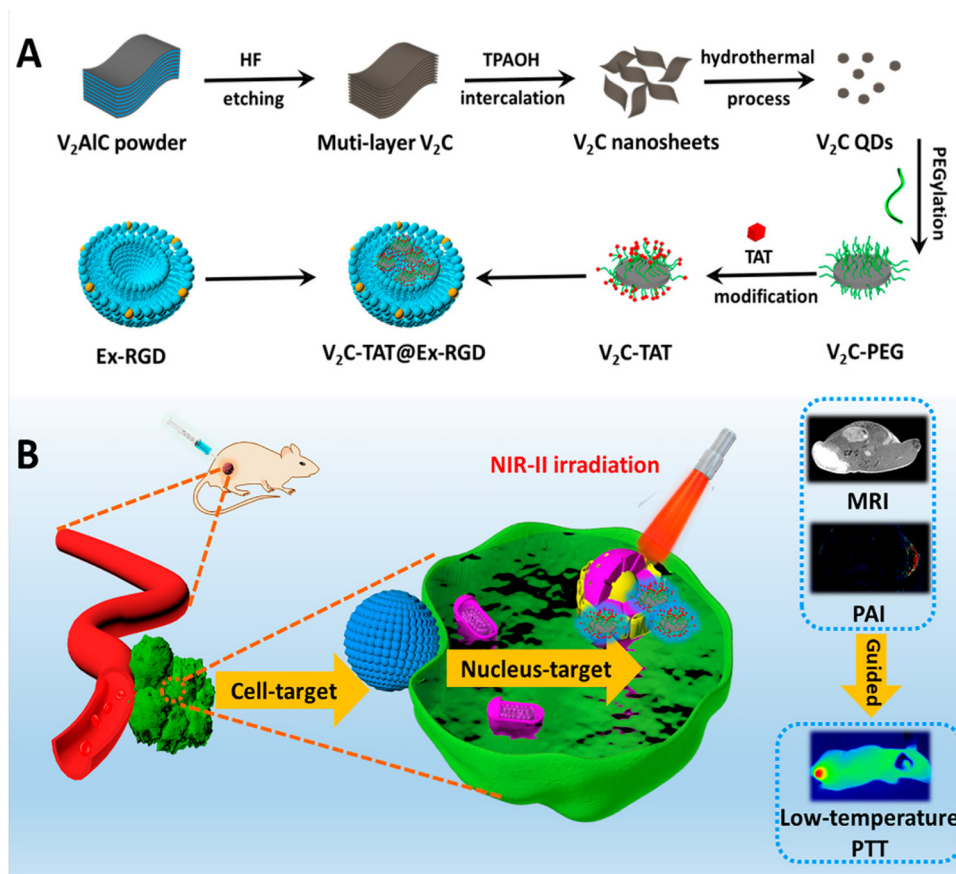


Fig. 6 (A) Preparation scheme of V<sub>2</sub>C-TAT@Ex-RGD. (B) Visual representation of a nanoagent, V<sub>2</sub>C-TAT@Ex-RGD, designed to target both the cancer cell membrane and the cell nucleus, enabling multimodal imaging-guided photothermal therapy (PTT) in the NIR-II biowindow at a low temperature. Reproduced from ref. 121 with permission from the American Chemical Society, copyright 2019.

these sensors comprise three essential elements: a sensor component for identifying the target analyte, a transducer for converting biochemical signals into electrical or optical signals, and a unit for interpreting the collected data. MXene-based nanomaterials are well-suited for biosensors due to their remarkable qualities, including outstanding hydrophilicity, extensive surface area, high conductivity, exceptional electrical and optical properties, as well as superior biocompatibility and safety, making them an ideal choice for this purpose.

Reactive oxygen, specifically hydrogen peroxide (H<sub>2</sub>O<sub>2</sub>), is a natural byproduct of various oxidase enzymes within the human body and exhibits a crucial role in the activities of phagocytic cells. However, in pathological conditions, excessive generation of reactive oxygen species can harm cell membranes and potentially damage proteins and cells. Therefore, early detection of H<sub>2</sub>O<sub>2</sub> is essential in diagnosing such diseases. Nagarajan and colleagues developed an efficient method for H<sub>2</sub>O<sub>2</sub> detection by creating a Ti<sub>3</sub>C<sub>2</sub>T<sub>x</sub>-Fe<sub>2</sub>O<sub>3</sub> composite through ultrasonication. This composite displayed a linear recognition range spanning from 10 to 1000 nM, a substantial surface area of 0.18 cm<sup>2</sup>, and demonstrated remarkable selectivity and sensitivity at 0.32 A nM<sup>-1</sup> cm<sup>-2</sup>. The composite's detection threshold was determined to be 7.46.<sup>122</sup>

In a separate study, a different researcher<sup>123</sup> developed MXene/La<sup>3+</sup>-doped ZnO/hemoglobin (Hb) nanocomposites for hydrothermal voltammetric detection of H<sub>2</sub>O<sub>2</sub>. The authors observed a poor detection limit of 0.08 M and a high correlation value of 0.9995. They established a linear profile for the range of 0.2–400.0 M at pH 7.0, with a remarkable recovery rate of nearly 100%. Furthermore, an electrocatalytic diagnostic for H<sub>2</sub>O<sub>2</sub> in a neutral medium was created using Flavin adenine dinucleotide/Ti<sub>3</sub>C<sub>2</sub>T<sub>x</sub>. This system exhibited a linear detection range from 5 nM to 2 M, a surface area of 0.13 cm<sup>2</sup>, and an impressive limit of detection at 0.7 nM. It maintained a high selectivity of 98% and displayed significant sensitivity at 0.125 A nM cm<sup>2</sup> compared to nonenzymatic sensors.<sup>124</sup> Another sensor based on Ti<sub>3</sub>C<sub>2</sub>T<sub>x</sub>/chitosan/Prussian blue was developed with excellent selectivity, a low detection limit of 4 nM, a wide linear range spanning from 50 nM to 667 M, and an outstanding recovery rate of 100.3% for monitoring H<sub>2</sub>O<sub>2</sub> in biological samples.<sup>125</sup>

Modifying the surface of MXenes can be advantageous for various sensor applications. MXene-based gas sensors utilize transitions in the conduction of MXenes during interactions with gas particles. Through density functional theory (DFT) calculations, it was determined that a single layer of Ti<sub>2</sub>CT<sub>x</sub> with oxygen-terminated ends exhibited significantly higher



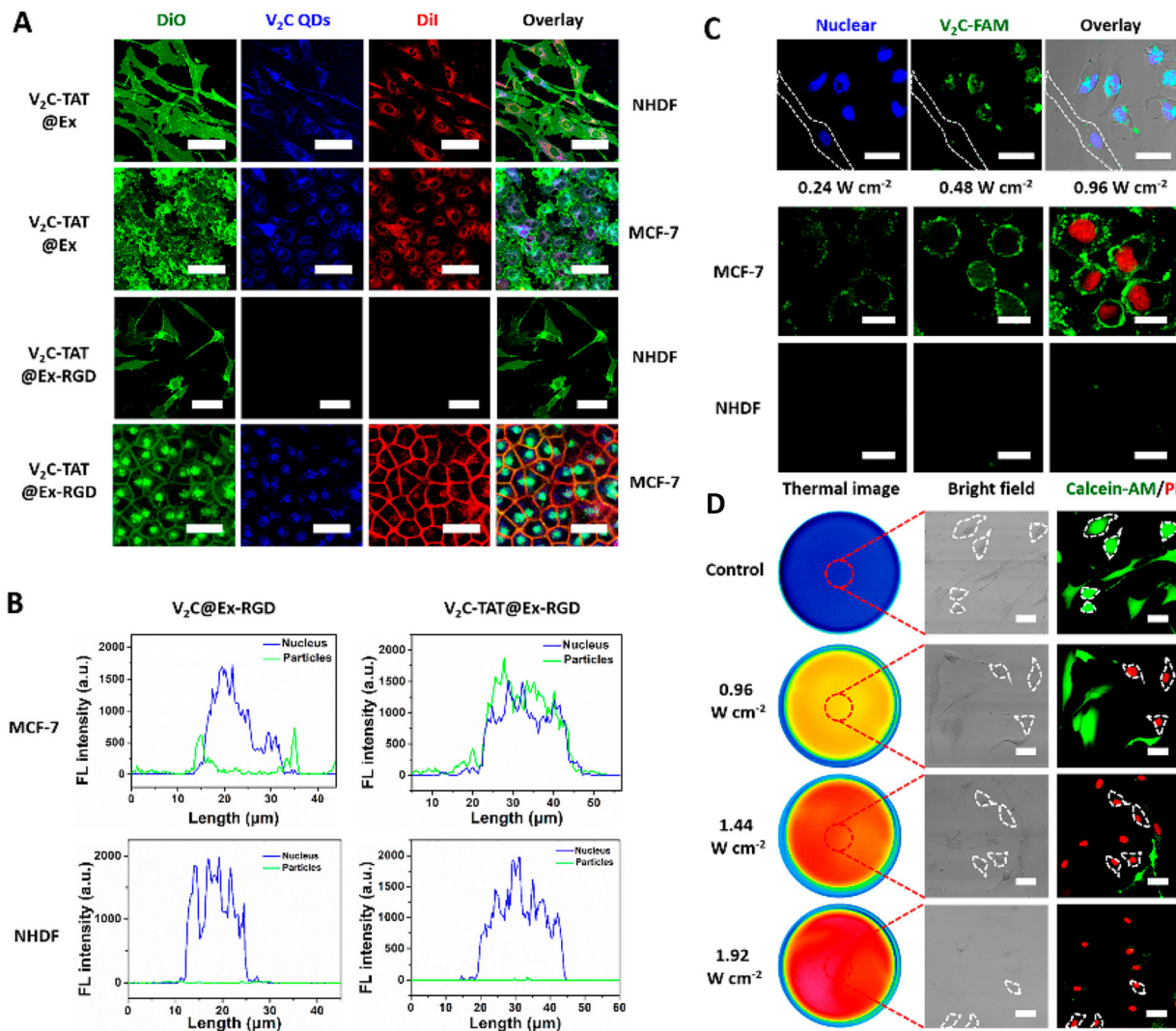


Fig. 7 (A) Confocal microscopic micrographs of co-cultured MCF-7 and NHDF cells indicating thermal images. (B) Line-scanning profiles of fluorescence intensity for MCF-7 cells and NHDF cells. (C) and (D) Confocal fluorescence micrographs of MCF-7 and NHDF cells, double-stained with Calcein-AM and PI imparting cellular uptake for phototherapeutic application. Reproduced from ref. 121 with permission from the American Chemical Society, copyright 2019.

specificity for ammonia ( $\text{NH}_3$ ) compared to other gas molecules. The findings indicated that  $\text{NH}_3$  molecules would strongly adhere to the oxygen-terminated ends of MXenes from the  $\text{M}_2\text{CT}_x$  family to facilitate charge transfer.

SPR biosensors have recently become indispensable research tools in the life sciences and pharmaceutical industries, offering a range of benefits such as real-time detection, enabling the dynamic tracking of entire biomolecular interaction processes. These biosensors utilize free-label samples, preserving molecular activity, and require very few samples, typically only 1 mg of protein on a surface. They boost a convenient and swift detection process, coupled with high sensitivity, a wide application range, and high throughput capabilities.

In a recent development, Wu *et al.* have proposed a  $\text{Ti}_3\text{C}_2$ -MXene-based sensing platform along with a multi-walled carbon nanotube (MWCNTs)-polydopamine (PDA)-Ag

nanoparticle (AgNPs) signal enhancer as an ultrasensitive SPR biosensor for detecting carcinoembryonic antigen (CEA). The strategy involved the use of Staphylococcal protein A (SPA) for aligning and fixing the monoclonal anti-CEA antibody (Ab1) through its Fc region. To achieve a dynamic range of  $2 \times 10^{-16}$  to  $2 \times 10^{-8}$  M for CEA determination, with a limit of detection of 0.07 fM, the combination of MWCNTs-PDA-AgNPs-polyclonal anti-CEA antibody (MWPAG-Ab2) was utilized in a sandwich format. This biosensing approach demonstrated reproducibility, specificity for CEA in actual serum samples, and holds promise for measuring CEA in human serum for early cancer detection and cancer surveillance.<sup>126</sup>

In addition to the previously mentioned methods, chemiluminescence and NIR PT immunoassay can also serve as techniques for detecting target analytes. For instance, Li and colleagues used a straightforward hydrothermal process to craft innovative 2D MXene- $\text{Ti}_3\text{C}_2/\text{CuS}$  nanocomposites endowed



with peroxidase-like capabilities. These nanocomposites exhibited a synergistic enhancement in peroxidase-like activity, catalyzing the reaction of 3,3,5,5-tetramethylbenzidine (TMB) in the presence of  $\text{H}_2\text{O}_2$ , resulting in a noticeable color change. This effect was not observed with individual MXene- $\text{Ti}_3\text{C}_2$  nanosheets or CuS nanoparticles alone.

Subsequently, a simple colorimetric technique was employed to detect  $\text{H}_2\text{O}_2$  and cholesterol in blood samples. The detection limit and linear range for  $\text{H}_2\text{O}_2$  were found to be 3.1 M and 0.1 nM, respectively, while cholesterol exhibited a detection limit and linear range of 1.9 M and 10–100 M, respectively.<sup>127</sup>

Apart from the methods mentioned earlier, chemiluminescence and near-infrared (NIR) photothermal immunoassay can be employed for detecting target analytes. As an example, Li and colleagues used a straightforward hydrothermal process to fabricate innovative 2D MXene- $\text{Ti}_3\text{C}_2$ /CuS nanocomposites endowed with peroxidase-like capabilities. These MXene- $\text{Ti}_3\text{C}_2$ /CuS nanocomposites demonstrated a synergistic enhancement in peroxidase-like activity, catalyzing the reaction of 3,3,5,5-tetramethylbenzidine (TMB) in the presence of  $\text{H}_2\text{O}_2$ , leading to a noticeable color change, which was not observed with individual MXene- $\text{Ti}_3\text{C}_2$  nanosheets or CuS nanoparticles. Subsequently, a simple colorimetric technique was employed to detect  $\text{H}_2\text{O}_2$  and cholesterol in blood samples.  $\text{H}_2\text{O}_2$  exhibited a detection limit and linear range of 3.1 M and 0.1 nM, respectively, while cholesterol had a detection limit and linear range of 1.9 M and 10–100 M, respectively.<sup>128</sup>

To monitor biological signals such as radial muscle contractions and wrist pulse, Guo and his team designed a wearable momentary pressure sensor using MXene nanosheets. They submerged tissue papers integrated with interdigitated electrodes in a solution containing MXene nanosheets at different concentrations, resulting in the creation of MXene/tissue paper for the pressure sensor. This highly sensitive wearable pressure sensor offered a broad detection range of up to 30 kPa and boosted a low detection limit of 10.2 Pa. Furthermore, it exhibited a speedy reaction time of just 11 ms while consuming a mere  $10^{-8}$  W of power. Impressively, even after undergoing more than 10 000 cycles, the sensors demonstrated exceptional repeatability. It is worth to note that the choice of materials for this sensor renders it susceptible to degradation.<sup>129</sup>

A recent development involves the creation of an ultra-stretchable, high-conductivity organohydrogel (M-OH) utilizing  $\text{Ti}_3\text{C}_2\text{T}_x$  MXene, lithium salt (LS), poly(acrylamide) (PAM), and poly(vinyl alcohol) (PVA) hydrogel. This innovative material has been designed for applications in human health monitoring and machine learning-assisted object recognition. The integration of machine learning (ML) further enhances its capabilities.

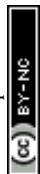
This study establishes that the ultra-stretchable, high-conductive M-OH exhibits exceptional performance in health monitoring and object identification. These findings open up a broad spectrum of potential applications in areas such as human-machine interfaces, personal healthcare, and artificial intelligence.<sup>130</sup> Due to the extraordinary thinness,<sup>131</sup> transparency,<sup>131</sup> and mechanical strength,<sup>132</sup> MXene-based

smart devices have recently gained considerable interest for possible applications in fitness, healthcare, human motion monitoring and EMG signal analysis.<sup>133</sup> MXenes can be printed, spun, plated, dip coated, or sprayed onto cellulose, which can then be incorporated into clothing for wearable applications.<sup>134</sup> This research introduces electromechanical sensors utilizing SnS/ $\text{Ti}_3\text{C}_2\text{T}_x$  nanohybrids, demonstrating their novel applications in sign-to-text translation and sitting posture monitoring. The piezoresistive sensor, in its original fabrication state, exhibits a high gauge factor and sensitivity value, measuring 7.41 and 7.49  $\text{kPa}^{-1}$ , respectively. Moreover, the nanohybrid-based sensor displays exceptional robustness and stability, with negligible performance changes observed across 3500 and 2500 cycles for strain and pressure characterizations, respectively.

Energy band diagrams are employed to elucidate the intrinsic piezoresistive mechanism in layered nanomaterials and the formation of Ohmic contact at the SnS/ $\text{Ti}_3\text{C}_2\text{T}_x$  heterojunction. Experimental determination of work function and  $E_{\text{HOMO}}$  values for both SnS and  $\text{Ti}_3\text{C}_2\text{T}_x$  is conducted using ultraviolet photoelectron spectroscopy (Fig. 8). The incorporation of piezoresistive sensors based on SnS/ $\text{Ti}_3\text{C}_2\text{T}_x$  nanohybrids for applications such as sign-to-text translation and e-cushion usage expands the realm of flexible and wearable electronics research.<sup>135</sup>

The utilization of clothing made from MXene-coated yarns in the context of fitness and health monitoring has been widely investigated. In one notable development, Yongjiu and colleagues<sup>138</sup> introduced an intriguing MXene-based smart device for analyzing sweat. This innovative system enabled the revealing of characteristic elements glucose and lactate materials in sweat through the use of an MXene/Prussian blue composite electrode-based sensor featuring a novel modular design that involves three phase interfaces of gas–solid–liquid. The sensor, tested with artificial sweat, achieved a sensitivity of 11.4  $\text{A mM}^{-1} \text{cm}^{-2}$  for lactate and 35.3  $\text{A mM}^{-1} \text{cm}^{-2}$  for glucose. Another significant advancement came from Han and collaborators,<sup>139</sup> who designed a smart mask integrated with a wireless real-time data communication and processing for the monitoring of respiration activity. This smart mask exhibited exceptional performance even in situations involving deformation and high humidity (with a 265% response at a relative humidity of 90%) and accurately recognized various respiratory patterns. The research on smart devices utilizing MXenes is progressing in tandem with MXene technology. Nevertheless, it is worth noting that MXene-based smart devices are still under development and have a more limited range of applications and devices compared to other 2D materials such as graphenes (Fig. 9).

Cutting-edge biosensors, capable of functioning through physical, chemical, and biological means, are transforming various industries that demand real-time evaluations, streamlined decision-making processes, and intelligent functionality. This transformation is made possible by their integration with technologies such as AI and IoT. Additionally, the global landscape is evolving towards increased intelligence and





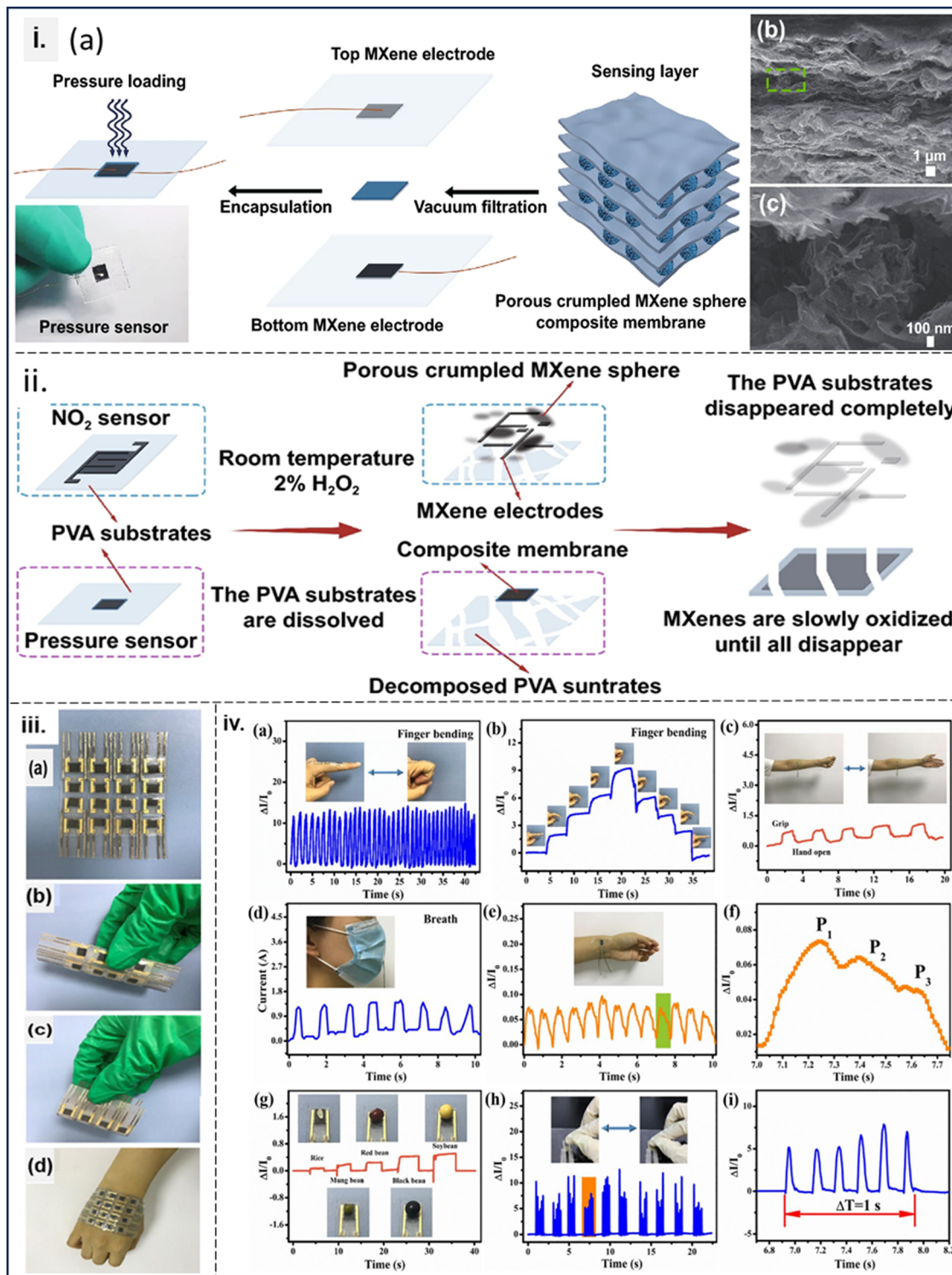


**Fig. 8** (i) (a) Schematic of the pressure sensor fabrication based on MS-2-10 and a photograph of the fabricated pressure sensor. (b) Cross-section SEM image of the composite membrane and (c) the close-up image of porous crumpled MXene sphere in the green box. (ii) Schematic of the degradation process of the transient  $\text{NO}_2$  and pressure sensors based on MS-2-10. Reproduced from ref. 136 with permission from Springer, copyright 2022. (iii) (a) Photograph of the assembled e-skin assembled from the MCF based pressure sensor with  $4 \times 4$  pixels. Photographs of the E-skin (b) and (c) under different bending states and (d) attached onto the hand. (iv) Real-time sensing signal of the MCF-based pressure sensor towards (a) repetitive finger bending and (b) different bending angles. Real-time sensing signal recording of the pressure sensor for different human physiological monitoring, including (c) arm muscle contraction, (d) breath and (e) and (f) wrist pulse. (g) Real-time sensing signal recording of the pressure sensor upon several small items with different weights (from left to right: rice, mung bean, red bean, black bean and soybean). (h) and (i) Real-time sensing signal of the pressure sensor for imitated knocking of early stage Parkinson's disease. Reproduced from ref. 137 with permission from Elsevier, copyright 2021.



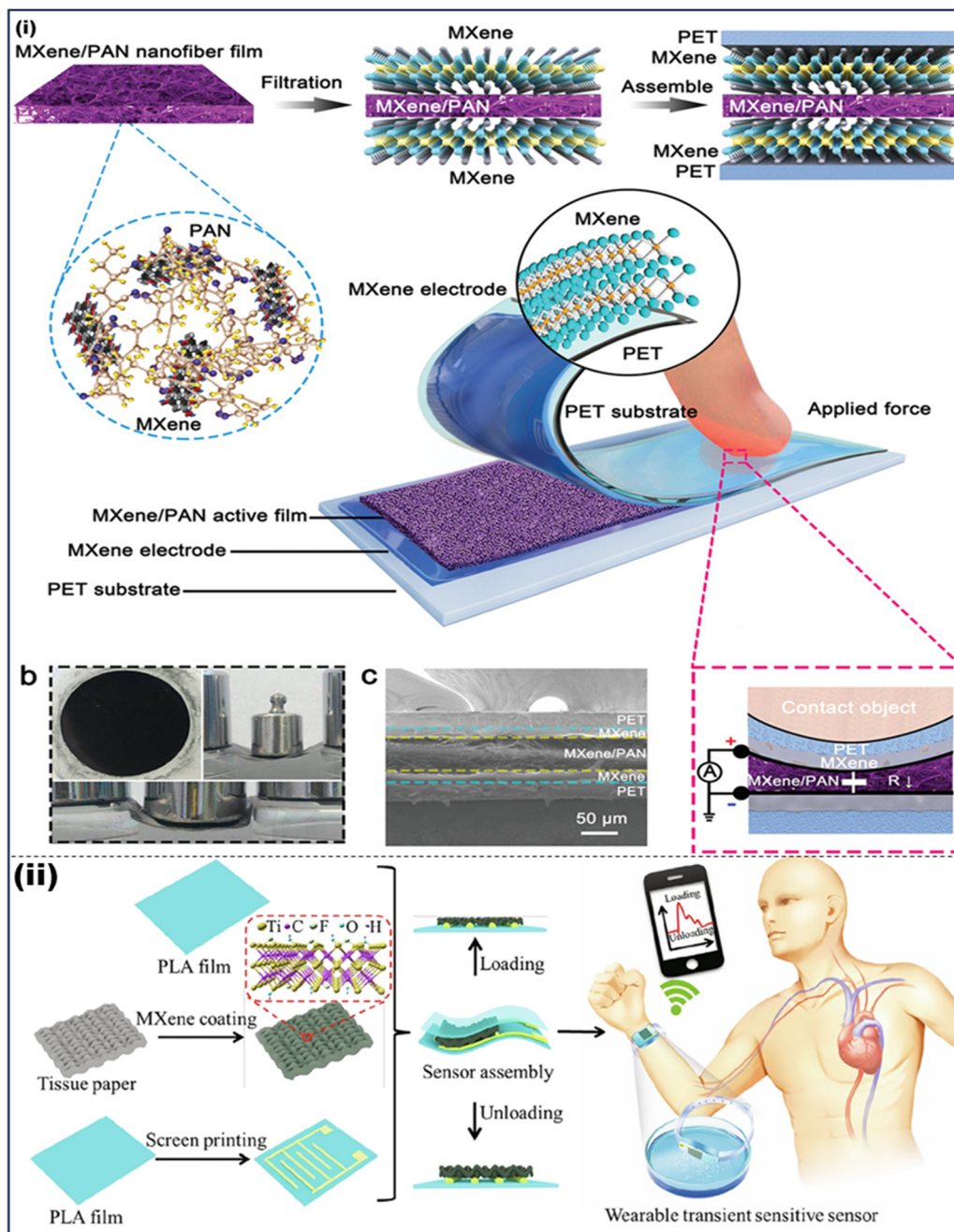


**Fig. 9** (i) Schematic of the hydrophilic, conductive, and redox-active sandwich-like PSGO-PEDOT nanosheets and their incorporation into hydrogels. (a) Fabrication process of the MXene/PAN-based flexible pressure sensor with the MXene electrode and working mechanism (inset). (b) Optical image of the MXene/PAN thin film with MXene electrodes and their mechanical flexibility and strength. (c) SEM image of the flexible pressure sensor with the sandwich structure. Reproduced from ref. 140 with permission from Wiley, copyright 2021. (ii) Schematic for the procedure to fabricate MXene nanosheet-based flexible wearable transient pressure sensors. Reproduced from ref. 141 with permission from the American Chemical Society, copyright 2019.

sophistication, driven by smart communities, precision agriculture, innovative technologies, and advanced medical services.<sup>142</sup> A recent development exemplifying this approach is the creation of a pristine MXene-based  $\text{Ti}_3\text{C}_2\text{T}_x$  liquid ink tailored for large-scale printing applications. This innovation holds potential applications in the manufacturing of 3D and 4D printed sensing devices, aligning with the demand for environmentally beneficial outcomes. Geravand and colleagues<sup>143</sup>

introduced an innovative biodegradable nano-filtration membrane by employing a hybrid nanocomposite made from polycaprolactone (PLC) and hydrophilic  $\text{Ti}_3\text{C}_2(\text{OH})_2$  MXene sheets. This membrane was designed for the treatment of dyed aqueous solutions. Similarly, Zhang and collaborators<sup>144</sup> unveiled a remarkable biodegradable multipurpose pressure sensor. This sensor was created using cross-attached collagen fibers (CCFs) combined with MXene aerogel, demonstrating an



impressive sensitivity response of  $61.99 \text{ kPa}^{-1}$  within a brief period of 0.30 seconds. Additionally, it exhibited rapid recovery within a few milliseconds (0.15 s), high thermal stability, and a small LDL (0.4 kPa).

#### 4.4. Tissue engineering and regenerative medicine

In the context of materialistic approach towards tissue repairing cascade, the possible immunomodulatory effects of  $\text{Ti}_3\text{C}_2$  MXene QDs have been investigated after injury.<sup>145</sup> These QDs consequently possessed innate immunomodulatory properties, especially reducing the activation of human CD4 + IFN- + T-lymphocytes while promoting the expansion of immunosuppressive CD4 + CD25 + FoxP3+ regulatory T-cells in an activated lymphocyte population. Additionally, they were highly biocompatible with mesenchymal stem cells and fibroblasts produced from stimulated pluripotent stem cells. Notably, a  $\text{Ti}_3\text{C}_2$  QD-anchored chitosan three-dimensional hydrogel architecture was developed with superior physicochemical properties for the delivery of stem cells and applicable as a wound healer. The developed hydrogel composites showed remarkable conductivity while retaining its injectability and thermosensitivity. These avant-garde intelligent biomaterials can not only trigger the inflammatory and degenerative diseases also fulfill the material translational gap, and restore tissue engineering using stem cell-based therapeutic approaches.<sup>145</sup> In a different study, immuno-engineered  $\text{Ta}_4\text{C}_3\text{T}_x$  MXene QDs were created for the *in vivo* treatment of transplant vasculopathy. These clever QDs with intriguing anti-inflammatory and anti-apoptotic properties can be taken into account for biomedical engineering. Surprisingly,  $\text{Ta}_4\text{C}_3\text{T}_x$  QDs were rapidly taken up by antigen-presenting endothelium cells, and they were able to change the expression of surface receptors to reduce their ability to activate allogeneic T-lymphocytes, which alleviated the cellular/structural changes associated with early allograft vasculopathy.<sup>146</sup> Additionally, the emerging application of MXenes in the realm of tissue engineering offers bone tissue engineering,<sup>147</sup> skin tissue engineering,<sup>148,149</sup> nerve tissue engineering and myocardial tissue engineering.<sup>145</sup>

In order to fabricate robust and bio-adaptable  $\text{Ti}_3\text{C}_2\text{T}_z$ -modulated poly lactic acid (PLA) nanocomposite membranes, Chen *et al.* developed a reliable methodology using *n*-octyltriethoxysilane (OTES) as the interfacial mediator. The presence of a robust bond between OTES- $\text{Ti}_3\text{C}_2\text{T}_z$  and PLA led to an improvement in the ultimate tensile strength (UTS) of the nanocomposite membranes comprising OTES- $\text{Ti}_3\text{C}_2\text{T}_z$  and PLA. Subsequently, the addition of these  $\text{Ti}_3\text{C}_2\text{T}_z$  nanosheets offered exceptional biocompatibility, leading to improved cell adhesion, osteogenic divergence and cell proliferation, all of which were highly dominant for bone resorption. Then, in order to assess  $\text{Ti}_3\text{C}_2\text{T}_x$  MXene's biocompatibility, potential to induce osteoporosis, and capacity for directed bone repair in both *in vitro* and *in vivo*.<sup>150</sup>

A multilayer  $\text{Ti}_3\text{C}_2\text{T}_x$  MXene memory was made by Zhang *et al.* The investigations' findings demonstrated the modified MXene membrane's endeavor to have a high grade of cell compatibility and ability to promote diversified osteogenesis

*in vitro* systems. When placed in the subcutaneous region and cranial defect of mice, the MXene membrane exhibited outstanding *in vivo* compatibility with the body, encouraged bone formation, and displayed remarkable bone regeneration properties.<sup>151</sup>

In relation to the engineering of nerve tissue, Nicolette group suggested a technique for creating flexible microelectrodes based on  $\text{Ti}_3\text{C}_2$ . A flexible assembly of  $\text{Ti}_3\text{C}_2$  MXene micro-electrodes have a significantly low resistance and can accurately and sensitively record neural activity because of the high electrical conductivity and specific surface area of the  $\text{Ti}_3\text{C}_2$  MXene films. In contrast to gold electrodes,  $\text{Ti}_3\text{C}_2$  electrodes exhibited an improved signal-to-noise ratio, reduced baseline noise, and a diminished susceptibility to interference at a frequency of 60 Hz. Neurons cultivated on  $\text{Ti}_3\text{C}_2$  have the same viability as control cultured neurons, according to the findings of neuronal biocompatibility tests. Additionally, they can adhere, develop axons, and create useful networks. In order to create high-resolution biological interfaces,  $\text{Ti}_3\text{C}_2$  MXene microelectrodes can be a possibility for strong platform technology.<sup>152</sup> Ye *et al.* miniaturized a biologically responsive engineered cardiac patch (ECP) by integrating hydrophilic and biocompatible conductive MXene/ $\text{Ti}_2\text{C}$  with hydrophilicity into a poly(ethylene glycol) diacrylate (PEGDA)-Gel-methacrylic anhydride (MA) cryogel. This integrated cardiac patch is highly effective in healing myocardial infarction (MI) like real heart. Chemical cryogelation technique has been adopted to fabricate a  $\text{Ti}_2\text{C}$  cryogel, wherein fast calcium expatriate and atune tissue-like beats were also visible in the artificial  $\text{Ti}_2\text{C}$ -8-cryogel ECP. Further transplantation into the embolism heart of the MI rat model can improve cardiac functionality, reduce infarct size, and prevent inflammation. The apparent vasoconstriction, particularly in the newly developed tiny arteries, was also discovered.<sup>153</sup>

MXene composites exhibit viscoelastic properties, combining elastic and viscous behaviors, which are crucial for mimicking the mechanical environment of biological tissues. These properties arise from the unique structure of MXenes, where their nanoscale layers provide stiffness and flexibility, and their integration with polymers or hydrogels enhances mechanical tunability.<sup>154</sup> The viscoelastic nature of MXene composites allows them to absorb and dissipate energy, adapt to dynamic biological environments, and support cell attachment, proliferation, and differentiation.

In tissue engineering, these characteristics are significant for creating biomimetic scaffolds that replicate the native extracellular matrix (ECM). In biomedical applications, besides conventional mechanical factors such as stiffness and strength, it is essential to ensure that the viscoelastic consistency of implant materials matches the native tissues due to the natural mechanical behavior of biological soft tissues.<sup>155-157</sup> A hybrid theory-experimental approach can effectively characterize multiscale viscoelastic changes in tissues, highlighting the mechanical differences in diseased and treated liver tissues and cells. Given this, understanding the viscoelastic properties of MXene-based composites is critical, especially in tissue



engineering applications. For instance, the tunable stiffness of MXene-based composites can match the mechanical properties of specific tissues, such as cartilage or muscle, facilitating proper cellular responses. Additionally, their ability to withstand cyclic loading makes them suitable for dynamic environments like vascular or musculoskeletal systems. The electrical conductivity of MXenes further enhances their utility by promoting cell signaling in electrically active tissues, such as nerve or cardiac tissue. By integrating viscoelasticity with biocompatibility and conductivity, MXene composites provide a robust platform for advancing tissue engineering and regenerative medicine.

## 5. Mxene-based therapeutic technologies and approaches

A range of biomedical applications, MXenes, a type of 2D transition metal carbides and nitrides, have shown promise as therapeutic agents. They have paved the path for groundbreaking techniques in drug administration, tissue engineering, and cancer therapy thanks to their exceptional synergism between electrical conductivity, mechanical strength, and biocompatibility.<sup>158</sup> Targeted drug delivery is made possible by MXene-based nanoparticles functionalized with certain ligands. This improves medication accumulation at disease locations while decreasing off-target effects. Apart from the conductive and supportive environment for cell proliferation and differentiation, MXene scaffolds offers extraordinary promise for tissue regeneration. Utilizing their capacity to convert light into heat and their capacity to produce reactive oxygen species upon light irradiation, MXenes have demonstrated success in photothermal and photodynamic therapies for the treatment of cancer. MXenes show great promise for transforming different biomedical fields as research in this developing topic moves forward since they provide flexible platforms for precise and efficient therapeutic treatments.

Advanced photothermal treatment (PTT) holds great promise in cancer therapeutics due to its exceptional ability to selectively target and eliminate cancer cells while minimizing damage to surrounding healthy tissue. PTT is a minimally invasive approach that utilizes photothermal agents—light-absorbing substances—to convert light energy into heat, inducing localized hyperthermia and resulting in the destruction of cancer cells. Tumor cells are particularly sensitive to elevated temperatures, and when a photothermal agent transforms near-infrared light into heat energy at the tumor site, it leads to increased temperatures, causing various risks such as protein denaturation, cell rupture, and damage to cell organelles.<sup>159,160</sup>

The ideal PT agent possesses high tissue selectivity, a large optical wavelength absorption cross-section, minimal toxicity, and ease of functionalization. Recent developments in the exploration of MXenes anchored to nanomaterials, such as gold nanorods, copper sulfide nanoparticles, and black phosphorus,<sup>161,162</sup> present a novel substrate for subcutaneous

regions of tissues due to their remarkable photothermal conversion efficiency (PTC) and strong absorbing sensitivity in the near-infrared (NIR) region.

Progress in MXene materials for PTT applications includes the development of Ta<sub>4</sub>C<sub>3</sub>T<sub>x</sub>-SP nanosheets enabling dual-mode CT scan and PA imaging of tumors, Nb<sub>2</sub>C with extremely high PTC efficiency in both the NIR-I and NIR-II regions, and MQDs with exceptionally high photothermal conversion efficiency.<sup>163</sup> Dai *et al.* introduced a Ti<sub>3</sub>C<sub>2</sub> material using the rational design, anchoring the (MnO)<sub>x</sub> composition to the surface of Ti<sub>3</sub>C<sub>2</sub> through a redox reaction.<sup>92</sup> The addition of soy phospholipids (SP) further enhanced the stability of (MnO)<sub>x</sub>/Ti<sub>3</sub>C<sub>2</sub>T<sub>x</sub>, leading to greater photothermal stability and a PTC efficiency of 22.9%, comparable to standard Au nanorods and Cu<sub>2-x</sub>Se carbon nanotubes.<sup>164</sup>

Moreover, Shao *et al.*'s research on nitride-based MXenes and Ti<sub>2</sub>NT<sub>x</sub> quantum dots demonstrated exceptionally high photothermal conversion efficiencies in both the first and second near-infrared (NIR) biological windows (NIR-I at 808 nm and NIR-II at 1064 nm).<sup>119</sup> The efficient degradation and fast excretion of Ti<sub>2</sub>NT<sub>x</sub> quantum dots, coupled with their effectiveness in photothermal therapy and favourable biocompatibility, contribute to their potential for efficient elimination from the body after the therapeutic impact becomes apparent.

Photodynamic therapy (PDT) stands out as an exceptionally promising light therapy for cancer treatment. The efficacy of PDT is significantly influenced by photosensitizers (PSS), which accumulate at the tumor site following local or systemic administration. Upon exposure to naturally occurring molecular oxygen species, especially singlet-state oxygen, activated photosensitizing molecules generate reactive oxygen species (ROS), ultimately leading to the death of cancer cells.

In a recent advancement, the Ru@MXene complex has introduced an innovative approach to creating multifunctional platforms responsive to light stimuli, effectively addressing highly resistant bacteria. This approach integrates photothermal therapy (PTT) and photodynamic therapy (PDT) for antibacterial purposes.<sup>165</sup>

Research conducted by Zhang and colleagues indicates that Mo<sub>2</sub>CT<sub>x</sub>, when subjected to laser stimulation, can generate elevated temperatures and reactive oxygen species (ROS), which play a substantial role in initiating apoptosis.<sup>87</sup> Fortunately, Guo *et al.* discovered that 3D MXenes have a better ROS production ability than Ti<sub>3</sub>C<sub>2</sub>T<sub>x</sub> nanosheets through the synthesis of honeycomb-structured 3D MXenes having anti-aggregation capabilities.<sup>166</sup> MXene-based materials are progressively showcasing potential applications in the realm of immunotherapy owing to their magnificent characteristics such as wide particular surface area, biocompatibility, and tumor-targeting accumulation. In recent years, an immune-engineered MXene nanosystem was designed to inhibit transplant rejection. An aggressive form of atherosclerosis known as cardiac allograft vasculopathy is a leading factor in the death of people who have received heart transplants. Endothelial cells (ECs) in blood vessels activate alloreactive T-lymphocytes, causing chronic inflammation. In this article, we describe for the



first time that  $\text{Ti}_3\text{C}_2\text{T}_x$  MXene nanosheets were used to prevent allograft vasculopathy. Human ECs were exposed to MXene nanosheets, which decreased the expression of genes involved in alloantigen presentation and, as a result, decreased the activation of allogeneic lymphocytes. A lymphocyte RNA-Seq investigation revealed that MXene therapy down-regulated the genes involved in allograft vasculopathy development, cell-mediated rejection, and transplant-induced T-cell activation.<sup>167</sup>

## 6. Unlocking the future of human–machine interfaces with Mxene electrodes

Soft skin-like MXene electrodes represent a groundbreaking advancement with profound significance in shaping the landscape of next-generation human–machine interactions. These flexible and biocompatible electrodes hold the potential to revolutionize various fields, from healthcare to robotics, by seamlessly bridging the gap between humans and machines. In this 1000-word paragraph, we will delve into the multifaceted significance of soft skin-like MXene electrodes in shaping the future of human–machine interactions (Fig. 9).

At the heart of the importance of MXene electrodes lies their unique ability to provide unparalleled comfort and wearability. Unlike traditional rigid electrodes, soft MXene electrodes conform effortlessly to the contours of the human body, offering a level of comfort that is crucial for long-term applications. Whether integrated into wearable technology, prosthetic limbs, or medical devices, MXene electrodes ensure that users can interact with machines for extended periods without discomfort or irritation. This comfort factor enhances the overall user experience, making human–machine interactions more accessible and user-friendly. In the context of deformable electronics resembling artificial skin, the key attributes of MXene electrodes that are of utmost significance include properties such as elasticity, self-repair capability, resilience, suitability for wear, and transparency, all akin to the characteristics of real skin. Utilizing a wide electrical conductivity range between 1 and  $15\,000\text{ S cm}^{-1}$ , the MXene family exhibits versatility for exploring various applications. To fabricate stretchable skin-like electrodes, the retention of electrical conductivity is of utmost importance when subject to mechanical deformation. Any disparity leads to ultimate dysfunction and complete mechanical failure of the fabricated devices. To address this issue, two methodological approaches have recently been adopted wherein mechanical stress dissipation and incorporation of elastomeric base matrices provide stretchable electronic and ionic conductors.<sup>168–170</sup> Moreover, the soft and conformable nature of MXene electrodes enhances their sensing capabilities, which is another pivotal aspect of their significance. These electrodes can intimately interface with the skin, enabling the sensitive and accurate monitoring of a wide range of physiological signals. From tracking vital signs such as heart rate and body temperature to detecting intricate muscle activity

patterns, MXene electrodes offer an unprecedented level of precision in data collection. In a recent development, Shipeng Zhang and colleagues downsized nanogenerators based on MXene/Ecoflex composites by incorporating flexible conductive fabric electrodes into 3D-printed gloves. The resulting nanogenerator exhibits a notable peak-to-peak voltage of 19.91 V, a high sensitivity of  $0.088\text{ V kPa}^{-1}$ , and an expansive pressure detection range of 0–120 kPa. This device holds versatile potential for applications in human–machine interactions, making it suitable for the next generation of artificial intelligence and interactive devices. Moreover, it generates high-quality output signals, enabling the accurate detection of various finger activities.<sup>171</sup>

In order to measure a person's health, it is critical to continuously monitor their body's numerous physiological signs. Contact charging and electrostatic induction coupling will be the pivotal principle behind nanogenerator fabrication. Cellulose nanofiber (CNF)-incorporated  $\text{Ti}_3\text{C}_2$  MXenes can detect the mass of a touched steel object weighing between 200 and 300 g. The fabricated triblock nanogenerator is tuned in such a way that it can be stretched to a maximum of 100% and generate various voltage signals of its initial length driven by the bending and folding angles.<sup>172</sup> This heightened sensitivity opens doors to more advanced applications, such as detecting subtle facial expressions or capturing neural signals, enabling machines to respond to human cues with greater subtlety and nuance.

Biocompatibility is a fundamental characteristic that distinguishes MXene electrodes. They have demonstrated excellent biocompatibility, meaning that they are unlikely to induce adverse reactions when in contact with biological tissues. This property is of utmost importance in medical applications, particularly in the realm of brain–computer interfaces (BCIs) and neuroprosthetics. Due to their biocompatible qualities, MXene nanosheets have recently attracted a lot of attention as electrodes for biomedical uses such as wound healing, tumor abscission and health assessment application. Hybrid electronic skin was tailored by omnipotent chitosan/MXene nanocomposites for monitoring respiration and heart health. To induce biocompatibility, chitosan is mimicked in biological tissues. Poly(*N*-isopropyl acrylamide) (PNIPAm)-based hydrogel was used to monitor health in real-time fashion.<sup>173</sup> Encapsulation with various polymers such as polyethylene glycol (PEG), poly(lactic-*co*-glycolic acid) (PLGA), chitosan, collagen and silk fibroin (SF) leads to reduced cytotoxicity.<sup>174–176</sup> Magnesium coating also renders the maximum cytotoxicity cell survey analysis, therefore additional research and optimization should be underway to provide an intrinsic footnote before human trial.

In these scenarios, electrodes must establish direct contact with the brain or nervous system without causing harm or triggering immune responses. Soft skin-like MXene electrodes offer a promising solution, potentially minimizing the risks associated with invasive medical interventions and enhancing the safety and reliability of human–machine interactions in healthcare. The conformability and flexibility of MXene



electrodes further accentuate their significance. These electrodes adapt to the dynamic and diverse contours of the human body, including irregular shapes and movements. This adaptability ensures a stable and reliable connection with the skin, even during physical activities or when applied to curved body parts. As a result, MXene electrodes can be seamlessly integrated into clothing or directly onto the skin, opening up possibilities for discreet and non-intrusive wearable technology that augments human capabilities while being practically imperceptible.

Reducing artifact and interference in signal recordings is another advantage of soft skin-like MXene electrodes. In applications such as electroencephalography (EEG) and electromyography (EMG), where precise data collection is paramount, unwanted noise and motion artifacts can compromise the quality of recordings. The soft nature of MXene electrodes can mitigate these challenges, ensuring that the data collected is of the highest fidelity (Fig. 10). This improvement in data quality is pivotal in enhancing the performance of human-machine interfaces, making them more reliable and effective.

MXene materials are renowned for their durability and transparency, which further contribute to the significance of soft skin-like MXene electrodes. These materials can withstand repeated use and exposure to various environmental conditions, making them suitable for long-term applications. This robustness is essential for devices intended for everyday use, such as assistive technologies or wearable health monitors. Perhaps the most profound significance of soft skin-like MXene electrodes lies in their ability to improve the overall user experience in human-machine interactions.

Wearable fabric bases exhibit a range of characteristics, including permeability, stretchability, breathability, and electrical conductivity. Typically, two methods are employed to produce fabric-based electrodes for use in wearable electronics on the skin (Fig. 10). The first method involves applying conductive nanoparticles to existing yarns. In the second method, composites of conductive nanoparticles and polymers are employed that can be spun into fibers, which are then woven in the form of conductive textiles. Nevertheless, these active fiber materials have a tendency to separate under mechanical deformations, leading to a reduction in their conductivity.<sup>180,181</sup>

A clever approach in the creation of conductive fabrics involves using the dip-coating technique. This method is utilized in the large-scale production of wearable fabric-based electronics, where yarns are submerged into a conductive solution, resulting in a layer of conductive material coating the fabric's surface.<sup>182</sup> Zhao and his team adopted this technique to produce conducting MXene fabrics by immersing cellulose fabric in an aqueous MXene solution.<sup>183</sup> In another approach, Shao and colleagues manufactured conductive and flexible textiles by electrospinning an MXene polymer solution onto PET yarns, creating yarns coated with nanofibers.<sup>184</sup> Additionally, to create a polymeric fiber matrix at the nano-scale, various materials such as PAA, PVA, poly(ethylene oxide)

(PEO), and alginate/PEO were incorporated with MXene nanosheets.<sup>185,186</sup>

Biscrolling is a technique that enhances the MXene-loading density and fiber production by combining MXenes with spinnable host materials (CNTs), achieving a high loading density of 98 wt%. It prevents delamination by trapping MXenes onto CNT corridors, enabling the creation of highly conductive and flexible MXene fibers. Zheng *et al.* used a roll-to-roll layer-by-layer assembly to fabricate CNT/MXene cellulose fabrics, where high pressures aided particle penetration, reducing delamination.<sup>187</sup> Researchers, including Wang *et al.*, have developed superhydrophobic wearable sensors by combining silicon nanoparticles with MXene nanosheets. This integration creates a hierarchical structure that maintains conductivity even under wet conditions.<sup>188</sup> To minimize the active agglomeration of nanoparticles and increase the spinnability, wet electrospinning technology, including electrospinning and wet spinning elements, is introduced to include MXene nanosheets throughout the entire yarn cross-section. Levitt *et al.* created conductive yarns with up to 90% nylon/MXene yarn loading by using hydrophilic (nylon) and hydrophobic (polyurethane) textiles.<sup>189</sup> Another method involves adding hydrophobic layers like PDMS and silicone rubber to MXene textiles, enhancing hydrophobicity and stability. Ma and colleagues successfully enhanced hydrophobicity (measured by a contact angle of 135.6°) by applying a PDMS coating to PDA/MXene-decorated paper. This step significantly improved the interaction between textiles and MXenes.<sup>190</sup> Another cost-effective and efficient method for imparting fabrics with hydrophobic characteristics is emulsion dipping, which involves the use of PDMS and MXenes.<sup>191</sup> In the healthcare sector, the implications of soft skin-like MXene electrodes are monumental. This, in turn, fosters a greater sense of integration and trust in technology. Whether it is a person with a prosthetic limb experiencing enhanced mobility and dexterity or a patient benefiting from a more comfortable and accurate medical monitoring device, MXene electrodes hold the promise of transforming the way we interact with machines. These devices equipped with MXene electrodes could revolutionize telemedicine, allowing healthcare providers to remotely monitor patients' conditions in real time, detect anomalies early, and intervene when necessary. Furthermore, in the field of rehabilitation, MXene-enabled prosthetic limbs could offer amputees a level of functionality and comfort previously unimaginable, allowing them to regain a sense of normalcy in their lives.

The significance of soft skin-like MXene electrodes extends beyond healthcare into the realm of human augmentation and robotics. In the development of exoskeletons and wearable robotic devices, these electrodes can facilitate more natural and intuitive control mechanisms. They enable machines to better understand and respond to the wearer's movements and intentions, blurring the line between the human body and machine. This advancement has the potential to revolutionize industries such as manufacturing, where workers can use wearable robotics to enhance their strength and precision, reducing the risk of injury and improving overall productivity.



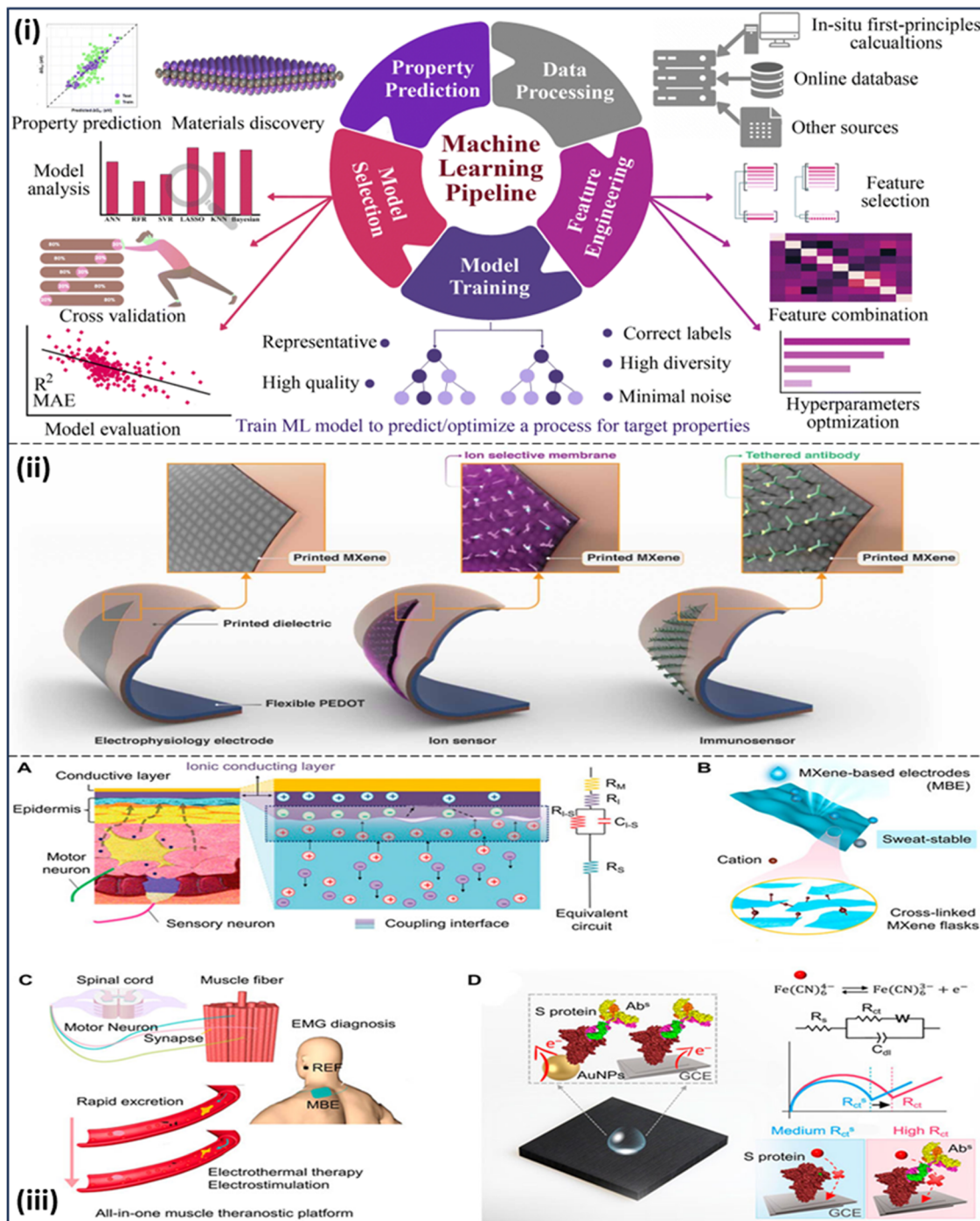


**Fig. 10** (i) Workflow of the machine learning approach, starting from data processing, feature engineering, model training, model selection and property prediction for the screening of ideal HER catalysts from MXenes. From first-principles calculations, the materials space is generated from a large number of possible combinations of the selected elements and functionalization. Reproduced from ref. 177 with permission from the Royal Society of Chemistry, copyright 2023. (ii) Schematic of three MXene electrodes printed on flexible self-standing PEDOT substrates. The mode of sensing is governed by the surface functionality of the printed MXene device. (Left) Electrophysiology electrode. (Middle) MXene-based ion sensor with an ion-selective membrane on the top of the MXene layer. (Right) Immunosensor made of MXene film tethered with specific antibodies. Reproduced from ref. 178 with permission from IOPscience, copyright 2020. (iii) (A) A flexible skin-adherent electrode with minimal electrochemical impedance attached to the epidermis. An equivalent circuit model is shown to the right. (B) Bioderived, air-permeable, and sweat-stable MXene-based electrode (top), where structural crosslinking exists throughout the nanoscopic structure (bottom). (C) A MXene-based "theranostic" device to provide electrothermal therapy if muscle fatigue is detected. (D) Loading a peptide onto a label-free EIS biosensor increases its sensitivity. Reproduced from ref. 179 with permission from Frontiers, copyright 2023.



Soft skin-like MXene electrodes are also poised to make a significant impact in the field of virtual and augmented reality (VR/AR). These electrodes can be integrated into headsets and gloves, enabling more immersive and intuitive experiences. Users can interact with virtual environments and objects in a manner that closely resembles natural human movements and sensations. This not only enhances the entertainment value of VR/AR but also extends into professional applications such as training simulations, where users can practice complex tasks in a risk-free virtual environment. By harnessing the power of machine learning, researchers have been able to analyze complex patterns and relationships within the MXene-based electrode's electrical properties, enabling more precise and adaptable sensor functionality. Machine learning algorithms can recognize and respond to subtle changes in skin conditions, making these electrodes valuable tools for various applications, such as health monitoring, prosthetics, and human-machine interfaces. In this context, symbolic regression (SR), multiple linear regression (MLR) model, decision tree (DT), and Recurrent Neural Network (RNN) model have been adopted to devise various machine learning interfaces. Epa and colleagues utilized multiple linear regression (MLR) to establish a nano-quantitative structure–activity relationship (nano-QSAR) aiming to forecast cellular biochemical responses and apoptosis. QSAR serves as a vital tool in drug discovery by establishing links between compound chemical attributes and their biological impacts.<sup>192</sup> J. Zhu *et al.* designed a flexible MXene electrode for screening the pesticide  $\alpha$ -naphthalene acetic acid. They employed genetic algorithm (GA) to investigate the materialistic content with 96.66 to 99.14% accuracy. GA, an effective optimization technique, requires parameter tuning and operator selection but applies Darwinian principles for self-learning. These studies highlight machine learning's efficacy in skin-like MXene electrode development.<sup>193</sup> In another finding, Shimadera and collaborators designed a haptic sensor using MXene technology, which can accurately sense contact force, location, and temperature at a micro-scale. This flexible device enables physical sensing inside the human body, proving beneficial for both scientific inquiries. The data collected by these MXene sensors underwent analysis through convolutional neural networks (CNN) and fully connected neural networks (FCNN).<sup>194</sup> Furthermore, in the context of human–computer interaction (HCI), soft MXene electrodes can lead to more responsive and adaptive interfaces. As machines better understand and respond to subtle physiological and emotional cues, the user experience becomes more personalized and engaging. This is particularly relevant in applications such as affective computing, where machines can assess a user's emotional state through physiological signals and adjust their responses accordingly. This capability has vast implications for fields like customer service, mental health support, and education. With this realization the intersection of skin-like characteristics and the identification of a novel and remarkably durable category of MXenes could profoundly transform our interactions with devices and the external environment.

## 7. Insights into the potential efficacy of Mxene nanocomposites in orthodontic implantation

Mxene nanocomposites hold substantial significance in the field of guided bone regeneration (GBR) due to their idiosyncratic properties. GBR is a technique used to restore lost or damaged bone, particularly in the realm of orthodontic implantation and periodontal regeneration. Mxene materials offer advantages such as biocompatibility, high surface area for enhanced cell adhesion, and the ability to promote osteogenesis. These properties enable them to serve as effective scaffolds for tissue engineering, aiding in the regeneration of bone by providing structural support and promoting the growth of new bone tissue. Mxene's excellent integration with bone tissue, antibacterial properties, electrical conductivity, and customizable degradation rates offer orthodontists the tools to design implants that not only provide structural support but also facilitate the healing and regeneration of bone tissue.<sup>195</sup>

In the field of tissue engineering biomaterial implants need additional concerns to regulate the endogenous surface morphology and electrical potential. To tune the top-notch electroactive microenvironment for mimicking the extracellular vicinity for bone regeneration Fu *et al.*<sup>196</sup> adopted electrospinning technique to fabricate PVDF/Mxene ferroelectric nanocomposites membrane.  $\text{Ti}_3\text{C}_2\text{T}_x$  MXene nanosheets were wrapped in a PVDF shell layer. Tailoring the content of Mxenes, the surface morphology was optimized and this allowed for the exact miniaturization of the nanosheets into a naturally occurring extracellular matrix (ECM) in bone tissue, as well as the uniform distribution of fibers subsequently upgraded the electric potential. Chen *et al.* created a robust and biocompatible membrane for GBR by integrating  $\text{Ti}_3\text{C}_2\text{T}_z$  nanosheets into a PLA matrix and using *n*-octyltriethoxysilane (OTES) as an interfacial mediating agent (Fig. 11). As compared to the PLA matrix, the OTES- $\text{Ti}_3\text{C}_2\text{T}_z$ /PLA nanocomposite membrane showed increased mechanical strength of 72 MPa.  $\text{Ti}_3\text{C}_2\text{T}_z$  nanosheets had a significant impact which bestowed the biocompatibility by advocating pre-osteoblast cell adhesion, osteogenic maturation and differentiation and cell migration than native 2D graphene oxide nanosheet.<sup>91</sup> To identify the underlying mechanism of endotheliocyte virtuous circle, Zhi-Chao Hu and his research team have developed a piezoresistive pressure transducer MXene/regenerated silk fibroin hydrogel (RSF). A unique and promising method for encouraging direct osteogenesis, controlling the immunological milieu and neovascularization under electrical stimulation, and reestablishing the electrical microenvironment for bone regeneration. The electroactive hydrogel could amplify the osteogenic induction by modulating the  $\text{Ca}^{2+}$ /CALM signaling pathway effective for bone tissue regeneration.<sup>197</sup> Awasthi *et al.* employed electrospinning to create fibers comprising MXene and polycaprolactone.

These fibers exhibited higher compatibility with pre-osteoblast cells during the regeneration process in comparison to fibroblast cells. The Mxene content of fiber mat (PCL)





promotes cellular adhesion and proliferation which might instigate the phosphorus/calcium deposition, thereby increasing *in vitro* bio-mineralization and osseointegration explored in

tissue engineering applications.<sup>147</sup> Furthermore, their radio-opacity aids in monitoring implant placement and post-operative assessment (Fig. 11). As research in this field

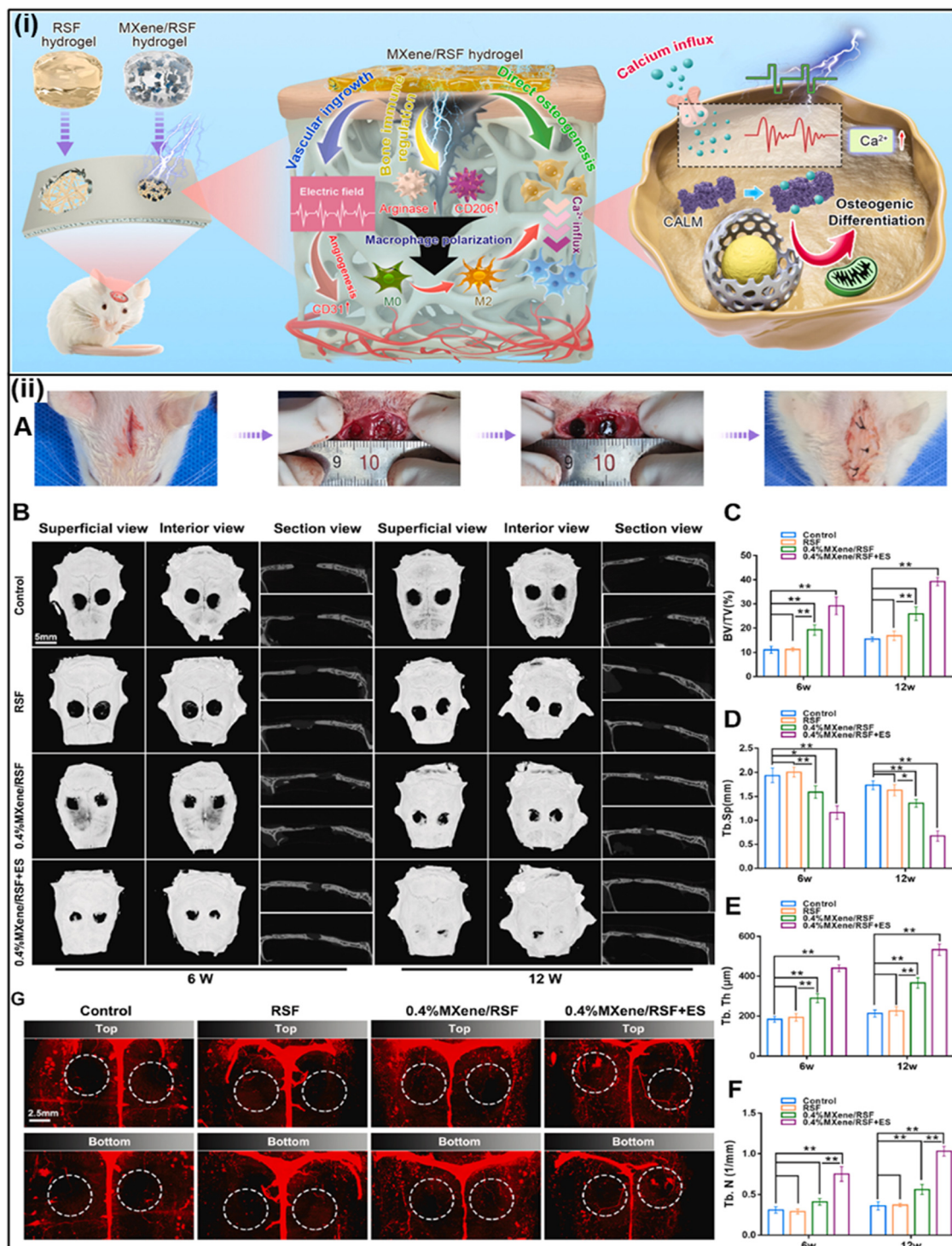


**Fig. 11** (i) Conceptual and effective mechanisms of the electroactive MXene/RSF hydrogels to re-establish the electrical microenvironment for bone regeneration. (ii) MXene/RSF hydrogels with ES potential accelerated bone regeneration. (A) Procedure for the establishment of the calvarial defect model in SD rats. (B) Cranial bone regeneration at 6 and 12 weeks after implantation presented by micro-CT. (C)–(F) BV/TV, Tb.Sp, Tb.Th, and Tb.N results calculated based on micro-CT. (G) Representative images of 3D reconstruction of the blood vessels at 12 weeks post-implantation. Reproduced from ref. 198 with permission from KeAi Communications, copyright 2023.



continues to evolve, Mxene nanocomposites have the potential to revolutionize orthodontic treatments, improving patient outcomes, and enhancing the long-term success of orthodontic implantations.

## 8. Biosafety and toxicity concerns

Unlike most organic entities, Mxenes and Mxene-based composites possess some unique characteristics such as tunable architecture, multifunctional potentials, exceptional physiological stability, biodegradability and biocompatibility which made them attractive materials in the realm of clinical and biomedical applications. For these 2D MXenes, biosafety, toxicity, and biocompatibility concerns must be further taken into consideration. Additionally, significant factors including dispersibility, solubility, and lasting toxic impact need to be thoroughly examined. In a particular study, the possible toxicity of MXene nanosheets was evaluated concerning early embryo stages and angiogenesis. It was found that they may have negative effects on the early phase of embryogenesis; approximately 46% of MXene-exposed embryos died within 1–5 days of exposure. Additionally, after five days of incubation at the investigated site, the chorioallantoic membrane's angiogenesis was inhibited by MXenes. Subsequent analysis using reverse transcription polymerase chain reaction (RT-PCR) revealed that seven critical regulatory genes were found to be relaxed in the heart, brain, and liver tissues of MXene-treated embryos in contrast to their respective control groups. Therefore, it is imperative to conduct more comprehensive investigations to assess the potential harmfulness and safety of MXenes and MXene-based structures.

In order to figure out biodegradation, the degradative act of Nb<sub>2</sub>C-PVP nanosheets was modelled using human myeloperoxidase (hMPO), which yields hypochlorous acid and active radical intermediates that break down carbon-based nanomaterials.<sup>17</sup> The nanosheet suspension turned translucent after the addition of hMPO and H<sub>2</sub>O<sub>2</sub>. After 24 hours of incubation with hMPO and H<sub>2</sub>O<sub>2</sub>, even Nb<sub>2</sub>C nearly vanished. Furthermore, studies of the mice's histopathology, blood biochemical indices, and hematological parameters over a 28-day period showed that intravenous Nb<sub>2</sub>C-PVP did not significantly affect kidney or liver toxicity, infection, inflammation, or infection, nor did it create any significant renal or hepatic toxicities. Additionally, the embedding of MXene thin films into subcutaneous tissues of rats led to a significant number of fibroblasts and capillaries as well as a mild granulation and inflammation in the tissue around the fractured MXenes. While significant inflammatory cell infiltration and necrosis were not seen, macrophages adhered to MXenes.

MXenes were taken up and biodegraded *in vivo* by phagocytosis. MXene nanosheets cause oxidative stress, which is harmful to cancer cells but has very little immediate cytotoxicity and causes only mild inflammation in healthy cells and tissues. The cornerstone for creating bio-applications is the fact that MXenes are extremely biocompatible and have a safe

biodegradation profile both *in vitro* and *in vivo* when used within the recommended dose range. The main challenge of MXenes' continued biomedical development would be maintaining a safe dosage while achieving optimal effectiveness.

## 9. Perspective, dilemmas and foreseeable future

Due to their unique physical and chemical properties, along with their strong biocompatibility and ease of modification compared to conventional organic materials, 2D MXene nanomaterials hold significant promise for various medical applications, *e.g.* bioimaging, biosensing, and drug delivery. Nevertheless, the translation of these materials into clinical use has presented substantial challenges. Despite the expansion of the 2D material family by MXenes and their diverse applications, the strategic development of MXenes and their derivatives for cancer theranostics, which include catalytic therapy, radiotherapy, photothermal and photodynamic therapy, and imaging capabilities, remains a significant hurdle in the field of biomedicine. For implementation in cancer therapy and diagnosis, these materials' mechanical, electrical, thermal, and optical properties can be enhanced by means of hybridization and surface functionalization or modification. The versatile applicability of 2D MXenes in biomedicine is somehow restricted due to its rapid accumulation, intricate surface engineering, insufficient strength, and potential toxicity. The degradation and resilience in the context of *in vivo* circulation are contingent on factors such as orientation, size, layer count, and oxidation level. However, there is a lack of discussion regarding metabolic pathway analysis, the potential negative impacts of MXene nano-films, and the interactions between these nanofilms and the physiological environment. It is utterly contradictory that rapid degradation might influence the anticipated therapeutic outcomes. To get the remarkable therapeutic outcomes and minimum toxicity, an appropriate degradation rate should be taken into account throughout the configuration and synthesis of MXenes. Subsequent studies should shift their emphasis away from immediate repercussions and instead concentrate on the enduring outcomes of nanomaterial exposure, particularly concerning the well-being of adult offspring, especially in the context of neurodevelopment. The next phase of research necessitates a more comprehensive exploration of cellular uptake patterns, mechanisms of immunogenicity, biodistribution, cytotoxicity, and the various factors that could influence the toxicity of MXenes and their derivative materials. This will make it easier to develop strategies for modulating their toxicity. It has been demonstrated that a 2D material's toxicity and biocompatibility may depend on its dispersion state, dimensions, solubility, chemical composition, and crystalline structure.

In order to simplify and reduce the costs of complex processes involved in the formulation of nanocarriers for anticancer drug administration and cancer diagnostic nanoplatforms, it is essential to adhere to methodologies and principles that prioritize controllability, reliability,



reproducibility, innovation, scalability, and practicality.<sup>118,119</sup> Another formidable challenge lies in successfully transitioning MXenes and their derivative materials from preclinical stages to practical clinical applications. This necessitates thorough investigations into pharmacodynamics, pharmacokinetics, tumor responses, and histopathology studies.<sup>99</sup>

Accurate assessments of MXenes' optical, mechanical, magnetic, and electrical properties, as well as optimization procedures, are crucial. Due to the inherent fragility of these nanostructures in complex physiological environments, MXenes can precipitate or aggregate in biological media. Therefore, there is a strong demand for surface multi-functionalization techniques, such as precise molecular or polymer surface modifications (e.g., polyvinylpyrrolidone (PVP) and soybean phospholipid), as well as the decoration of MXenes with multifunctional inorganic nanoparticles. These techniques are highly desirable to ensure the dispersity and stability of MXenes and its derivative-based systems under physiological conditions.

The bottom-up synthesis approach provides superior control when compared to the top-down synthesis method, as it enables the regulation of size distribution and repeatability. Investigating further morphological attributes of MXenes, such as nanotubes and nanocages, in conjunction with the examination of thin films and quantum dots, presents valuable opportunities. In the pursuit of launching biomedical applications based on MXenes, current research is directed towards blending MXenes along with other relevant functional materials to develop hybrid materials that leverage the advantages of various materials. The future of MXenes in the field of biomedical applications holds great promise and has the potential to revolutionize various aspects of healthcare, fostering groundbreaking discoveries. Thanks to their unique blend of biocompatibility, adaptable properties, and multifunctional capabilities, MXene-based nanocomposites are poised to usher in a new era of precision medicine. This future may involve tailored drug delivery and non-invasive therapies based on individual genetic and physiological profiles. Moreover, MXenes' ability to integrate diagnostics and therapies into a single platform enables simultaneous treatment, precise disease identification, and real-time monitoring, ultimately leading to early interventions and improved patient outcomes.

MXenes are expected to revolutionize implant technology, brain interfaces, and regenerative medicine as improvements are made because they provide biocompatible and conductive materials that naturally merge with the human body. While obstacles still exist, the combined efforts of scientists, doctors, and regulatory agencies are poised to move MXenes from ground-breaking research to useful clinical applications, ultimately influencing the development of safer, more efficient, and individualized healthcare solutions.

## Data availability

All the data supporting the study mentioned in this article have been presented through figures and tables. Additional data are

available in the supplementary files included in the submission request.

## Conflicts of interest

There are no conflicts to declare.

## Acknowledgements

The authors wish to appreciate DST West Bengal and Central DST the Centre for Research in Nanoscience and Nanotechnology, and the Department of Polymer Science and Technology University of Calcutta for their financial and technical support. Dr Sriparna De would like to acknowledge the SEED Research grant, Brainware University (BWU/PRJ/SMG/22-23/001) for providing research support and facilities. Dr Suresh K. Verma acknowledges infrastructure support available through DBT-BUILDER program (BT/INF/22/SP42155/2021) at KIIT UNIVERSITY. The authors also acknowledge NRF Korea (2021R1A6A1A03038785, 2021R1F1A1055694), and Kwangwoon University for financial grants in 2024.

## References

- 1 A. Gupta, T. Sakhivel and S. Seal, Recent development in 2D materials beyond graphene, *Prog. Mater. Sci.*, 2015, **73**, 44–126, DOI: [10.1016/j.pmatsci.2015.02.002](https://doi.org/10.1016/j.pmatsci.2015.02.002).
- 2 V. H. Nguyen, B. S. Nguyen, C. Hu, C. C. Nguyen, D. L. T. Nguyen, M. T. N. Dinh, D. V. N. Vo, Q. T. Trinh, M. Shokouhimehr, A. Hasani, S. Y. Kim and Q. Van Le, Novel architecture titanium carbide (Ti<sub>3</sub>C<sub>2</sub>T<sub>x</sub>) MXene cocatalysts toward photocatalytic hydrogen production: a mini-review, *Nanomaterials*, 2020, **10**(4), 602, DOI: [10.3390/nano10040602](https://doi.org/10.3390/nano10040602).
- 3 S. De, S. Mohanty, S. K. Nayak, S. K. Verma and M. Suar, Nanotoxicity of rare earth metal oxide anchored graphene nanohybrid: a facile synthesis and *in vitro* cellular response studies, *Nano*, 2015, **10**, 1550091, DOI: [10.1142/S1793292015500915](https://doi.org/10.1142/S1793292015500915).
- 4 Z. Ayreen, U. Khatoun, A. Kirti, A. Sinha, A. Gupta, S. S. Lenka, A. Yadav, R. Mohanty, S. S. Naser, R. Mishra, R. S. Chouhan, S. K. Samal, N. K. Kaushik, D. Singh, M. Suar and S. K. Verma, Perilous paradigm of graphene oxide and its derivatives in biomedical applications: insight to immunocompatibility, *Biomed. Pharmacother.*, 2024, **176**, 116842, DOI: [10.1016/j.biopha.2024.116842](https://doi.org/10.1016/j.biopha.2024.116842).
- 5 K. Rasool, M. Helal, A. Ali, C. E. Ren, Y. Gogotsi and K. A. Mahmoud, Antibacterial Activity of Ti<sub>3</sub>C<sub>2</sub>T<sub>x</sub> MXene, *ACS Nano*, 2016, **10**, 3674–3684, DOI: [10.1021/acsnano.6b00181](https://doi.org/10.1021/acsnano.6b00181).
- 6 M. Naguib, V. N. Mochalin, M. W. Barsoum and Y. Gogotsi, MXenes: a new family of two-dimensional materials, *Adv. Mater.*, 2014, **26**, 992–1005.
- 7 A. Gupta, A. Prasad, N. Mulchandani, M. Shah, M. Ravi Sankar, S. Kumar and V. Katiyar, Multifunctional



- Nanohydroxyapatite-Promoted Toughened High-Molecular-Weight Stereocomplex Poly(lactic acid)-Based Bionanocomposite for Both 3D-Printed Orthopedic Implants and High-Temperature Engineering Applications, *ACS Omega*, 2017, 2, 4039–4052, DOI: [10.1021/acsomega.7b00915](https://doi.org/10.1021/acsomega.7b00915).
- 8 X. Li, M. Li, Q. Yang, G. Liang, Z. Huang, L. Ma, D. Wang, F. Mo, B. Dong, Q. Huang and C. Zhi, In Situ Electrochemical Synthesis of MXenes without Acid/Alkali Usage in/for an Aqueous Zinc Ion Battery, *Adv. Energy Mater.*, 2020, 10, 2001791, DOI: [10.1002/aenm.202001791](https://doi.org/10.1002/aenm.202001791).
  - 9 S. Y. Pang, Y. T. Wong, S. Yuan, Y. Liu, M. K. Tsang, Z. Yang, H. Huang, W. T. Wong and J. Hao, Universal Strategy for HF-Free Facile and Rapid Synthesis of Two-dimensional MXenes as Multifunctional Energy Materials, *J. Am. Chem. Soc.*, 2019, 141, 9610–9616, DOI: [10.1021/jacs.9b02578](https://doi.org/10.1021/jacs.9b02578).
  - 10 T. Li, L. Yao, Q. Liu, J. Gu, R. Luo, J. Li, X. Yan, W. Wang, P. Liu, B. Chen, W. Zhang, W. Abbas, R. Naz and D. Zhang, Fluorine-Free Synthesis of High-Purity  $Ti_3C_2T_x$  (T = OH, O) via Alkali Treatment, *Angew. Chem., Int. Ed.*, 2018, 57, 6115–6119, DOI: [10.1002/anie.201800887](https://doi.org/10.1002/anie.201800887).
  - 11 A. Prasad, Bioabsorbable polymeric materials for biofilms and other biomedical applications: recent and future trends, *Mater. Today Proc.*, 2021, 44, 2447–2453, DOI: [10.1016/j.matpr.2020.12.489](https://doi.org/10.1016/j.matpr.2020.12.489).
  - 12 M. Li, J. Lu, K. Luo, Y. Li, K. Chang, K. Chen, J. Zhou, J. Rosen, L. Hultman, P. Eklund, P. O. Å. Persson, S. Du, Z. Chai, Z. Huang and Q. Huang, Element Replacement Approach by Reaction with Lewis Acidic Molten Salts to Synthesize Nanolaminated MAX Phases and MXenes, *J. Am. Chem. Soc.*, 2019, 141, 4730–4737, DOI: [10.1021/jacs.9b00574](https://doi.org/10.1021/jacs.9b00574).
  - 13 P. Urbankowski, B. Anasori, K. Hantanasirisakul, L. Yang, L. Zhang, B. Haines, S. J. May, S. J. L. Billinge and Y. Gogotsi, 2D molybdenum and vanadium nitrides synthesized by ammoniation of 2D transition metal carbides (MXenes), *Nanoscale*, 2017, 9, 17722–17730, DOI: [10.1039/c7nr06721f](https://doi.org/10.1039/c7nr06721f).
  - 14 J. Xuan, Z. Wang, Y. Chen, D. Liang, L. Cheng, X. Yang, Z. Liu, R. Ma, T. Sasaki and F. Geng, Organic-Base-Driven Intercalation and Delamination for the Production of Functionalized Titanium Carbide Nanosheets with Superior Photothermal Therapeutic Performance, *Angew. Chem.*, 2016, 128, 14789–14794, DOI: [10.1002/ange.201606643](https://doi.org/10.1002/ange.201606643).
  - 15 A. Prasad, B. Devendar, M. R. Sankar and P. S. Robi, Micro-Scratch Based Tribological Characterization of Hydroxyapatite (HAp) Fabricated through Fish Scales, *Mater. Today Proc.*, 2015, 2, 1216–1224, DOI: [10.1016/j.matpr.2015.07.034](https://doi.org/10.1016/j.matpr.2015.07.034).
  - 16 K. Chen, N. Qiu, Q. Deng, M. H. Kang, H. Yang, J. U. Baek, Y. H. Koh, S. Du, Q. Huang and H. E. Kim, Cytocompatibility of  $Ti_3AlC_2$ ,  $Ti_3SiC_2$ , and  $Ti_2AlN$ : In Vitro Tests and First-Principles Calculations, *ACS Biomater. Sci. Eng.*, 2017, 3, 2293–2301, DOI: [10.1021/acsbomaterials.7b00432](https://doi.org/10.1021/acsbomaterials.7b00432).
  - 17 H. Lin, S. Gao, C. Dai, Y. Chen and J. Shi, A Two-Dimensional Biodegradable Niobium Carbide (MXene) for Photothermal Tumor Eradication in NIR-I and NIR-II Biowindows, *J. Am. Chem. Soc.*, 2017, 139, 16235–16247, DOI: [10.1021/jacs.7b07818](https://doi.org/10.1021/jacs.7b07818).
  - 18 S. Guo, K. Wu, C. Li, H. Wang, Z. Sun, D. Xi, S. Zhang, W. Ding, M. E. Zaghoul, C. Wang, F. A. Castro, D. Yang and Y. Zhao, Integrated contact lens sensor system based on multifunctional ultrathin  $MoS_2$  transistors, *Matter*, 2021, 4, 969–985, DOI: [10.1016/j.matt.2020.12.002](https://doi.org/10.1016/j.matt.2020.12.002).
  - 19 Y. Lei, W. Zhao, Y. Zhang, Q. Jiang, J. He, A. J. Baeumner, O. S. Wolfbeis, Z. L. Wang, K. N. Salama and H. N. Alshareef, A Mxene-Based Wearable Biosensor System for High-Performance In Vitro Perspiration Analysis, *Small*, 2019, 15, 1901190, DOI: [10.1002/smll.201901190](https://doi.org/10.1002/smll.201901190).
  - 20 J. S. Nah, S. C. Barman, M. A. Zahed, M. Sharifuzzaman, H. Yoon, C. Park, S. Yoon, S. Zhang and J. Y. Park, A wearable microfluidics-integrated impedimetric immunosensor based on  $Ti_3C_2T$  MXene incorporated laser-burned graphene for noninvasive sweat cortisol detection, *Sens. Actuators, B*, 2021, 329, 129206, DOI: [10.1016/j.snb.2020.129206](https://doi.org/10.1016/j.snb.2020.129206).
  - 21 Y.-C. Yang, Y.-T. Lin, J. Yu, H.-T. Chang, T.-Y. Lu, T.-Y. Huang, A. Preet, Y.-J. Hsu, L. Wang and T.-E. Lin, MXene Nanosheet-Based Microneedles for Monitoring Muscle Contraction and Electrostimulation Treatment, *ACS Appl. Nano Mater.*, 2021, 4, 7917–7924, DOI: [10.1021/acsanm.1c01237](https://doi.org/10.1021/acsanm.1c01237).
  - 22 S. K. Verma, E. Jha, P. K. Panda, A. Thirumurugan, S. K. S. Parashar, S. Patro and M. Suar, Mechanistic insight into size-dependent enhanced cytotoxicity of industrial antibacterial titanium oxide nanoparticles on colon cells because of reactive oxygen species quenching and neutral lipid alteration, *ACS Omega*, 2018, 3, 1244–1262, DOI: [10.1021/acsomega.7b01522](https://doi.org/10.1021/acsomega.7b01522).
  - 23 K. Huang, Z. Li, J. Lin, G. Han and P. Huang, Two-dimensional transition metal carbides and nitrides (MXenes) for biomedical applications, *Chem. Soc. Rev.*, 2018, 47, 5109–5124, DOI: [10.1039/c7cs00838d](https://doi.org/10.1039/c7cs00838d).
  - 24 A. Prasad, S. M. Bhasney, V. Prasannavenkadesan, M. R. Sankar and V. Katiyar, Nano-hydroxyapatite reinforced polylactic acid bioabsorbable cancellous screws for bone fracture fixations, *J. Appl. Polym. Sci.*, 2023, 140, e54577, DOI: [10.1002/app.54577](https://doi.org/10.1002/app.54577).
  - 25 G. Chakraborty, R. Padmashree and A. Prasad, Recent advancement of surface modification techniques of 2-D nanomaterials, *Mater. Sci. Eng., B*, 2023, 297, 116817, DOI: [10.1016/j.mseb.2023.116817](https://doi.org/10.1016/j.mseb.2023.116817).
  - 26 A. Prasad, State of art review on bioabsorbable polymeric scaffolds for bone tissue engineering, *Mater. Today Proc.*, 2021, 44, 1391–1400, DOI: [10.1016/j.matpr.2020.11.622](https://doi.org/10.1016/j.matpr.2020.11.622).
  - 27 M. Naguib, M. Kurtoglu, V. Presser, J. Lu, J. Niu, M. Heon, L. Hultman, Y. Gogotsi and M. W. Barsoum, Two-Dimensional Nanocrystals Produced by Exfoliation of  $Ti_3AlC_2$ , *Adv. Mater.*, 2011, 23, 4248–4253, DOI: [10.1002/adma.201102306](https://doi.org/10.1002/adma.201102306).
  - 28 Y. Wang, W. Feng and Y. Chen, Chemistry of two-dimensional MXene nanosheets in theranostic nanomedicine, *Chin. Chem. Lett.*, 2020, 31, 937–946, DOI: [10.1016/j.cclet.2019.11.016](https://doi.org/10.1016/j.cclet.2019.11.016).



- 29 A. Lipatov, M. Alhabeab, M. R. Lukatskaya, A. Boson, Y. Gogotsi and A. Sinitskii, Effect of Synthesis on Quality, Electronic Properties and Environmental Stability of Individual Monolayer  $Ti_3C_2$  MXene Flakes, *Adv. Electron. Mater.*, 2016, **2**, 1600255, DOI: [10.1002/aelm.201600255](https://doi.org/10.1002/aelm.201600255).
- 30 S. Yang, P. Zhang, F. Wang, A. G. Ricciardulli, M. R. Lohe, P. W. M. Blom and X. Feng, Fluoride-Free Synthesis of Two-Dimensional Titanium Carbide (MXene) Using A Binary Aqueous System, *Angew. Chem., Int. Ed.*, 2018, **57**, 15491–15495, DOI: [10.1002/anie.201809662](https://doi.org/10.1002/anie.201809662).
- 31 A. Vijayaprabakaran and M. Kathiresan, Fluorine-free synthesized tantalum carbide ( $Ta_2C$  MXene) as an efficient electrocatalyst for water reduction and nitro compound reduction, *Mater. Adv.*, 2023, **4**, 3593–3602, DOI: [10.1039/D3MA00223C](https://doi.org/10.1039/D3MA00223C).
- 32 M. Ghidui, M. R. Lukatskaya, M. Q. Zhao, Y. Gogotsi and M. W. Barsoum, Conductive two-dimensional titanium carbide “clay” with high volumetric capacitance, *Nature*, 2015, **516**, 78–81, DOI: [10.1038/nature13970](https://doi.org/10.1038/nature13970).
- 33 M. R. Lukatskaya, J. Halim, B. Dyatkin, M. Naguib, Y. S. Buranova, M. W. Barsoum and Y. Gogotsi, Room-temperature carbide-derived carbon synthesis by electrochemical etching of MAX phases, *Angew. Chem., Int. Ed.*, 2014, **53**, 4877–4880, DOI: [10.1002/anie.201402513](https://doi.org/10.1002/anie.201402513).
- 34 W. Sun, S. A. Shah, Y. Chen, Z. Tan, H. Gao, T. Habib, M. Radovic and M. J. Green, Electrochemical etching of  $Ti_2AlC$  to  $Ti_2CT_x$  (MXene) in low-concentration hydrochloric acid solution, *J. Mater. Chem. A*, 2017, **5**, 21663–21668, DOI: [10.1039/C7TA05574A](https://doi.org/10.1039/C7TA05574A).
- 35 A. Djire, H. Zhang, J. Liu, E. M. Miller and N. R. Neale, Electrocatalytic and Optoelectronic Characteristics of the Two-Dimensional Titanium Nitride  $Ti_4N_3T_x$  MXene, *ACS Appl. Mater. Interfaces*, 2019, **11**, 11812–11823, DOI: [10.1021/acsami.9b01150](https://doi.org/10.1021/acsami.9b01150).
- 36 X. Xie, Y. Xue, L. Li, S. Chen, Y. Nie, W. Ding and Z. Wei, Surface Al leached  $Ti_3AlC_2$  as a substitute for carbon for use as a catalyst support in a harsh corrosive electrochemical system, *Nanoscale*, 2014, **6**, 11035–11040, DOI: [10.1039/c4nr02080d](https://doi.org/10.1039/c4nr02080d).
- 37 G. Zou, Q. Zhang, C. Fernandez, G. Huang, J. Huang and Q. Peng, Heterogeneous  $Ti_3SiC_2@C$ -Containing  $Na_2Ti_7O_{15}$  Architecture for High-Performance Sodium Storage at Elevated Temperatures, *ACS Nano*, 2017, **11**, 12219–12229, DOI: [10.1021/acsnano.7b05559](https://doi.org/10.1021/acsnano.7b05559).
- 38 Y. Wei, P. Zhang, R. A. Soomro, Q. Zhu and B. Xu, Advances in the Synthesis of 2D MXenes, *Adv. Mater.*, 2021, **33**, 2103148, DOI: [10.1002/adma.202103148](https://doi.org/10.1002/adma.202103148).
- 39 H. Shi, P. Zhang, Z. Liu, S. Park, M. R. Lohe, Y. Wu, A. Shaygan Nia, S. Yang and X. Feng, Ambient-Stable Two-Dimensional Titanium Carbide (MXene) Enabled by Iodine Etching, *Angew. Chem.*, 2021, **133**, 8771–8775, DOI: [10.1002/ange.202015627](https://doi.org/10.1002/ange.202015627).
- 40 R. Sankar, Mamilla, *Process for the preparation of polymer based Cancellous screws and pins*, 2023.
- 41 L. Verger, C. Xu, V. Natu, H. M. Cheng, W. Ren and M. W. Barsoum, Overview of the synthesis of MXenes and other ultrathin 2D transition metal carbides and nitrides, *Curr. Opin. Solid State Mater. Sci.*, 2019, **23**, 149–163, DOI: [10.1016/j.cossms.2019.02.001](https://doi.org/10.1016/j.cossms.2019.02.001).
- 42 C. Xu, L. Wang, Z. Liu, L. Chen, J. Guo, N. Kang, X. L. Ma, H. M. Cheng and W. Ren, Large-area high-quality 2D ultrathin  $Mo_2C$  superconducting crystals, *Nat. Mater.*, 2015, **14**, 1135–1141, DOI: [10.1038/nmat4374](https://doi.org/10.1038/nmat4374).
- 43 X. Xiao, H. Yu, H. Jin, M. Wu, Y. Fang, J. Sun, Z. Hu, T. Li, J. Wu, L. Huang, Y. Gogotsi and J. Zhou, Salt-Templated Synthesis of 2D Metallic MoN and Other Nitrides, *ACS Nano*, 2017, **11**, 2180–2186, DOI: [10.1021/acsnano.6b08534](https://doi.org/10.1021/acsnano.6b08534).
- 44 B. Yang, Y. Chen and J. Shi, Material Chemistry of Two-Dimensional Inorganic Nanosheets in Cancer Theranostics, *Chem*, 2018, **4**, 1284–1313, DOI: [10.1016/j.chempr.2018.02.012](https://doi.org/10.1016/j.chempr.2018.02.012).
- 45 S. K. Verma, E. Jha, K. J. Kiran, S. Bhat, M. Suar and P. S. Mohanty, Synthesis and characterization of novel polymer-hybrid silver nanoparticles and its biomedical study, *Mater. Today Proc.*, 2016, **3**, 1949–1957, DOI: [10.1016/j.matpr.2016.04.096](https://doi.org/10.1016/j.matpr.2016.04.096).
- 46 M. Carey, Z. Hinton, M. Sokol, N. J. Alvarez and M. W. Barsoum, Nylon-6/ $Ti_3C_2T_x$  MXene Nanocomposites Synthesized by *in Situ* Ring Opening Polymerization of  $\epsilon$ -Caprolactam and Their Water Transport Properties, *ACS Appl. Mater. Interfaces*, 2019, **11**, 20425–20436, DOI: [10.1021/acsami.9b05027](https://doi.org/10.1021/acsami.9b05027).
- 47 Z. Zhang, S. Yang, P. Zhang, J. Zhang, G. Chen and X. Feng, Mechanically strong MXene/Kevlar nanofiber composite membranes as high-performance nanofluidic osmotic power generators, *Nat. Commun.*, 2019, **10**, 2920, DOI: [10.1038/s41467-019-10885-8](https://doi.org/10.1038/s41467-019-10885-8).
- 48 X. Jin, J. Wang, L. Dai, X. Liu, L. Li, Y. Yang, Y. Cao, W. Wang, H. Wu and S. Guo, Flame-retardant poly(vinyl alcohol)/MXene multilayered films with outstanding electromagnetic interference shielding and thermal conductive performances, *Chem. Eng. J.*, 2020, **380**, 122475, DOI: [10.1016/j.cej.2019.122475](https://doi.org/10.1016/j.cej.2019.122475).
- 49 X. Wu, B. Han, H. Bin Zhang, X. Xie, T. Tu, Y. Zhang, Y. Dai, R. Yang and Z. Z. Yu, Compressible, durable and conductive polydimethylsiloxane-coated MXene foams for high-performance electromagnetic interference shielding, *Chem. Eng. J.*, 2020, **381**, 122622, DOI: [10.1016/j.cej.2019.122622](https://doi.org/10.1016/j.cej.2019.122622).
- 50 M. Wu, Q. Zhang, Y. Fang, C. Deng, F. Zhou, Y. Zhang, X. Wang, Y. Tang and Y. Wang, Polylysine-modified MXene nanosheets with highly loaded glucose oxidase as cascade nanoreactor for glucose decomposition and electrochemical sensing, *J. Colloid Interface Sci.*, 2021, **586**, 20–29, DOI: [10.1016/j.jcis.2020.10.065](https://doi.org/10.1016/j.jcis.2020.10.065).
- 51 H. Zhang, Z. Wang, F. Wang, Y. Zhang, H. Wang and Y. Liu,  $Ti_3C_2$  MXene mediated Prussian blue in situ hybridization and electrochemical signal amplification for the detection of exosomes, *Talanta*, 2021, **224**, 121879, DOI: [10.1016/j.talanta.2020.121879](https://doi.org/10.1016/j.talanta.2020.121879).
- 52 M. Ankitha, N. Shabana and P. A. Rasheed, A novel  $ReS_2-Nb_2CT_x$  composite as a sensing platform for ultrasensitive



- and selective electrochemical detection of dipyridole from human serum, *Graphene 2D Mater.*, 2023, **8**, 27–37, DOI: [10.1007/s41127-022-00055-x](https://doi.org/10.1007/s41127-022-00055-x).
- 53 W. Luo, H. Liu, X. Liu, L. Liu and W. Zhao, Biocompatibility nanoprobe of MXene N-Ti<sub>3</sub>C<sub>2</sub> quantum dot/Fe<sup>3+</sup> for detection and fluorescence imaging of glutathione in living cells, *Colloids Surf., B*, 2021, **201**, 111631, DOI: [10.1016/j.colsurfb.2021.111631](https://doi.org/10.1016/j.colsurfb.2021.111631).
- 54 Y. Nie, Z. Liang, P. Wang, Q. Ma and X. Su, MXene-Derived Quantum Dot@Gold Nanobones Heterostructure-Based Electrochemiluminescence Sensor for Triple-Negative Breast Cancer Diagnosis, *Anal. Chem.*, 2021, **93**, 17086–17093, DOI: [10.1021/acs.analchem.1c04184](https://doi.org/10.1021/acs.analchem.1c04184).
- 55 Y. Xu, X. Wang, C. Ding and X. Luo, Ratiometric antifouling electrochemical biosensors based on multifunctional peptides and MXene loaded with Au nanoparticles and methylene blue, *ACS Appl. Mater. Interfaces*, 2021, **13**, 20388–20396, DOI: [10.1021/acsami.1c04933](https://doi.org/10.1021/acsami.1c04933).
- 56 L. Liu, Y. Yao, K. Ma, C. Shangguan, S. Jiao, S. Zhu and X. Xu, Ultrasensitive photoelectrochemical detection of cancer-related miRNA-141 by carrier recombination inhibition in hierarchical Ti<sub>3</sub>C<sub>2</sub>@ReS<sub>2</sub>, *Sens. Actuators, B*, 2021, **331**, 129470, DOI: [10.1016/j.snb.2021.129470](https://doi.org/10.1016/j.snb.2021.129470).
- 57 P. Zhang, X. J. Yang, P. Li, Y. Zhao and Q. J. Niu, Fabrication of novel MXene (Ti<sub>3</sub>C<sub>2</sub>)/polyacrylamide nanocomposite hydrogels with enhanced mechanical and drug release properties, *Soft Matter*, 2019, **16**, 162–169, DOI: [10.1039/c9sm01985e](https://doi.org/10.1039/c9sm01985e).
- 58 C. Xing, S. Chen, X. Liang, Q. Liu, M. Qu, Q. Zou, J. Li, H. Tan, L. Liu, D. Fan and H. Zhang, Two-Dimensional MXene (Ti<sub>3</sub>C<sub>2</sub>)-Integrated Cellulose Hydrogels: Toward Smart Three-Dimensional Network Nanoplatfoms Exhibiting Light-Induced Swelling and Bimodal Photothermal/Chemotherapy Anticancer Activity, *ACS Appl. Mater. Interfaces*, 2018, **10**, 27631–27643, DOI: [10.1021/acsami.8b08314](https://doi.org/10.1021/acsami.8b08314).
- 59 K. Rasool, K. A. Mahmoud, D. J. Johnson, M. Helal, G. R. Berdiyrov and Y. Gogotsi, Efficient Antibacterial Membrane based on Two-Dimensional Ti<sub>3</sub>C<sub>2</sub>T<sub>x</sub> (MXene) Nanosheets, *Sci. Rep.*, 2017, **7**, 1598, DOI: [10.1038/s41598-017-01714-3](https://doi.org/10.1038/s41598-017-01714-3).
- 60 Y. Fu, J. B. Zhang, H. Lin and A. Mo, 2D titanium carbide(MXene) nanosheets and 1D hydroxyapatite nanowires into free standing nanocomposite membrane: in vitro and in vivo evaluations for bone regeneration, *Mater. Sci. Eng., C*, 2021, **118**, 111367, DOI: [10.1016/j.msec.2020.111367](https://doi.org/10.1016/j.msec.2020.111367).
- 61 Y. Li, M. Han, Y. Cai, B. Jiang, Y. Zhang, B. Yuan, F. Zhou and C. Cao, Muscle-inspired MXene/PVA hydrogel with high toughness and photothermal therapy for promoting bacteria-infected wound healing, *Biomater. Sci.*, 2022, **10**, 1068–1082, DOI: [10.1039/d1bm01604k](https://doi.org/10.1039/d1bm01604k).
- 62 C. Yang, Y. Luo, H. Lin, M. Ge, J. Shi and X. Zhang, Niobium Carbide MXene Augmented Medical Implant Elicits Bacterial Infection Elimination and Tissue Regeneration, *ACS Nano*, 2021, **15**, 1086–1099, DOI: [10.1021/acsnano.0c08045](https://doi.org/10.1021/acsnano.0c08045).
- 63 Q. Yang, H. Yin, T. Xu, D. Zhu, J. Yin, Y. Chen, X. Yu, J. Gao, C. Zhang, Y. Chen and Y. Gao, Engineering 2D Mesoporous Silica@MXene-Integrated 3D-Printing Scaffolds for Combinatory Osteosarcoma Therapy and NO-Augmented Bone Regeneration, *Small*, 2020, **16**, 1906814, DOI: [10.1002/smll.201906814](https://doi.org/10.1002/smll.201906814).
- 64 X. Xu, S. Wang, H. Wu, Y. Liu, F. Xu and J. Zhao, A multimodal antimicrobial platform based on MXene for treatment of wound infection, *Colloids Surf., B*, 2021, **207**, 111979, DOI: [10.1016/j.colsurfb.2021.111979](https://doi.org/10.1016/j.colsurfb.2021.111979).
- 65 A. Adhikari, D. Mandal, D. Rana, J. Nath, A. Bose, N. Sonika, J. T. Orasugh, S. De and D. Chattopadhyay, COVID-19 mitigation: nanotechnological intervention, perspective, and future scope, *Mater. Adv.*, 2022, **4**, 52–78, DOI: [10.1039/d2ma00797e](https://doi.org/10.1039/d2ma00797e).
- 66 S. Li, B. Gu, X. Li, S. Tang, L. Zheng, E. Ruiz-Hitzky, Z. Sun, C. Xu and X. Wang, MXene-Enhanced Chitin Composite Sponges with Antibacterial and Hemostatic Activity for Wound Healing, *Adv. Healthcare Mater.*, 2022, **11**, 2102367, DOI: [10.1002/adhm.202102367](https://doi.org/10.1002/adhm.202102367).
- 67 A. Prasad, M. R. Sankar and V. Katiyar, State of Art on Solvent Casting Particulate Leaching Method for Orthopedic ScaffoldsFabrication, *Mater. Today Proc.*, 2017, **4**, 898–907, DOI: [10.1016/j.matpr.2017.01.101](https://doi.org/10.1016/j.matpr.2017.01.101).
- 68 Y. Yang, H. Zhang, F. Zeng, Q. Jia, L. Zhang, A. Yu and B. Duan, A quaternized chitin derivatives, egg white protein and montmorillonite composite sponge with antibacterial and hemostatic effect for promoting wound healing, *Composites, Part B*, 2022, **234**, 109661, DOI: [10.1016/j.compositesb.2022.109661](https://doi.org/10.1016/j.compositesb.2022.109661).
- 69 L. Guo, K. Hu and H. Wang, Antimicrobial and Mechanical Properties of Ag@Ti<sub>3</sub>C<sub>2</sub>T<sub>x</sub>-Modified PVA Composite Hydrogels Enhanced with Quaternary Ammonium Chitosan, *Polymers*, 2023, **15**, 2352, DOI: [10.3390/polym15102352](https://doi.org/10.3390/polym15102352).
- 70 J. Li, Z. Li, X. Liu, C. Li, Y. Zheng, K. W. K. Yeung, Z. Cui, Y. Liang, S. Zhu, W. Hu, Y. Qi, T. Zhang, X. Wang and S. Wu, Interfacial engineering of Bi<sub>2</sub>S<sub>3</sub>/Ti<sub>3</sub>C<sub>2</sub>T<sub>x</sub> MXene based on work function for rapid photo-excited bacteria-killing, *Nat. Commun.*, 2021, **12**, 1224, DOI: [10.1038/s41467-021-21435-6](https://doi.org/10.1038/s41467-021-21435-6).
- 71 M. Khatami, P. Irvani, G. Jamalipour Soufi and S. Irvani, MXenes for antimicrobial and antiviral applications: recent advances, *Mater. Technol.*, 2022, **37**, 1890–1905, DOI: [10.1080/10667857.2021.2002587](https://doi.org/10.1080/10667857.2021.2002587).
- 72 Y. Zheng, Y. Yan, L. Lin, Q. He, H. Hu, R. Luo, D. Xian, J. Wu, Y. Shi, F. Zeng, C. Wu, G. Quan and C. Lu, Titanium carbide MXene-based hybrid hydrogel for chemophotothermal combinational treatment of localized bacterial infection, *Acta Biomater.*, 2022, **142**, 113–123, DOI: [10.1016/j.actbio.2022.02.019](https://doi.org/10.1016/j.actbio.2022.02.019).
- 73 X. Zhou, Z. Wang, Y. K. Chan, Y. Yang, Z. Jiao, L. Li, J. Li, K. Liang and Y. Deng, Infection Micromilieu-Activated Nanocatalytic Membrane for Orchestrating Rapid Sterilization and Stalled Chronic Wound Regeneration, *Adv. Funct. Mater.*, 2022, **32**, 2109469, DOI: [10.1002/adfm.202109469](https://doi.org/10.1002/adfm.202109469).
- 74 K. Rasool, M. Helal, A. Ali, C. E. Ren, Y. Gogotsi and K. A. Mahmoud, Antibacterial Activity of Ti<sub>3</sub>C<sub>2</sub>T<sub>x</sub> MXene,



- ACS Nano*, 2016, **10**, 3674–3684, DOI: [10.1021/acsnano.6b00181](https://doi.org/10.1021/acsnano.6b00181).
- 75 Z. P. Li, D. Xu, Z. Deng, J. Yin, Y. Qian, J. T. Hou, X. Ding, J. Shen and X. He, Single-Atom-Catalyzed MXene-Based nanoplatform with Photo-Enhanced Peroxidase-Like activity nanotherapeutics for Staphylococcus aureus infection, *Chem. Eng. J.*, 2023, **452**(4), 139587, DOI: [10.1016/j.cej.2022.139587](https://doi.org/10.1016/j.cej.2022.139587).
- 76 H. Yuan, X. Hong, H. Ma, C. Fu, Y. Guan, W. Huang, J. Ma, P. Xia, M. Cao, L. Zheng, X. Xu, C. Xu, D. Liu, Z. Li, Q. Geng and J. Wang, MXene-Based Dual Functional Nanocomposite with Photothermal Nanozyme Catalytic Activity to Fight Bacterial Infections, *ACS Mater. Lett.*, 2023, **5**, 762–774, DOI: [10.1021/acsmaterialslett.2c00771](https://doi.org/10.1021/acsmaterialslett.2c00771).
- 77 X. Sun, X. He, Y. Zhu, E. Obeng, B. Zeng, H. Deng, J. Shen and R. Hu, Valence-Switchable and Biocatalytic Vanadium-Based Mxene Nanoplatform with Photothermal-Enhanced Dual Enzyme-Like Activities for Anti-Infective Therapy, *SSRN Electron. J.*, 2022, 138985, DOI: [10.2139/ssrn.4156471](https://doi.org/10.2139/ssrn.4156471).
- 78 L. Zhou, H. Zheng, Z. Liu, S. Wang, Z. Liu, F. Chen, H. Zhang, J. Kong, F. Zhou and Q. Zhang, Conductive Antibacterial Hemostatic Multifunctional Scaffolds Based on  $Ti_3C_2T_x$  MXene Nanosheets for Promoting Multidrug-Resistant Bacteria-Infected Wound Healing, *ACS Nano*, 2021, **15**, 2468–2480, DOI: [10.1021/acsnano.0c06287](https://doi.org/10.1021/acsnano.0c06287).
- 79 R. P. Pandey, K. Rasool, V. E. Madhavan, B. Aïssa, Y. Gogotsi and K. A. Mahmoud, Ultrahigh-flux and fouling-resistant membranes based on layered silver/MXene ( $Ti_3C_2T_x$ ) nanosheets, *J. Mater. Chem. A*, 2018, **6**, 3522–3533, DOI: [10.1039/C7TA10888E](https://doi.org/10.1039/C7TA10888E).
- 80 Z. Li, Y. Wei, X. Gao, L. Ding, Z. Lu, J. Deng, X. Yang, J. Caro and H. Wang, Antibiotics Separation with MXene Membranes Based on Regularly Stacked High-Aspect-Ratio Nanosheets, *Angew. Chem.*, 2020, **132**, 9838–9843, DOI: [10.1002/ange.202002935](https://doi.org/10.1002/ange.202002935).
- 81 M. Malaki, A. Maleki and R. S. Varma, MXenes and ultrasonication, *J. Mater. Chem. A*, 2019, **7**, 10843–10857, DOI: [10.1039/c9ta01850f](https://doi.org/10.1039/c9ta01850f).
- 82 D. Chen, Z. Jin, B. Zhao, Y. Wang and Q. He, MBene as a Theranostic Nanoplatform for Photocontrolled Intratumoral Retention and Drug Release, *Adv. Mater.*, 2021, **33**, 2008089, DOI: [10.1002/adma.202008089](https://doi.org/10.1002/adma.202008089).
- 83 X. Yang, C. Zhang, D. Deng, Y. Gu, H. Wang and Q. Zhong, Multiple Stimuli-Responsive MXene-Based Hydrogel as Intelligent Drug Delivery Carriers for Deep Chronic Wound Healing, *Small*, 2022, **18**, 2104368, DOI: [10.1002/smll.202104368](https://doi.org/10.1002/smll.202104368).
- 84 W. Sinshaw, A. Kebede, A. Bitew, E. Tesfaye, M. Tadesse, Z. Mehamed, B. Yenew, M. Amare, B. Dagne, G. Diriba, A. Alemu, M. Getahun, D. Fikadu, K. Desta and H. H. Tola, Prevalence of tuberculosis, multidrug resistant tuberculosis and associated risk factors among smear negative presumptive pulmonary tuberculosis patients in Addis Ababa, Ethiopia, *BMC Infect. Dis.*, 2019, **19**, 641, DOI: [10.1186/s12879-019-4241-7](https://doi.org/10.1186/s12879-019-4241-7).
- 85 M. Mathew and C. S. Rout, Electrochemical biosensors based on  $Ti_3C_2T_x$  MXene: future perspectives for on-site analysis, *Curr. Opin. Electrochem.*, 2021, **30**, 100782, DOI: [10.1016/j.coelec.2021.100782](https://doi.org/10.1016/j.coelec.2021.100782).
- 86 J. Zhang, Y. Li, S. Duan and F. He, Highly electrically conductive two-dimensional  $Ti_3C_2$  Mxenes-based 16S rDNA electrochemical sensor for detecting Mycobacterium tuberculosis, *Anal. Chim. Acta*, 2020, **1123**, 9–17, DOI: [10.1016/j.aca.2020.05.013](https://doi.org/10.1016/j.aca.2020.05.013).
- 87 Q. Zhang, W. Huang, C. Yang, F. Wang, C. Song, Y. Gao, Y. Qiu, M. Yan, B. Yang and C. Guo, The theranostic nanoagent  $Mo_2C$  for multi-modal imaging-guided cancer synergistic phototherapy, *Biomater. Sci.*, 2019, **7**, 2729–2739, DOI: [10.1039/c9bm00239a](https://doi.org/10.1039/c9bm00239a).
- 88 Z. Liu, M. Zhao, H. Lin, C. Dai, C. Ren, S. Zhang, W. Peng and Y. Chen, 2D magnetic titanium carbide MXene for cancer theranostics, *J. Mater. Chem. B*, 2018, **6**, 3541–3548, DOI: [10.1039/c8tb00754c](https://doi.org/10.1039/c8tb00754c).
- 89 A. Szuplewska, D. Kulpińska, A. Dybko, A. M. Jastrzębska, T. Wojciechowski, A. Rozmysłowska, M. Chudy, I. Grabowska-Jadach, W. Ziemkowska, Z. Brzózka and A. Olszyna, 2D  $Ti_2C$  (MXene) as a novel highly efficient and selective agent for photothermal therapy, *Mater. Sci. Eng., C*, 2019, **98**, 874–886, DOI: [10.1016/j.msec.2019.01.021](https://doi.org/10.1016/j.msec.2019.01.021).
- 90 X. Han, X. Jing, D. Yang, H. Lin, Z. Wang, H. Ran, P. Li and Y. Chen, Therapeutic mesopore construction on 2D  $Nb_2C$  MXenes for targeted and enhanced chemo-photothermal cancer therapy in NIR-II biowindow, *Theranostics*, 2018, **8**, 4491–4508, DOI: [10.7150/thno.26291](https://doi.org/10.7150/thno.26291).
- 91 Y. Fu, S. Huang, Z. Feng, L. Huang, X. Zhang, H. Lin and A. Mo, MXene-Functionalized Ferroelectric Nanocomposite Membranes with Modulating Surface Potential Enhance Bone Regeneration, *ACS Biomater. Sci. Eng.*, 2023, **9**, 900–917, DOI: [10.1021/acsbiomaterials.2c01174](https://doi.org/10.1021/acsbiomaterials.2c01174).
- 92 C. Dai, Y. Chen, X. Jing, L. Xiang, D. Yang, H. Lin, Z. Liu, X. Han and R. Wu, Two-Dimensional Tantalum Carbide (MXenes) Composite Nanosheets for Multiple Imaging-Guided Photothermal Tumor Ablation, *ACS Nano*, 2017, **11**, 12696–12712, DOI: [10.1021/acsnano.7b07241](https://doi.org/10.1021/acsnano.7b07241).
- 93 A. Zavabeti, A. Jannat, L. Zhong, A. A. Haidry, Z. Yao and J. Z. Ou, Two-Dimensional Materials in Large-Areas: Synthesis, Properties and Applications, *Nano-Micro Lett.*, 2020, **12**, 66, DOI: [10.1007/s40820-020-0402-x](https://doi.org/10.1007/s40820-020-0402-x).
- 94 W. Tang, Z. Dong, R. Zhang, X. Yi, K. Yang, M. Jin, C. Yuan, Z. Xiao, Z. Liu and L. Cheng, Multifunctional Two-Dimensional Core-Shell MXene@Gold Nanocomposites for Enhanced Photo-Radio Combined Therapy in the Second Biological Window, *ACS Nano*, 2019, **13**, 284–294, DOI: [10.1021/acsnano.8b05982](https://doi.org/10.1021/acsnano.8b05982).
- 95 S. Zada, W. Dai, Z. Kai, H. Lu, X. Meng, Y. Zhang, Y. Cheng, F. Yan, P. Fu, X. Zhang and H. Dong, Algae Extraction Controllable Delamination of Vanadium Carbide Nanosheets with Enhanced Near-Infrared Photothermal Performance, *Angew. Chem.*, 2020, **132**, 6663–6668, DOI: [10.1002/ange.201916748](https://doi.org/10.1002/ange.201916748).
- 96 H. Lin, Y. Wang, S. Gao, Y. Chen and J. Shi, Theranostic 2D Tantalum Carbide (MXene), *Adv. Mater.*, 2018, **30**, 1703284, DOI: [10.1002/adma.201703284](https://doi.org/10.1002/adma.201703284).



- 97 X. Chang, Q. Wu, Y. Wu, X. Xi, J. Cao, H. Chu, Q. Liu, Y. Li, W. Wu, X. Fang and F. Chen, Multifunctional Au Modified  $Ti_3C_2$ -MXene for Photothermal/Enzyme Dynamic/Immune Synergistic Therapy, *Nano Lett.*, 2022, 22, 8321–8330, DOI: [10.1021/acs.nanolett.2c03260](https://doi.org/10.1021/acs.nanolett.2c03260).
- 98 Y. Zhu, Z. Wang, R. Zhao, Y. Zhou, L. Feng, S. Gai and P. Yang, Pt Decorated  $Ti_3C_2T_x$  MXene with NIR-II Light Amplified Nanozyme Catalytic Activity for Efficient Phototheranostics, *ACS Nano*, 2022, 16, 3105–3118, DOI: [10.1021/acsnano.1c10732](https://doi.org/10.1021/acsnano.1c10732).
- 99 T. Liao, Z. Chen, Y. Kuang, Z. Ren, W. Yu, W. Rao, L. Li, Y. Liu, Z. Xu, B. Jiang and C. Li, Small-size  $Ti_3C_2T_x$  MXene nanosheets coated with metal-polyphenol nanodots for enhanced cancer photothermal therapy and anti-inflammation, *Acta Biomater.*, 2023, 159, 312–323, DOI: [10.1016/j.actbio.2023.01.049](https://doi.org/10.1016/j.actbio.2023.01.049).
- 100 Y. Lu, X. Zhang, X. Hou, M. Feng, Z. Cao and J. Liu, Functionalized 2D  $Nb_2C$  nanosheets for primary and recurrent cancer photothermal/immune-therapy in the NIR-II biowindow, *Nanoscale*, 2021, 13, 17822–17836, DOI: [10.1039/d1nr05126a](https://doi.org/10.1039/d1nr05126a).
- 101 Z. Wang, H. Li, W. She, X. Zhang, Y. Liu, Y. Liu and P. Jiang, 3-Bromopyruvate-Loaded  $Ti_3C_2$  MXene/ $Cu_2O$  Nanosheets for Photoacoustic Imaging-Guided and Hypoxia-Relieving Enhanced Photothermal/Chemodynamic Therapy, *Anal. Chem.*, 2023, 95, 1710–1720, DOI: [10.1021/acs.analchem.2c04953](https://doi.org/10.1021/acs.analchem.2c04953).
- 102 Z. Huang, X. Cui, S. Li, J. Wei, P. Li, Y. Wang and C. S. Lee, Two-dimensional MXene-based materials for photothermal therapy, *Nanophotonics*, 2020, 9, 2233–2249, DOI: [10.1515/nanoph-2019-0571](https://doi.org/10.1515/nanoph-2019-0571).
- 103 M. Aghajanzadeh, M. Zamani, F. R. Kouchi, J. Eixenberger, D. Shirini, D. Estrada and F. Shirini, Synergic Antitumor Effect of Photodynamic Therapy and Chemotherapy Mediated by Nano Drug Delivery Systems, *Pharmaceutics*, 2022, 14(2), 322, DOI: [10.3390/pharmaceutics14020322](https://doi.org/10.3390/pharmaceutics14020322).
- 104 Z. Bai, L. Zhao, H. Feng, H. Xu, N. Zhang, Y. Li, J. Song, Y. Bai, R. Yang and F. Feng, Fabricating Aptamer-functionalized  $Ti_3C_2$  therapeutic nanoplatform for targeted chemo-photothermal therapy of cancer, *Mater. Des.*, 2023, 226, 111656, DOI: [10.1016/j.matdes.2023.111656](https://doi.org/10.1016/j.matdes.2023.111656).
- 105 B. Anasori, M. R. Lukatskaya and Y. Gogotsi, 2D metal carbides and nitrides (MXenes) for energy storage, *MXenes From Discov. to Appl. Two-Dimensional Met. Carbides Nitrides*, 2023, pp. 677–722, DOI: [10.1201/9781003306511-35](https://doi.org/10.1201/9781003306511-35).
- 106 H. Assad, I. Fatma, A. Kumar, S. Kaya, D. V. N. Vo, A. Al-Gheethi and A. Sharma, An overview of MXene-Based nanomaterials and their potential applications towards hazardous pollutant adsorption, *Chemosphere*, 2022, 298, 134221, DOI: [10.1016/j.chemosphere.2022.134221](https://doi.org/10.1016/j.chemosphere.2022.134221).
- 107 S. S. Naser, B. Ghosh, F. Z. Simnani, D. Singh, A. Choudhury, A. Nandi, A. Sinha, E. Jha, P. K. Panda, M. Suar and S. K. Verma, Emerging Trends in the Application of Green Synthesized Biocompatible ZnO Nanoparticles for Translational Paradigm in Cancer Therapy, *J. Nanotheranostics*, 2023, 4, 248–279, DOI: [10.3390/jnt4030012](https://doi.org/10.3390/jnt4030012).
- 108 M. Soleymaniha, M. A. Shahbazi, A. R. Rafieerad, A. Maleki and A. Amiri, Promoting Role of MXene Nanosheets in Biomedical Sciences: Therapeutic and Biosensing Innovations, *Adv. Healthcare Mater.*, 2019, 8, 1801137, DOI: [10.1002/adhm.201801137](https://doi.org/10.1002/adhm.201801137).
- 109 Z. Xie, S. Chen, Y. Duo, Y. Zhu, T. Fan, Q. Zou, M. Qu, Z. Lin, J. Zhao, Y. Li, L. Liu, S. Bao, H. Chen, D. Fan and H. Zhang, Biocompatible Two-Dimensional Titanium Nanosheets for Multimodal Imaging-Guided Cancer Theranostics, *ACS Appl. Mater. Interfaces*, 2019, 11, 22129–22140, DOI: [10.1021/acsami.9b04628](https://doi.org/10.1021/acsami.9b04628).
- 110 P. Patel, A. Nandi, E. Jha, A. Sinha, S. Mohanty, P. K. Panda, S. Mishra, S. K. Verma and M. Suar, Magnetic nanoparticles: fabrication, characterization, properties, and application for environment sustainability, *Magn Nanoparticle-Based Hybrid Mater. Fundam. Appl.*, 2021, pp. 33–64, DOI: [10.1016/B978-0-12-823688-8.00017-X](https://doi.org/10.1016/B978-0-12-823688-8.00017-X).
- 111 S. S. Naser, D. Singh, S. Preetam, S. Kishore, L. Kumar, A. Nandi, F. Z. Simnani, A. Choudhury, A. Sinha, Y. K. Mishra, M. Suar, P. K. Panda, S. Malik and S. K. Verma, Posterity of nanoscience as lipid nanosystems for Alzheimer's disease regression, *Mater. Today Bio*, 2023, 21, 100701, DOI: [10.1016/j.mtmbio.2023.100701](https://doi.org/10.1016/j.mtmbio.2023.100701).
- 112 P. K. Panda, S. K. Verma and M. Suar, Nanoparticle-biological interactions: the renaissance of bionomics in the myriad nanomedical technologies, *Nanomedicine*, 2021, 16, 2249–2254, DOI: [10.2217/nnm-2021-0174](https://doi.org/10.2217/nnm-2021-0174).
- 113 B. Zhou, H. Yin, C. Dong, L. Sun, W. Feng, Y. Pu, X. Han, X. Li, D. Du, H. Xu and Y. Chen, Biodegradable and Excretable 2D  $W_{1.33C}$  i-MXene with Vacancy Ordering for Theory-Oriented Cancer Nanotheranostics in Near-Infrared Biowindow, *Adv. Sci.*, 2021, 8, 2101043, DOI: [10.1002/advs.202101043](https://doi.org/10.1002/advs.202101043).
- 114 A. Gazzì, L. Fusco, A. Khan, D. Bedognetti, B. Zavan, F. Vitale, A. Yilmazer and L. G. Delogu, Photodynamic therapy based on graphene and MXene in cancer theranostics, *Front. Bioeng. Biotechnol.*, 2019, 7, 295, DOI: [10.3389/fbioe.2019.00295](https://doi.org/10.3389/fbioe.2019.00295).
- 115 V. S. Sivasankarapillai, A. K. Somakumar, J. Joseph, S. Nikazar, A. Rahdar and G. Z. Kyzas, Cancer theranostic applications of MXene nanomaterials: recent updates, *Nano-Struct. Nano-Objects*, 2020, 22, 100457, DOI: [10.1016/j.nanoso.2020.100457](https://doi.org/10.1016/j.nanoso.2020.100457).
- 116 G. Liu, J. Zou, Q. Tang, X. Yang, Y. Zhang, Q. Zhang, W. Huang, P. Chen, J. Shao and X. Dong, Surface Modified  $Ti_3C_2$  MXene Nanosheets for Tumor Targeting Photothermal/Photodynamic/Chemo Synergistic Therapy, *ACS Appl. Mater. Interfaces*, 2017, 9, 40077–40086, DOI: [10.1021/acsami.7b13421](https://doi.org/10.1021/acsami.7b13421).
- 117 D. Y. Zhang, H. Liu, M. R. Younis, S. Lei, Y. Chen, P. Huang and J. Lin, *In situ*  $TiO_{2-x}$  decoration of titanium carbide MXene for photo/sono-responsive antitumor theranostics, *J. Nanobiotechnol.*, 2022, 20, 53, DOI: [10.1186/s12951-022-01253-8](https://doi.org/10.1186/s12951-022-01253-8).





- 118 S. Irvani and R. S. Varma, Smart MXene Quantum Dot-Based Nanosystems for Biomedical Applications, *Nanomaterials*, 2022, **12**, 1200, DOI: [10.3390/nano12071200](https://doi.org/10.3390/nano12071200).
- 119 J. Shao, J. Zhang, C. Jiang, J. Lin and P. Huang, Biodegradable titanium nitride MXene quantum dots for cancer phototheranostics in NIR-I/II biowindows, *Chem. Eng. J.*, 2020, **400**, 126009, DOI: [10.1016/j.cej.2020.126009](https://doi.org/10.1016/j.cej.2020.126009).
- 120 B. Singh, R. Bahadur, P. Maske, M. Gandhi, D. Singh and R. Srivastava, Preclinical safety assessment of red emissive gold nanocluster conjugated crumpled MXene nanosheets: a dynamic duo for image-guided photothermal therapy, *Nanoscale*, 2023, **15**, 2932–2947, DOI: [10.1039/d2nr05773e](https://doi.org/10.1039/d2nr05773e).
- 121 Y. Cao, T. Wu, K. Zhang, X. Meng, W. Dai, D. Wang, H. Dong and X. Zhang, Engineered Exosome-Mediated Near-Infrared-II Region V<sub>2</sub>C Quantum Dot Delivery for Nucleus-Target Low-Temperature Photothermal Therapy, *ACS Nano*, 2019, **13**(2), 1499–1510, DOI: [10.1021/acsnano.8b07224](https://doi.org/10.1021/acsnano.8b07224).
- 122 R. D. Nagarajan, A. Sundaramurthy and A. K. Sundramoorthy, Synthesis and characterization of MXene (Ti<sub>3</sub>C<sub>2</sub>T<sub>x</sub>)/Iron oxide composite for ultrasensitive electrochemical detection of hydrogen peroxide, *Chemosphere*, 2022, **286**, 131478, DOI: [10.1016/j.chemosphere.2021.131478](https://doi.org/10.1016/j.chemosphere.2021.131478).
- 123 F. Beigmoradi and H. Beitollahi, MXene/La<sup>3+</sup> Doped ZnO/Hb Nanocomposite Modified Glassy Carbon Electrode as Novel Voltammetric Sensor for Determination of Hydrogen Peroxide, *Surf. Eng. Appl. Electrochem.*, 2021, **57**, 708–714, DOI: [10.3103/S106837552106003X](https://doi.org/10.3103/S106837552106003X).
- 124 R. D. Nagarajan, P. Murugan, K. Palaniyandi, R. Atchudan and A. K. Sundramoorthy, Biocompatible MXene (Ti<sub>3</sub>C<sub>2</sub>T<sub>x</sub>) immobilized with flavin adenine dinucleotide as an electrochemical transducer for hydrogen peroxide detection in ovarian cancer cell lines, *Micromachines*, 2021, **12**, 862, DOI: [10.3390/mi12080862](https://doi.org/10.3390/mi12080862).
- 125 F. Zhu, X. Wang, X. Yang, C. Zhao, Y. Zhang, S. Qu, S. Wu and W. Ji, Reasonable design of an MXene-based enzyme-free amperometric sensing interface for highly sensitive hydrogen peroxide detection, *Anal. Methods*, 2021, **13**, 2512–2518, DOI: [10.1039/d1ay00568e](https://doi.org/10.1039/d1ay00568e).
- 126 Q. Wu, N. Li, Y. Wang, Y. Liu, Y. Xu, S. Wei, J. Wu, G. Jia, X. Fang, F. Chen and X. Cui, A 2D transition metal carbide MXene-based SPR biosensor for ultrasensitive carcinoembryonic antigen detection, *Biosens. Bioelectron.*, 2019, **144**, 111697, DOI: [10.1016/j.bios.2019.111697](https://doi.org/10.1016/j.bios.2019.111697).
- 127 Y. Li, Z. Kang, L. Kong, H. Shi, Y. Zhang, M. Cui and D. P. Yang, MXene-Ti<sub>3</sub>C<sub>2</sub>/CuS nanocomposites: enhanced peroxidase-like activity and sensitive colorimetric cholesterol detection, *Mater. Sci. Eng., C*, 2019, **104**, 110000, DOI: [10.1016/j.msec.2019.110000](https://doi.org/10.1016/j.msec.2019.110000).
- 128 G. Cai, Z. Yu, P. Tong and D. Tang, Ti<sub>3</sub>C<sub>2</sub> MXene quantum dot-encapsulated liposomes for photothermal immunoassays using a portable near-infrared imaging camera on a smartphone, *Nanoscale*, 2019, **11**, 15659–15667, DOI: [10.1039/c9nr05797h](https://doi.org/10.1039/c9nr05797h).
- 129 Y. Guo, M. Zhong, Z. Fang, P. Wan and G. Yu, A Wearable Transient Pressure Sensor Made with MXene Nanosheets for Sensitive Broad-Range Human–Machine Interfacing, *Nano Lett.*, 2019, **19**, 1143–1150, DOI: [10.1021/acs.nanolett.8b04514](https://doi.org/10.1021/acs.nanolett.8b04514).
- 130 Q. Li, X. Zhi, Y. Xia, S. Han, W. Guo, M. Li and X. Wang, Ultrastretchable High-Conductivity MXene-Based Organohydrogels for Human Health Monitoring and Machine-Learning-Assisted Recognition, *ACS Appl. Mater. Interfaces*, 2023, **15**, 19435–19446, DOI: [10.1021/acsmi.3c00432](https://doi.org/10.1021/acsmi.3c00432).
- 131 A. C. Y. Yuen, T. B. Y. Chen, B. Lin, W. Yang, I. I. Kabir, I. M. De Cachinho Cordeiro, A. E. Whitten, J. Mata, B. Yu, H. D. Lu and G. H. Yeoh, Study of structure morphology and layer thickness of Ti<sub>3</sub>C<sub>2</sub> MXene with Small-Angle Neutron Scattering (SANS), *Compos., Part C: Open Access*, 2021, **5**, 100155, DOI: [10.1016/j.jcomc.2021.100155](https://doi.org/10.1016/j.jcomc.2021.100155).
- 132 K. L. Firestein, J. E. von Treifeldt, D. G. Kvashnin, J. F. S. Fernando, C. Zhang, A. G. Kvashnin, E. V. Podryabinkin, A. V. Shapeev, D. P. Siriwardena, P. B. Sorokin and D. Golberg, Young's Modulus and Tensile Strength of Ti<sub>3</sub>C<sub>2</sub> MXene Nanosheets As Revealed by In Situ TEM Probing, AFM Nanomechanical Mapping, and Theoretical Calculations, *Nano Lett.*, 2020, **20**, 5900–5908, DOI: [10.1021/acs.nanolett.0c01861](https://doi.org/10.1021/acs.nanolett.0c01861).
- 133 J. Luo, S. Gao, H. Luo, L. Wang, X. Huang, Z. Guo, X. Lai, L. Lin, R. K. Y. Li and J. Gao, Superhydrophobic and breathable smart MXene-based textile for multifunctional wearable sensing electronics, *Chem. Eng. J.*, 2021, **406**, 126898, DOI: [10.1016/j.cej.2020.126898](https://doi.org/10.1016/j.cej.2020.126898).
- 134 C. Jin and Z. Bai, MXene-Based Textile Sensors for Wearable Applications, *ACS Sens.*, 2022, **7**, 929–950, DOI: [10.1021/acssensors.2c00097](https://doi.org/10.1021/acssensors.2c00097).
- 135 V. Adepu, A. Kunchur, M. Tathacharya, V. Mattela and P. Sahatiya, SnS/Ti<sub>3</sub>C<sub>2</sub>T<sub>x</sub>(MXene) Nanohybrid-Based Wearable Electromechanical Sensors for Sign-to-Text Translation and Sitting Posture Analysis, *ACS Appl. Electron. Mater.*, 2022, **4**, 1756–1768, DOI: [10.1021/acsaem.2c00026](https://doi.org/10.1021/acsaem.2c00026).
- 136 Z. Yang, S. Lv, Y. Zhang, J. Wang, L. Jiang, X. Jia, C. Wang, X. Yan, P. Sun, Y. Duan, F. Liu and G. Lu, Self-Assembly 3D Porous Crumpled MXene Spheres as Efficient Gas and Pressure Sensing Material for Transient All-MXene Sensors, *Nano-Micro Lett.*, 2022, **14**, 56, DOI: [10.1007/s40820-022-00796-7](https://doi.org/10.1007/s40820-022-00796-7).
- 137 Y. Zheng, R. Yin, Y. Zhao, H. Liu, D. Zhang, X. Shi, B. Zhang, C. Liu and C. Shen, Conductive MXene/cotton fabric based pressure sensor with both high sensitivity and wide sensing range for human motion detection and E-skin, *Chem. Eng. J.*, 2021, **420**, 127720, DOI: [10.1016/j.cej.2020.127720](https://doi.org/10.1016/j.cej.2020.127720).
- 138 Y. Lei, W. Zhao, Y. Zhang, Q. Jiang, J. H. He, A. J. Baeumner, O. S. Wolfbeis, Z. L. Wang, K. N. Salama and H. N. Alshareef, A MXene-Based Wearable Biosensor System for High-Performance In Vitro Perspiration Analysis, *Small*, 2019, **15**, 1901190, DOI: [10.1002/sml.201901190](https://doi.org/10.1002/sml.201901190).
- 139 H. Xing, X. Li, Y. Lu, Y. Wu, Y. He, Q. Chen, Q. Liu and R. P. S. Han, Mxene/Mwcnt Electronic Fabric with Enhanced Mechanical Robustness on Humidity Sensing



- for Real-Time Respiration Monitoring, *SSRN Electron. J.*, 2022, 131704, DOI: [10.2139/ssrn.4016292](https://doi.org/10.2139/ssrn.4016292).
- 140 X. Fu, L. Wang, L. Zhao, Z. Yuan, Y. Zhang, D. Wang, D. Wang, J. Li, D. Li, V. Shulga, G. Shen and W. Han, Controlled Assembly of MXene Nanosheets as an Electrode and Active Layer for High-Performance Electronic Skin, *Adv. Funct. Mater.*, 2021, **31**, 2010533, DOI: [10.1002/adfm.202010533](https://doi.org/10.1002/adfm.202010533).
- 141 Y. Guo, M. Zhong, Z. Fang, P. Wan and G. Yu, A Wearable Transient Pressure Sensor Made with MXene Nanosheets for Sensitive Broad-Range Human–Machine Interfacing, *Nano Lett.*, 2019, **19**, 1143–1150, DOI: [10.1021/acs.nanolett.8b04514](https://doi.org/10.1021/acs.nanolett.8b04514).
- 142 P. Mohanty, P. K. Singh, B. Lenka, T. K. Adhya, S. K. Verma, Z. Ayreen, S. Patro, B. Sarkar, R. K. Mohapatra and S. Mishra, Biofabricated nanomaterials in sustainable agriculture: insights, challenges and prospects, *Biofabrication*, 2024, **16**, 042003, DOI: [10.1088/1758-5090/ad60f7](https://doi.org/10.1088/1758-5090/ad60f7).
- 143 M. H. Abbasi Geravand, E. Saljoughi, S. M. Mousavi and S. Kiani, Biodegradable polycaprolactone/MXene nanocomposite nanofiltration membranes for the treatment of dye solutions, *J. Taiwan Inst. Chem. Eng.*, 2021, **128**, 124–139, DOI: [10.1016/j.jtice.2021.08.048](https://doi.org/10.1016/j.jtice.2021.08.048).
- 144 W. Zhang, Z. Pan, J. Ma, L. Wei, Z. Chen and J. Wang, Degradable Cross-Linked Collagen Fiber/MXene Composite Aerogels as a High-Performing Sensitive Pressure Sensor, *ACS Sustainable Chem. Eng.*, 2022, **10**, 1408–1418, DOI: [10.1021/acssuschemeng.1c05757](https://doi.org/10.1021/acssuschemeng.1c05757).
- 145 A. Rafieerad, W. Yan, G. L. Sequiera, N. Sareen, E. Abu-El-Rub, M. Moudgil and S. Dhingra, Application of Ti<sub>3</sub>C<sub>2</sub> MXene Quantum Dots for Immunomodulation and Regenerative Medicine, *Adv. Healthcare Mater.*, 2019, **8**, 1900569, DOI: [10.1002/adhm.201900569](https://doi.org/10.1002/adhm.201900569).
- 146 A. Rafieerad, W. Yan, K. N. Alagarsamy, A. Srivastava, N. Sareen, R. C. Arora and S. Dhingra, Fabrication of Smart Tantalum Carbide MXene Quantum Dots with Intrinsic Immunomodulatory Properties for Treatment of Allograft Vasculopathy, *Adv. Funct. Mater.*, 2021, **31**, 2106786, DOI: [10.1002/adfm.202106786](https://doi.org/10.1002/adfm.202106786).
- 147 G. P. Awasthi, B. Maharjan, S. Shrestha, D. P. Bhattarai, D. Yoon, C. H. Park and C. S. Kim, Synthesis, characterizations, and biocompatibility evaluation of polycaprolactone–MXene electrospun fibers, *Colloids Surf., A*, 2020, **586**, 124282, DOI: [10.1016/j.colsurfa.2019.124282](https://doi.org/10.1016/j.colsurfa.2019.124282).
- 148 N. Driscoll, K. Maleski, A. G. Richardson, B. Murphy, B. Anasori, T. H. Lucas, Y. Gogotsi and F. Vitale, Fabrication of Ti<sub>3</sub>C<sub>2</sub> MXene microelectrode arrays for in vivo neural recording, *J. Visualized Exp.*, 2020, **2020**, 156, DOI: [10.3791/60741](https://doi.org/10.3791/60741).
- 149 H. Rastin, B. Zhang, A. Mazinani, K. Hassan, J. Bi, T. T. Tung and D. Losic, 3D bioprinting of cell-laden electroconductive MXene nanocomposite bioinks, *Nanoscale*, 2020, **12**, 16069–16080, DOI: [10.1039/d0nr02581j](https://doi.org/10.1039/d0nr02581j).
- 150 J. H. Jang, J. S. Oh, E. J. Lee and C. M. Han, Electrophoretically deposition of Ti<sub>3</sub>C<sub>2</sub> on titanium surface for hard tissue implant applications, *Coatings*, 2021, **11**(7), 761, DOI: [10.3390/coatings11070761](https://doi.org/10.3390/coatings11070761).
- 151 J. Zhang, Y. Fu and A. Mo, Multilayered titanium carbide MXene film for guided bone regeneration, *Int. J. Nanomed.*, 2019, **14**, 10091–10103, DOI: [10.2147/IJN.S227830](https://doi.org/10.2147/IJN.S227830).
- 152 N. Driscoll, A. G. Richardson, K. Maleski, B. Anasori, O. Adewole, P. Lelyukh, L. Escobedo, D. K. Cullen, T. H. Lucas, Y. Gogotsi and F. Vitale, Two-Dimensional Ti<sub>3</sub>C<sub>2</sub> MXene for High-Resolution Neural Interfaces, *ACS Nano*, 2018, **12**, 10419–10429, DOI: [10.1021/acsnano.8b06014](https://doi.org/10.1021/acsnano.8b06014).
- 153 G. Ye, Z. Wen, F. Wen, X. Song, L. Wang, C. Li, Y. He, S. Prakash and X. Qiu, Mussel-inspired conductive Ti<sub>2</sub>C-cryogel promotes functional maturation of cardiomyocytes and enhances repair of myocardial infarction, *Theranostics*, 2020, **10**, 2047–2066, DOI: [10.7150/thno.38876](https://doi.org/10.7150/thno.38876).
- 154 A. Bigham, A. Zarepour, A. Khosravi, S. Iravani and A. Zarrabi, 3D and 4D Printing of MXene-based Composites: From Fundamentals to Emerging Applications, *Mater. Horiz.*, 2024, **11**, 6257–6288, DOI: [10.1039/d4mh01056f](https://doi.org/10.1039/d4mh01056f).
- 155 Z. Chang, L. Zhang, J. T. Hang, W. Liu and G. K. Xu, Viscoelastic Multiscale Mechanical Indexes for Assessing Liver Fibrosis and Treatment Outcomes, *Nano Lett.*, 2023, **23**, 9618–9625, DOI: [10.1021/acs.nanolett.3c03341](https://doi.org/10.1021/acs.nanolett.3c03341).
- 156 Z. Chang, J. Zhang, Y. Liu, H. Gao and G. K. Xu, New Mechanical Markers for Tracking the Progression of Myocardial Infarction, *Nano Lett.*, 2023, **23**, 7350–7357, DOI: [10.1021/acs.nanolett.3c01712](https://doi.org/10.1021/acs.nanolett.3c01712).
- 157 Z. Chang, L. Y. Li, Z. J. Shi, W. Liu and G. K. Xu, Beyond stiffness: multiscale viscoelastic features as biomechanical markers for assessing cell types and states, *Biophys. J.*, 2024, **123**, 1869–1881, DOI: [10.1016/j.bpj.2024.05.033](https://doi.org/10.1016/j.bpj.2024.05.033).
- 158 A. Kirti, F. Z. Simnani, S. Jena, S. S. Lenka, C. Kalalpitaya, S. S. Naser, D. Singh, A. Choudhury, R. N. Sahu, A. Yadav, A. Sinha, A. Nandi, P. K. Panda, N. K. Kaushik, M. Suar and S. K. Verma, Nanoparticle-mediated metronomic chemotherapy in cancer: a paradigm of precision and persistence, *Cancer Lett.*, 2024, **594**, 216990, DOI: [10.1016/j.canlet.2024.216990](https://doi.org/10.1016/j.canlet.2024.216990).
- 159 S. Wang, A. Riedinger, H. Li, C. Fu, H. Liu, L. Li, T. Liu, L. Tan, M. J. Barthel, G. Pugliese, F. De Donato, M. Scotto D'Abbusco, X. Meng, L. Manna, H. Meng and T. Pellegrino, Plasmonic copper sulfide nanocrystals exhibiting near-infrared photothermal and photodynamic therapeutic effects, *ACS Nano*, 2015, **9**, 1788–1800, DOI: [10.1021/nn506687t](https://doi.org/10.1021/nn506687t).
- 160 Y. Chen, Y. Wu, B. Sun, S. Liu and H. Liu, Two-Dimensional Nanomaterials for Cancer Nanotheranostics, *Small*, 2017, **13**, 1603446, DOI: [10.1002/smll.201603446](https://doi.org/10.1002/smll.201603446).
- 161 L. Rao, L. L. Bu, L. Ma, W. Wang, H. Liu, D. Wan, J. F. Liu, A. Li, S. S. Guo, L. Zhang, W. F. Zhang, X. Z. Zhao, Z. J. Sun and W. Liu, Platelet-Facilitated Photothermal Therapy of Head and Neck Squamous Cell Carcinoma, *Angew. Chem., Int. Ed.*, 2018, **57**, 986–991, DOI: [10.1002/anie.201709457](https://doi.org/10.1002/anie.201709457).
- 162 B. Chen, L. Mei, R. Fan, Y. Wang, C. Nie, A. Tong and G. Guo, Facile construction of targeted pH-responsive DNA-conjugated gold nanoparticles for synergistic



- photothermal-chemotherapy, *Chin. Chem. Lett.*, 2021, **32**, 1775–1779, DOI: [10.1016/j.ccllet.2020.12.058](https://doi.org/10.1016/j.ccllet.2020.12.058).
- 163 C. Dai, H. Lin, G. Xu, Z. Liu, R. Wu and Y. Chen, Biocompatible 2D Titanium Carbide (MXenes) Composite Nanosheets for pH-Responsive MRI-Guided Tumor Hyperthermia, *Chem. Mater.*, 2017, **29**, 8637–8652, DOI: [10.1021/acs.chemmater.7b02441](https://doi.org/10.1021/acs.chemmater.7b02441).
- 164 X. Yu, X. Cai, H. Cui, S. W. Lee, X. F. Yu and B. Liu, Fluorine-free preparation of titanium carbide MXene quantum dots with high near-infrared photothermal performances for cancer therapy, *Nanoscale*, 2017, **9**, 17859–17864, DOI: [10.1039/c7nr05997c](https://doi.org/10.1039/c7nr05997c).
- 165 X. Liu, H. Xie, S. Zhuo, Y. Zhou, M. S. Selim, X. Chen and Z. Hao, Ru(II) Complex Grafted Ti<sub>3</sub>C<sub>2</sub>T<sub>x</sub> MXene Nano Sheet with Photothermal/Photodynamic Synergistic Antibacterial Activity, *Nanomaterials*, 2023, **13**(6), 958, DOI: [10.3390/nano13060958](https://doi.org/10.3390/nano13060958).
- 166 Y. Guo, H. Wang, X. Feng, Y. Zhao, C. Liang, L. Yang, M. Li, Y. Zhang and W. Gao, 3D MXene microspheres with honeycomb architecture for tumor photothermal/ photodynamic/chemo combination therapy, *Nanotechnology*, 2021, **32**, 195701, DOI: [10.1088/1361-6528/abe153](https://doi.org/10.1088/1361-6528/abe153).
- 167 W. Yan, A. Rafieerad, K. N. Alagarsamy, L. R. Saleth, R. C. Arora and S. Dhingra, Immunoengineered MXene nanosystem for mitigation of alloantigen presentation and prevention of transplant vasculopathy, *Nano Today*, 2023, **48**, 101706, DOI: [10.1016/j.nantod.2022.101706](https://doi.org/10.1016/j.nantod.2022.101706).
- 168 K. S. Kim, Y. Zhao, H. Jang, S. Y. Lee, J. M. Kim, K. S. Kim, J. H. Ahn, P. Kim, J. Y. Choi and B. H. Hong, Large-scale pattern growth of graphene films for stretchable transparent electrodes, *Nature*, 2009, **457**, 706–710.
- 169 A. Prasad, S. M. Bhasney, V. Prasannavenkadesan, M. R. Sankar and V. Katiyar, Polylactic acid reinforced with nano-hydroxyapatite bioabsorbable cortical screws for bone fracture treatment, *J. Polym. Res.*, 2023, **30**, 177, DOI: [10.1007/s10965-023-03542-8](https://doi.org/10.1007/s10965-023-03542-8).
- 170 S. Baik, H. R. Choi, Y.-J. Kim, J.-H. Ahn, K.-Y. Chun, J. Rho and Y. Oh, Highly conductive, printable and stretchable composite films of carbon nanotubes and silver, *Nat. Nanotechnol.*, 2010, **5**, 853–857.
- 171 S. Zhang, S. S. Rana, T. Bhatta, G. B. Pradhan, S. Sharma, H. Song, S. Jeong and J. Y. Park, 3D printed smart glove with pyramidal MXene/Ecoflex composite-based toroidal triboelectric nanogenerators for wearable human-machine interaction applications, *Nano Energy*, 2023, **106**, 108110, DOI: [10.1016/j.nanoen.2022.108110](https://doi.org/10.1016/j.nanoen.2022.108110).
- 172 J. Fan, M. Yuan, L. Wang, Q. Xia, H. Zheng and A. Zhou, MXene supported by cotton fabric as electrode layer of triboelectric nanogenerators for flexible sensors, *Nano Energy*, 2023, **105**, 107973, DOI: [10.1016/j.nanoen.2022.107973](https://doi.org/10.1016/j.nanoen.2022.107973).
- 173 F. Hao, L. Wang, B. Chen, L. Qiu, J. Nie and G. Ma, Bifunctional Smart Hydrogel Dressing with Strain Sensitivity and NIR-Responsive Performance, *ACS Appl. Mater. Interfaces*, 2021, **13**, 46938–46950, DOI: [10.1021/acsami.1c15312](https://doi.org/10.1021/acsami.1c15312).
- 174 A. Szuplewska, D. Kulpińska, A. Dybko, A. M. Jastrzębska, T. Wojciechowski, A. Rozmysłowska, M. Chudy, I. Grabowska-Jadach, W. Ziemkowska, Z. Brzózka and A. Olszyna, 2D Ti<sub>2</sub>C (MXene) as a novel highly efficient and selective agent for photothermal therapy, *Mater. Sci. Eng., C*, 2019, **98**, 874–886, DOI: [10.1016/j.msec.2019.01.021](https://doi.org/10.1016/j.msec.2019.01.021).
- 175 E. A. Mayerberger, R. M. Street, R. M. McDaniel, M. W. Barsoum and C. L. Schauer, Antibacterial properties of electrospun Ti<sub>3</sub>C<sub>2</sub>T<sub>x</sub> (MXene)/chitosan nanofibers, *RSC Adv.*, 2018, **8**, 35386–35394, DOI: [10.1039/c8ra06274a](https://doi.org/10.1039/c8ra06274a).
- 176 A. Rozmysłowska-Wojciechowska, A. Szuplewska, T. Wojciechowski, S. Poźniak, J. Mitrzak, M. Chudy, W. Ziemkowska, L. Chlubny, A. Olszyna and A. M. Jastrzębska, A simple, low-cost and green method for controlling the cytotoxicity of MXenes, *Mater. Sci. Eng., C*, 2020, **111**, 110790, DOI: [10.1016/j.msec.2020.110790](https://doi.org/10.1016/j.msec.2020.110790).
- 177 B. M. Abraham, P. Sinha, P. Halder and J. K. Singh, Fusing a machine learning strategy with density functional theory to hasten the discovery of 2D MXene-based catalysts for hydrogen generation, *J. Mater. Chem. A*, 2023, **11**, 8091–8100, DOI: [10.1039/D3TA00344B](https://doi.org/10.1039/D3TA00344B).
- 178 A. Saleh, S. Wustoni, E. Bihar, J. K. El-Demellawi, Y. Zhang, A. Hama, V. Druet, A. Yudhanto, G. Lubineau, H. N. Alshareef and S. Inal, Inkjet-printed Ti<sub>3</sub>C<sub>2</sub>T<sub>x</sub> MXene electrodes for multimodal cutaneous biosensing, *JPhys Mater.*, 2020, **3**, 044004, DOI: [10.1088/2515-7639/abb361](https://doi.org/10.1088/2515-7639/abb361).
- 179 J. Chen, B. Arianpour, K. Wang, S. Wang, J. Yin, Y. Zhang, E. Zhu and T. K. Hsiai, Emerging nanomaterials to enhance electrochemical impedance spectroscopy for biomedical applications, *Front. Mater.*, 2023, **10**, 1146045, DOI: [10.3389/fmats.2023.1146045](https://doi.org/10.3389/fmats.2023.1146045).
- 180 J. Xiong, M. F. Lin, J. Wang, S. L. Gaw, K. Parida and P. S. Lee, Wearable All-Fabric-Based Triboelectric Generator for Water Energy Harvesting, *Adv. Energy Mater.*, 2017, **7**, 1701243, DOI: [10.1002/aenm.201701243](https://doi.org/10.1002/aenm.201701243).
- 181 J. Xiong, P. Cui, X. Chen, J. Wang, K. Parida, M. F. Lin and P. S. Lee, Skin-touch-actuated textile-based triboelectric nanogenerator with black phosphorus for durable biomechanical energy harvesting, *Nat. Commun.*, 2018, **9**, 4280, DOI: [10.1038/s41467-018-06759-0](https://doi.org/10.1038/s41467-018-06759-0).
- 182 L. Yuan, M. Zhang, T. Zhao, T. Li, H. Zhang, L. Chen and J. Zhang, Flexible and breathable strain sensor with high performance based on MXene/nylon fabric network, *Sens. Actuators, A*, 2020, **315**, 112192, DOI: [10.1016/j.sna.2020.112192](https://doi.org/10.1016/j.sna.2020.112192).
- 183 X. Zhao, L. Y. Wang, C. Y. Tang, X. J. Zha, Y. Liu, B. H. Su, K. Ke, R. Y. Bao, M. B. Yang and W. Yang, Smart Ti<sub>3</sub>C<sub>2</sub>T<sub>x</sub> MXene Fabric with Fast Humidity Response and Joule Heating for Healthcare and Medical Therapy Applications, *ACS Nano*, 2020, **14**, 8793–8805, DOI: [10.1021/acsnano.0c03391](https://doi.org/10.1021/acsnano.0c03391).
- 184 E. A. Mayerberger, O. Urbanek, R. M. McDaniel, R. M. Street, M. W. Barsoum and C. L. Schauer, Preparation and characterization of polymer-Ti<sub>3</sub>C<sub>2</sub>T<sub>x</sub> (MXene) composite nanofibers produced via electrospinning, *J. Appl. Polym. Sci.*, 2017, **134**, 45295, DOI: [10.1002/app.45295](https://doi.org/10.1002/app.45295).
- 185 W. Shao, M. Tebyetekerwa, I. Marriam, W. Li, Y. Wu, S. Peng, S. Ramakrishna, S. Yang and M. Zhu, Polyester@MXene nanofibers-based yarn electrodes,



- J. Power Sources*, 2018, **396**, 683–690, DOI: [10.1016/j.jpowsour.2018.06.084](https://doi.org/10.1016/j.jpowsour.2018.06.084).
- 186 S. S. Naser, A. Gupta, A. Choudhury, A. Yadav, A. Sinha, A. Kirti, D. Singh, M. Kujawska, N. K. Kaushik, A. Ghosh, S. De and S. K. Verma, Biophysical translational paradigm of polymeric nanoparticle: embarked advancement to brain tumor therapy, *Biomed. Pharmacother.*, 2024, **179**, 117372, DOI: [10.1016/j.biopha.2024.117372](https://doi.org/10.1016/j.biopha.2024.117372).
- 187 X. Zheng, Q. Hu, Z. Wang, W. Nie, P. Wang and C. Li, Roll-to-roll layer-by-layer assembly bark-shaped carbon nanotube/Ti<sub>3</sub>C<sub>2</sub>T<sub>x</sub> MXene textiles for wearable electronics, *J. Colloid Interface Sci.*, 2021, **602**, 680–688, DOI: [10.1016/j.jcis.2021.06.043](https://doi.org/10.1016/j.jcis.2021.06.043).
- 188 Z. Wang, S. Qin, S. Seyedin, J. Zhang, J. Wang, A. Levitt, N. Li, C. Haines, R. Ovalle-Robles, W. Lei, Y. Gogotsi, R. H. Baughman and J. M. Razal, High-Performance Biscrolled MXene/Carbon Nanotube Yarn Supercapacitors, *Small*, 2018, **14**, 1802225, DOI: [10.1002/sml.201802225](https://doi.org/10.1002/sml.201802225).
- 189 A. Levitt, S. Seyedin, J. Zhang, X. Wang, J. M. Razal, G. Dion and Y. Gogotsi, Bath Electrospinning of Continuous and Scalable Multifunctional MXene-Infiltrated Nanoyarns, *Small*, 2020, **16**, 2002158, DOI: [10.1002/sml.202002158](https://doi.org/10.1002/sml.202002158).
- 190 C. Ma, Q. Yuan, H. Du, M. G. Ma, C. Si and P. Wan, Multiresponsive MXene (Ti<sub>3</sub>C<sub>2</sub>T<sub>x</sub>)-Decorated Textiles for Wearable Thermal Management and Human Motion Monitoring, *ACS Appl. Mater. Interfaces*, 2020, **12**, 34226–34234, DOI: [10.1021/acsami.0c10750](https://doi.org/10.1021/acsami.0c10750).
- 191 W. Xin, M. G. Ma and F. Chen, Silicone-Coated MXene/Cellulose Nanofiber Aerogel Films with Photothermal and Joule Heating Performances for Electromagnetic Interference Shielding, *ACS Appl. Nano Mater.*, 2021, **4**, 7234–7243, DOI: [10.1021/acsnm.1c01185](https://doi.org/10.1021/acsnm.1c01185).
- 192 J. Li, C. Wang, L. Yue, F. Chen, X. Cao and Z. Wang, Nano-QSAR modeling for predicting the cytotoxicity of metallic and metal oxide nanoparticles: a review, *Ecotoxicol. Environ. Saf.*, 2022, **243**, 113955, DOI: [10.1016/j.ecoenv.2022.113955](https://doi.org/10.1016/j.ecoenv.2022.113955).
- 193 X. Zhu, L. Lin, R. Wu, Y. Zhu, Y. Sheng, P. Nie, P. Liu, L. Xu and Y. Wen, Portable wireless intelligent sensing of ultra-trace phyto regulator  $\alpha$ -naphthalene acetic acid using self-assembled phosphorene/Ti<sub>3</sub>C<sub>2</sub>-MXene nanohybrid with high ambient stability on laser induced porous graphene as nanozyme flexible electrode, *Biosens. Bioelectron.*, 2021, **179**, 113062, DOI: [10.1016/j.bios.2021.113062](https://doi.org/10.1016/j.bios.2021.113062).
- 194 S. Shimadera, K. Kitagawa, K. Sagehashi, Y. Miyajima, T. Niiyama and S. Sunada, Speckle-based high-resolution multimodal soft sensing, *Sci. Rep.*, 2022, **12**, 13096, DOI: [10.1038/s41598-022-17026-0](https://doi.org/10.1038/s41598-022-17026-0).
- 195 M. C. Bottino, V. Thomas, G. Schmidt, Y. K. Vohra, T. M. G. Chu, M. J. Kowolik and G. M. Janowski, Recent advances in the development of GTR/GBR membranes for periodontal regeneration – A materials perspective, *Dent. Mater.*, 2012, **28**, 703–721, DOI: [10.1016/j.dental.2012.04.022](https://doi.org/10.1016/j.dental.2012.04.022).
- 196 K. Sarkar, K. Dutta, A. Chatterjee, J. Sarkar, D. Das, A. Prasad, D. Chattopadhyay, K. Acharya, M. Das, S. K. Verma and S. De, Nanotherapeutic potential of antibacterial folic acid-functionalized nanoceria for wound-healing applications, *Nanomedicine*, 2023, **18**, 109–123, DOI: [10.2217/nnm-2022-0233](https://doi.org/10.2217/nnm-2022-0233).
- 197 K. Chen, Y. Chen, Q. Deng, S. H. Jeong, T. S. Jang, S. Du, H. E. Kim, Q. Huang and C. M. Han, Strong and biocompatible poly(lactic acid) membrane enhanced by Ti<sub>3</sub>C<sub>2</sub>T<sub>z</sub> (MXene) nanosheets for Guided bone regeneration, *Mater. Lett.*, 2018, **229**, 114–117, DOI: [10.1016/j.matlet.2018.06.063](https://doi.org/10.1016/j.matlet.2018.06.063).
- 198 Z.-C. Hu, J.-Q. Lu, T.-W. Zhang, H.-F. Liang, H. Yuan, D.-H. Su, W. Ding, R.-X. Lian, Y.-X. Ge, B. Liang, J. Dong, X.-G. Zhou and L.-B. Jiang, Piezoresistive MXene/Silk fibroin nanocomposite hydrogel for accelerating bone regeneration by Re-establishing electrical microenvironment, *Bioact. Mater.*, 2023, **22**, 1–17, DOI: [10.1016/j.bioactmat.2022.08.025](https://doi.org/10.1016/j.bioactmat.2022.08.025).

